Doctoral Dissertations and Master's Theses

Summer 8-10-2023

Tests of General Relativity through Searches for Lorentz and CPT Symmetry Breaking

Kellie Ault
Embry-Riddle Aeronautical University, aultk@my.erau.edu

Follow this and additional works at: https://commons.erau.edu/edt

Part of the Cosmology, Relativity, and Gravity Commons, and the Other Astrophysics and Astronomy Commons

Tests of General Relativity through Searches for Lorentz and CPT Symmetry Breaking

By

Kellie O'Neal-Ault

A Dissertation submitted in Partial Fulfillment of the Requirements for the Degree

of

Doctor of Philosophy in Engineering Physics

Embry-Riddle Aeronautical University

Department of Physical Sciences

Daytona Beach, FL 32114

August 10th, 2023

Tests of General Relativity through Searches for Lorentz and CPT Symmetry Breaking

By Kellie O'Neal-Ault

This dissertation was prepared with the guidance of the candidate's dissertation committee chair, Dr. Quentin G. Bailey, Department of Physics and Astronomy, Prescott, AZ, and has been approved by the members of his dissertation committee. It was submitted to the Department of Physical Sciences, Daytona Beach, FL, and was accepted in partial fulfillment of the requirements for the
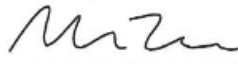
Degree of

Doctor of Philosophy in Engineering Physics

DISSERTATION COMMITTEE:
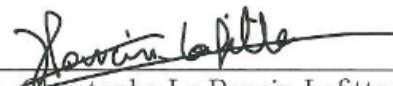
_8-11-23_
Dr. Quentin G. Bailey, Ph.D.,
Committee Chair

_8/11/2023_
Dr. Michele Zanolin, Ph.D.,
Committee Member

August 14, 2023
Dr. Lijing Shao, Ph.D.,
Committee Member

Dr. Christophe Le Poncin-Lafitte, Ph.D.,
Committee Member

Edwin Mierkiewicz Digitally signed by Edwin Mierkiewicz
DN: cn=Edwin Mierkiewicz, o, ou,
email=mierkiee@erau.edu, c=US
Date: 2023.08.23 19:21:32 -05'00'

Dr. Edwin J. Mierkiewicz, Ph.D.,
Graduate Program Chair,
Engineering Physics

Digitally signed by Dr. John Hughes
Date: 2023.08.24 08:29:08 -04'00'

Dr. John Hughes, Ph.D.,
Department Chair, Physical Sciences

Peter Hoffmann Digitally signed by Peter Hoffmann
Date: 2023.08.24 12:17:29 -04'00'

Dr. Peter Hoffmann, Ph.D.,
Dean, College of Arts and Sciences

Acknowledgments

Contents

Abstract

An effective field theory framework, the Standard Model Extension (SME), provides an agnostic, systematic test of General Relativity (GR) and its founding spacetime symmetries, Lorentz and CPT symmetry. Violating these symmetries may provide clues toward unifying the physics of the General Relativity and the Standard Model of particle physics.

Part of this work involves the merge of theory, data analysis and experiments with gravitational wave (GW) signals from LIGO/Virgo/KAGRA (LVK) detectors. A modified dispersion relation derived from the SME of GWs is implemented into the LIGO Scientific Collaboration Algorithm Library Suite (LALSuite), where a joint Bayesian inference of the source parameters and coefficients for spacetime symmetry-breaking is performed for binary black hole and neutron star events. Using 45 events from the GWTC-3 LVK catalogue, constraints are placed on the symmetry-breaking coefficients.

Additional work involves a 3+1 formulation of the SME in the gravitational sector with a Dirac Hamiltonian analysis. The assumption of explicit local Lorentz and diffeomorphism symmetry breaking is made. This work shows significant differences in the structure of the dynamics when comparing to General Relativity and focus is given to cosmological solutions, which produce modified Friedmann equations and altered conservation laws. This research also find terms within the framework to match certain modified gravity models along with noting further potential impact toward other gravitational models, theories and phenomenology including quantum gravity.

List of Figures

List of Tables

Chapter 1

Introduction

Physicists search for the truths that describe the Nature and universe that we exist within. It is the research and exploration itself, the appreciation of the beauty learned during their career and the potential for special moments of discovery that give purpose among the vastness in both established concepts and even more, the mysteries yet understood.

Strong instinctual curiosity makes focusing within a subset area of physics quite difficult for some. The sole physicist can learn to appreciate the significance of a shared group of minds, with varying skills and perspectives. A single human is limited and biased, adding to the unique experiences as one explores the essence of our world. Yet if one wishes to experience more, possibly heading toward an unknown unified theory, there is an overwhelming amount of knowledge along the way that one can try to acquire within countless paths and avenues. This is where the community of different minds, when acting together, allow a broader experience and view of the immense landscape of physics.

A physicists can also look at nature around them and note our instinctual desire to see symmetries. A rose with its pedals, trees with spreading branches, clouds, waters

and mountains may not seem to have obvious perfect symmetries, possibly having partial symmetries, yet are beautiful and admired. It is even unusual when one finds perfect symmetry in nature, something that stands out. It is no surprise then, the fascination with symmetries and the devotion of studies into trying to comprehend them. Whether by finding their pure forms, or by breaking them, it is in the hopes of seeing hints into the underlying fabric of our reality.

1.1 Research Motivation

General Relativity (GR), the current theory of gravity, and the Standard Model (SM) of particle physics are well-tested, successful theories for over a century, yet it still remains a challenge to find a fundamental unified theory that encompasses the two. It is expected that GR and the SM describe the low-energy limits for this unified theory, a theory of quantum gravity. Some theorists believe this should emerge around some ultraviolet cutoff scale, commonly thought to be the Planck energy scale of 10^{19} GeV [43]. Experiments to probe such scales are not yet feasible and so one must look for hints of this underlying fundamental physics. One approach is to take the foundational symmetries of GR and the SM and test for any violations, investigating any possible exposed clues that could guide us toward this unified physics. Many proposed theories and models suggest symmetries can be broken, searching for space-time breaking effects within sensitive tests [84, 51, 40, 16, 10, 88, 3, 4, 5, 9, 7]. The research in this thesis is devoted toward the searches for Lorentz and CPT symmetry breaking, focusing efforts on gravity.

1.2 Notation and units

For most of this thesis, work is done within natural units more common among the SM community, where $\hbar = c = 1$, and Newton's gravitational constant is $G_N \neq 1$. Note that later in this work, a devoted section is given to elaborating on different notation used and their conversions when applicable. In regards to the chapter involving gravitational waves, the metric signature is taken to be the standard choice for GR $(- + ++)$. For tensors and their components, Greek letters are used for spacetime indices and Latin letters for spatial indices. The operator ∇_μ is used for the spacetime covariant derivative and $\mathcal{D}_\mu$ for the covariant derivative that is defined on a spatial hypersurface parameterized by time.

1.3 Spacetime Symmetries

Special Relativity (SR) states that the laws of physics are the same for any inertial observer and the speed of light is the same for all inertial observers. When referring to flat, Minkowski spacetime, this refers to the absence of gravity. As a result of SR, a symmetry becomes apparent under certain transformations. As an illustrative example, imagine a sphere. Under a rotation, the geometry does not change and thus the sphere has a symmetric geometry. Likewise, in SR, the laws of physics are the symmetry that do not change under transformations known as Lorentz transformations (LT). There are 6 Lorentz transformations one can apply to a frame $\mathcal{O}$ with coordinates x^μ to transform to the new primed frame $\mathcal{O}'$ with coordinates x'^μ. These include 3 rotations about the frame's coordinate axes and 3 boosts, where the $\mathcal{O}$ frame is given a boost velocity along a coordinate axis (see Fig. 1.1). The LT are contained within the Lorentz transformation, Λ^μ_ν, where a vector B^μ transforms as $B'^\mu = \Lambda'^\mu_\nu B^\nu$.
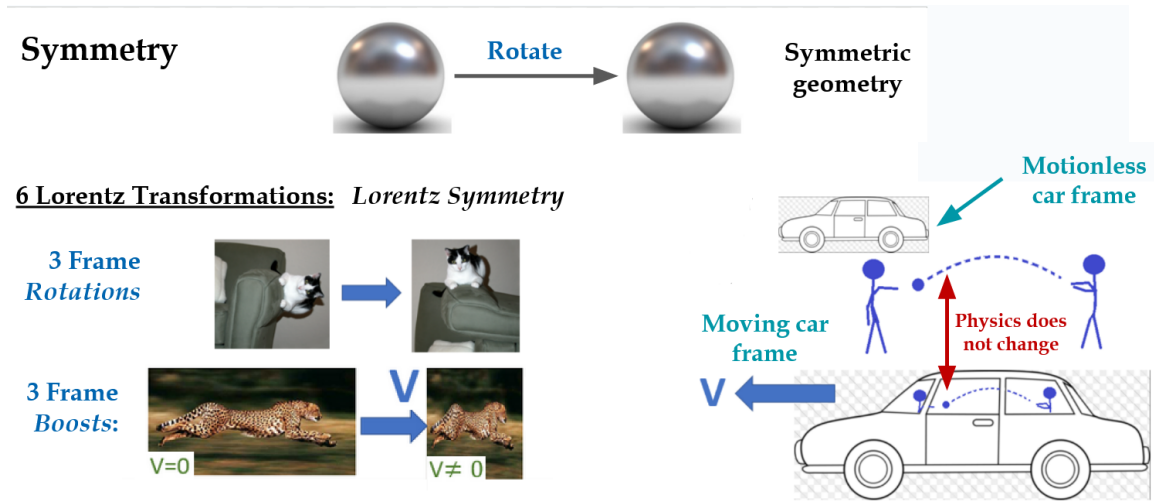
Figure 1.1: As a result of SR, six Lorentz transformations that can be applied to the observer frame will preserve the laws of physics: three rotations and three boosts.

There is also charge conjugation, parity inversion, and time reversal (CPT) symmetries that are *discrete* symmetries in comparison to the continuous Lorentz symmetries. The existence of an antiparticle for every particle with an opposite charge refers to charge conjugation; parity inversion describes the mirror-image counterpart of particles and their interactions; time reversal refers to invariance of the laws of physics that describe the particle interactions under a reversal of time.

A principle foundation for GR is the Einstein Equivalence Principle where in any local Lorentz frame, the form for physical laws are the same as in any freely falling inertial frames in SR (in the absence of gravitational fields). In GR, spacetime is no longer flat and has curvature; its symmetry reduces to local Lorentz symmetry for any one point P in spacetime and is defined to preserve Lorentz symmetry as shown in 1.2. . The Minkowski metric is defined in SR for flat spacetime, i.e., $\eta_{\mu\nu}$ while in GR, the metric is $g_{\mu\nu}$. The metric $g_{\mu\nu}$ can be connected to the local Lorentz frame defined at point P via the vierbein $e^\mu_a(P) \equiv \frac{\partial x^\mu}{\partial \xi^a}(P)$ using the form $g_{\mu\nu} = e^a_\mu \, e^b_\nu \, \eta_{ab}$. There is also 4 diffeomorphism symmetries associated with translations ξ^μ within the
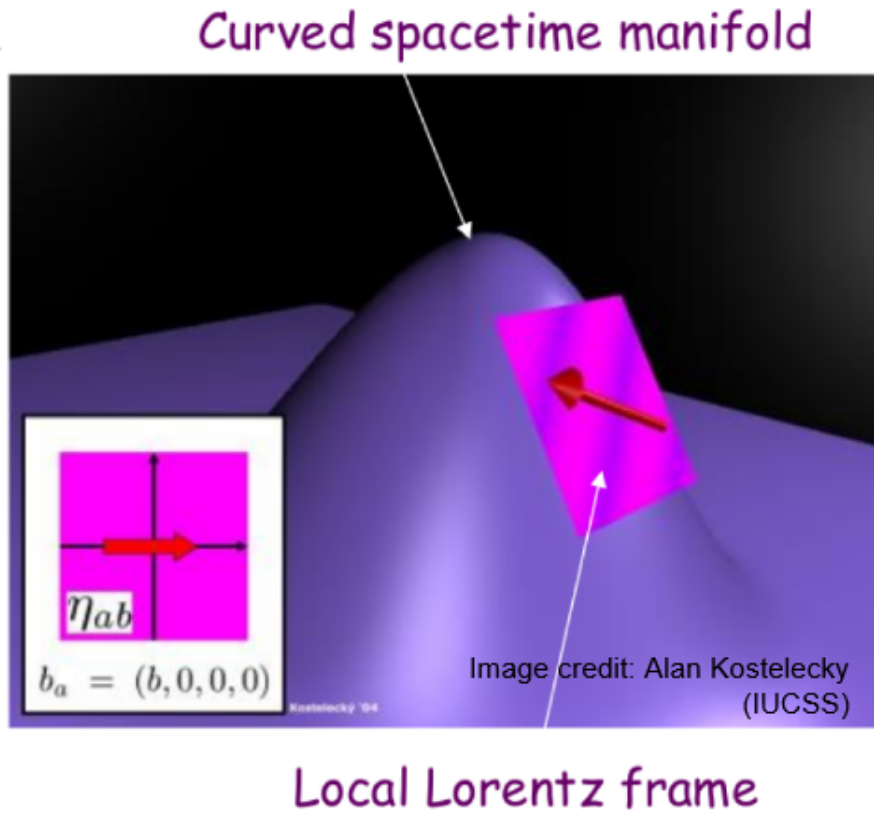
Figure 1.2: Spacetime can have curvature in GR, while points are defined in a local Lorentz frame (flat spacetime).

spacetime, where for a vector B^μ,

$$B^\mu \rightarrow B^\mu + (\partial_\nu \xi^\mu)B^\nu - \xi^\nu \partial_\nu B^\mu.$$

These are additional, local transformation symmetries within a pseudo Riemann manifold. Additional information can be found within textbook sources including [92, 127, 58].

1.4 Standard-Model Extension

One method that allows for the test of fundamental symmetries of GR and the SM is an effective field theory framework, named the Standard-Model Extension (SME) [43, 72]. This model-independent framework provides a systematic, agnostic approach for testing Lorentz and CPT symmetries as depicted in Fig. 1.3. It starts at the level of
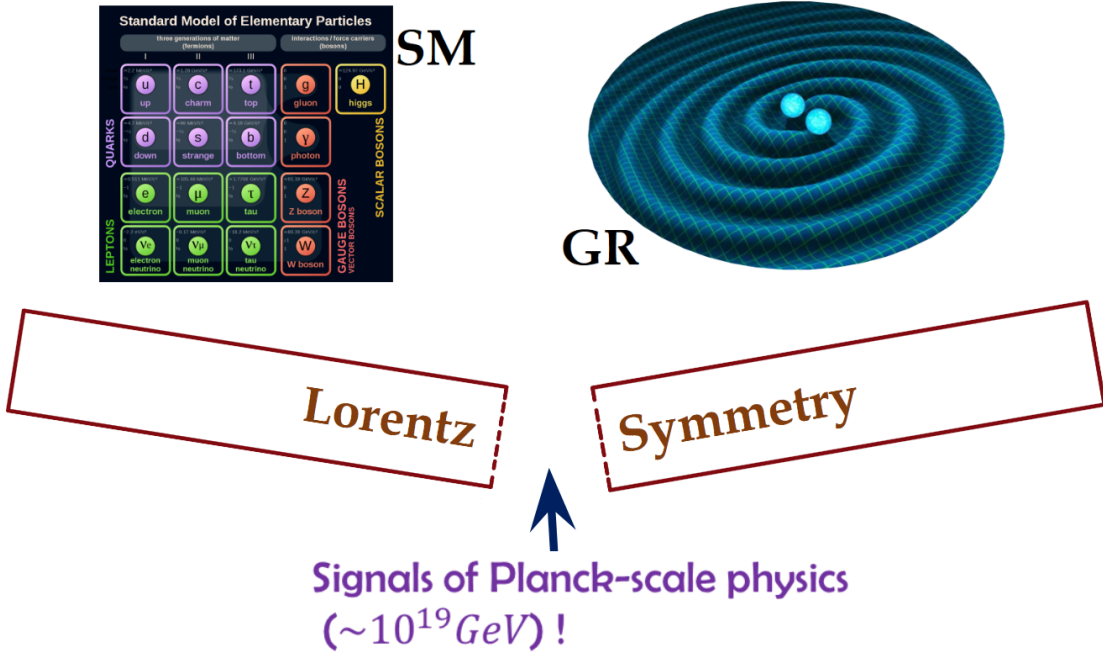
Figure 1.3: The SME framework allows for tests that break foundational spacetime-symmetry breaking to search for clues for some unified physics that is expected emerge at Planck-scale physics. *Image inspiration: Matthew Mewes and Quentin G. Bailey.*

the action S, containing the known physics of GR within the Lagrange density $\mathcal{L}_{GR}$, the SM of particle physics within $\mathcal{L}_{SM}$, plus an arbitrary number of terms that allow for spacetime-breaking within $\mathcal{L}_{SME}$ [44, 43, 72, 24, 67, 23, 29, 80, 78, 73],

$$S = \int d^4x (\mathcal{L}_{GR} + \mathcal{L}_{SM} + \mathcal{L}_{SME}). \tag{1.1}$$

The last term includes tests of local Lorentz, CPT and diffeomorphism symmetries. The additional terms in $\mathcal{L}_{SME}$ contain operators derived from known physics fields like that of gravity, which act on coefficients for spacetime-symmetry breaking that control the degree of symmetry breaking within observable physics. Though there are an arbitrary number of additional terms, in practice, one often chooses to truncate to those of lower mass dimension, as in the case of the *minimal* SME, containing terms of mass dimensions 3 and 4. The mass dimension is defined in terms of the chosen natural units, e.g., GR is a mass dimension 4 term.

The SME is a framework and not a theory or model that covers many sectors of physics as depicted in Fig. 1.1. Numerous literature provide both experimental and theoretically-derived bounds on the SME coefficients. A collection of this decades-worth progress is displayed within [81]. The focus of this research is the gravity sector of the SME.

There are also many publications that devote efforts toward mapping existing modified physics to terms within the SME. The table 1.4 displays current progress within the gravity sector of the SME [22, 102]. A mapping between Hořava-Lifshitz gravity and terms within the SME is elaborated on later in chapter 3.

1.5   Linkage to Scientific Papers and Overview

The chapters 2 and 3 contain the main body of this research, focusing on investigating possible effects from spacetime symmetry-breaking in the pure gravity sector within the SME framework. Most of the work has been published within peer-reviewed journals and conference proceedings and can be accessed through:

`https://inspirehep.net/authors/1815931.`

Chapter 2 follows the research involving gravitational waves, and is based on

Different Sectors of Physics Within the SME Framework:
Electron Sector
Charged-lepton Sector
Proton Sector
Neutrino Sector
Neutron Sector
Quark Sector
Nonminimal QED Sector
Gluon Sector
Gravity Sector

Table 1.1: There are 46 data tables compiled from current literature that cover many sectors of physics when testing symmetry-breaking within the SME framework. The focus of this dissertation is the gravity sector.

published works of the dissertation author [104, 55, 99, 97, 64, 102]. Chapter 3 contains the research regarding the 3+1 formulation of the gravity sector within the SME framework, along with a Dirac-Hamiltonian analysis, and is based on the publication of the dissertation author [103].

Mapping

Models ⟷ *Framework*

Model	Link to SME	Lorentz-violating fields	General Test Framework
PPN	Yes	None (α_1, α_2, w^j)	Yes, metric
SME, gravity sector	Yes	tensors, flavor dependent	Yes, EFT
Bumblebee	Yes	vector	No
Einstein-Aether	Partial	vector	No
Horava gravity	Yes	vector	No
ATT model	Yes	Anti-symm. two-tensor	No
Cardinal	Yes	symm. two tensor	No
Massive gravity	Yes	two-tensor	?
Chern-Simons gravity	Yes	scalar	No
GW modified dispersion	Yes	None (parameters)	Yes, Disp. Rel.
NC gravity	Yes	$\Theta\mu\nu$	No

Figure 1.4: The figure shows current progress toward mapping modified physics models and theories to terms within the SME. *Table credit: Quentin G. Bailey*

Chapter 2

Gravitational Wave Tests of Spacetime Symmetries

Since the discovery of the first GW signal on September 14, 2015 [3], nearly one hundred confidently-detected events [6, 41, 15] have opened a ripe, new testing ground for gravitational physics. There are many specific models that have investigated the effects from Lorentz-symmetry breaking for gravitational waves [24, 80, 78, 129, 130, 96, 91]. Other works test for deviations from GR via parameterization [5, 9, 125, 123]. Many more do so through the SME framework [131, 26, 18, 48, 120, 125, 123, 110, 86, 118, 126, 80, 101, 8, 124], including comparison tests between gravity and light [2] and related works within this thesis [104, 55, 54].

2.1   Background Theory of Gravitational Waves

One can expand the spacetime metric $g_{\mu\nu}$ as a perturbation $h_{\mu\nu}$ around a flat Minkwoski background $\eta_{\mu\nu}$,

$$g_{\mu\nu} = \eta_{\mu\nu} + h_{\mu\nu}. \tag{2.1}$$

Near gravitational wave sources in the near zone, one finds strong, nonlinear gravity; far from such sources in the radiation zone, propagating GWs can be represented as small perturbations, i.e., $h_{\mu\nu} << \eta_{\mu\nu}$, having strain around the order of 10^{-21}. Tensors including the Riemann and Ricci tensors, can be rewritten in a linear form, up to the first order in $h_{\mu\nu}$. The Einstein field equations can be written in a "relaxed form",

$$(G_L)^{\mu\nu} = \kappa[(T_M)^{\mu\nu} + \tau^{\mu\nu}], \tag{2.2}$$

where $\kappa = 8\pi G_N$, $(T_M)^{\mu\nu}$ is the matter stress-energy tensor, $\tau^{\mu\nu}$ is the energy-momentum pseudo tensor [107] containing terms of second and higher order in $h_{\mu\nu}$, and $(G_L)^{\mu\nu}$ is the linearized Einstein tensor. Gravitational Waves travel through the vacuum, and in regions far from the source, reducing to, (2.2)

$$\Box h_{\mu\nu} = 0. \tag{2.3}$$

The general solution to ((2.3)) for a plane wave is a linear superposition for the metric perturbation,

$$h_{\mu\nu} = e_{\mu\nu}e^{ik_\alpha x^\alpha} + e^*_{\mu\nu}e^{-ik_\alpha x^\alpha}, \tag{2.4}$$

where $k_\alpha = (\omega, \vec{p})$ is the four-momentum, $x^\alpha = (t, \vec{x})$ the configuration coordinates, and $e_{\mu\nu}$ is a two-tensor that is labeled as the *polarization tensor*. Note that indices for all tensors can be raised and lowered via the Minkowski metric, and thus the polarization tensor is symmetric. When applying the solution to the equation in (2.3) for the nontrivial case of $h_{\mu\nu} \neq 0$, one finds the dispersion relation,

$$k^\alpha k_\alpha = 0. \tag{2.5}$$

One can choose to impose the Lorentz gauge,

$$\partial_\alpha h^\alpha_\beta = \tfrac{1}{2}\partial_\beta h, \tag{2.6}$$

where $h \equiv h^\alpha_\alpha$. Applying the general solution (2.4) to the Lorentz gauge, another useful relation is found,

$$k_\alpha e^\alpha_\beta = \tfrac{1}{2}k_\beta e^\alpha_\alpha. \tag{2.7}$$

The symmetric polarization tensor has initially 10 independent components and when imposing the condition (2.7), four equations are found containing 10 unknown components, leaving six independent components. One can also use the usual GR linear gauge transformation $h_{\mu\nu} \to h_{\mu\nu} - \partial_\mu\xi_\nu - \partial_\nu\xi_\mu$, where ξ^μ is an arbitrary vector. Choosing the form $\xi^\mu(x) = i\epsilon^\mu e^{ik_\alpha x^\alpha} - i\epsilon^{*\mu}e^{-ik_\alpha x^\alpha}$ transforms the polarization tensor into a new primed coordinate system as,

$$e'_{\mu\nu} = e_\mu\nu + k_\nu\epsilon_\mu + k_\mu\epsilon_\nu. \tag{2.8}$$

Since both $e'_{\mu\nu}$ and $e_{\mu\nu}$ must represent the same physical situation for the arbitrary parameters k_μ and ϵ_μ, the number of linearly independent components is narrowed down to two polarizations. One can refer to textbook sources for further details on this derivation [92, 127]. The two physical components are labeled as "+" and "×" polarizations, having a phase angle difference of $\pi/4$. The gauge used is the

transverse-traceless gauge (TT-gauge) which expresses the $h_{\mu\nu}$ components as,

$$h_{\mu\nu} = \begin{pmatrix} 0 & 0 & 0 & 0 \\ 0 & h_+ & h_\times & 0 \\ 0 & h_\times & -h_+ & 0 \\ 0 & 0 & 0 & 0 \end{pmatrix}. \tag{2.9}$$

In order for the gravitational perturbation $h_{\mu\nu}$ to be observable, it must interact and provide a means to measure changes with some type of detector, e.g., the LVK ground based detectors.

2.2 Era of Ground-Based Gravitational Wave Detectors

The LVK collaboration includes a network of four ground based detectors, two of which are located within the United States (LIGO), one in Italy (Virgo), and one in Japan (KAGRA). The detectors are designed after the Michelson-Morley experiment over a hundred years prior to the founding of the first LIGO detector [90]. Each detector has two perpendicular laser trajectory paths a few kilometers in length, with inertial tests mass mirrors at their ends. A laser source produces an electromagnetic wave that is split into two separate, equal beams before propagating along perpendicular arms (see Figure 2.1). The end mirrors reflect the beams back to the beam splitter a few hundred times before ultimately, they are recombined at the origin center point, producing an output signal at a photo detector [11, 12]. In the absence of GW effects, the output signal is designed to produce a full destructive interference, yet in the presence of a gravitational wave, the travel time of each propagating beam
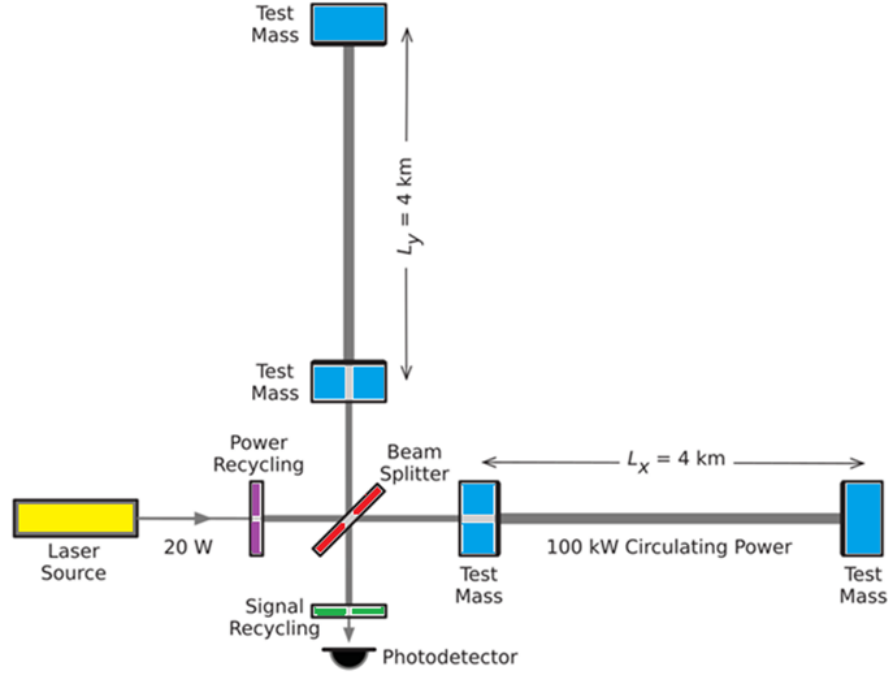
Figure 2.1: The above image provides a basic layout of a LIGO GW detector, where the laser source beam is split evenly, each then traveling down their respective arm, reflecting, and recombining to produce an interference pattern observed at the photo detector.

can be altered, producing a possible interference pattern at the photo detector.

The observable signal can be represented as a projection of the GW's plus and cross polarizations onto the detector arms,

$$S_A(t, \theta, \phi, \psi) = F_{A,+}(\theta, \phi, \psi)\, h_+(t, \theta, \phi, \psi, \tau) \; + \; F_{A,\times}(\theta, \phi, \psi)\, h_\times(t, \theta, \phi, \psi, \tau), \quad (2.10)$$

where the antenna response patterns are the $F_{A,*}$ functions. These functions depend on the source's sky localization angles θ and ϕ, the time delay between the detectors receiving the signal τ, and the GW frame rotation with respect to the frame of the detectors ψ (see Figure 2.2). Each term within (2.10) is not gauge independent
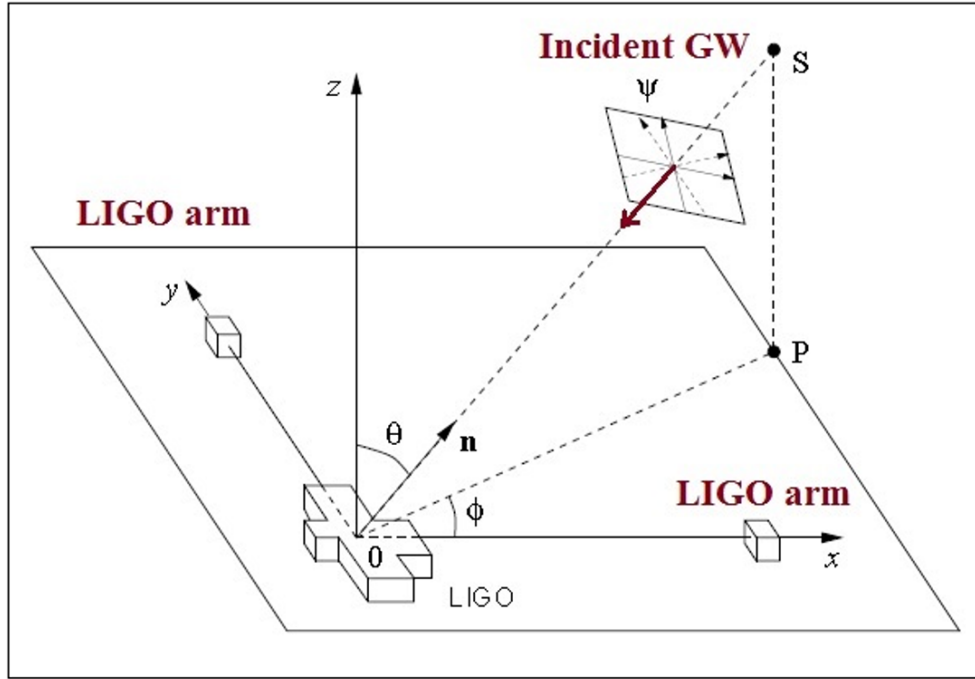
Figure 2.2: The projection of the incident GW frame onto the detector frame and the relative angles.

considering they rely on the ψ, yet the entire observable signal is.

2.2.1 Demonstrating Simplified Detector Response and Sensitivity

To expand some on the base understanding of the response behavior and sensitivities of the detectors to GWs, consider a case where the wavelength of the GW becomes comparable to the arm length of the detectors [112, 111] [1] Consider the input signal as the GW, the response function as the LIGO equipment and related physics, and the output signal as the recombined laser beam. Normally, it is assumed the GW wavelength is much larger than the effective travel length of the beam. A traveling photon experiences a small portion of the GW's wavelength, or approximately only a

---

[1]The current actual characterization of systematic error in Advance LIGO calibration is not discussed within this work and can be found in [14].

particular phase during the complete trip to the end mirror and back. Yet consider the case when the traveling photon experiences a complete GW cycle over its total trip: the result would be no altered effect in the output signal. A form for the response functions can be formed, where the simple case of light traveling down one arm is first considered, subject to a GW passing through. The response system function for this EM wave along one arm is,

$$
\begin{aligned}
F(f_{GW}, n_x) \quad &= \tfrac{1}{i2f_{GW}}[(1 - e^{-iN(1-n_x)f_{GW}})/(1 - n_x) \\
&\quad - e^{i2Nf_{GW}}(1 - e^{iN(1+n_x)f_{GW}})(1 + n_x)],
\end{aligned}
\tag{2.11}
$$

where $N = (2\pi L)/c$ and the dependence on the GW frame orientation with respect to the detector frame is included within $n_x = \sin\theta\cos\phi$, $n_y = \sin\theta\sin\phi$ and $n_z = \cos\theta$ as noted in Figure 2.2. The unperturbed travel length is L while f_{GW} is the GW frequency. If there is no GW signal, there is no phase shift, and if the GW wavelength approaches the effective length of the arms, the sensitivity to this signal can be negligible.

One can also consider incorporating the effect of the Fabry-Perot cavities that are situated along each LIGO arm, which effectively extend the detector arm lengths via reflecting the laser beam several hundred times before passing it back to the out port. The response function is modified by including the function $C(f)$ as a product $F(f_{GW}, n_x)C(f)$ where,

$$
C(f) = \exp\left(2i\pi f_{GW}T\frac{\sinh(2\pi f_0 T)}{\sinh[2\pi f_0 T(1 + if_{GW}/f_0)]}\right),
\tag{2.12}
$$

and $f_0 = \frac{|\ln(r_1 r_2)|}{4\pi T}$, which includes the dependence on the mirrors' reflectivities r_1 and r_2. The unperturbed travel time is T. The response functions (2.11) are plotted in
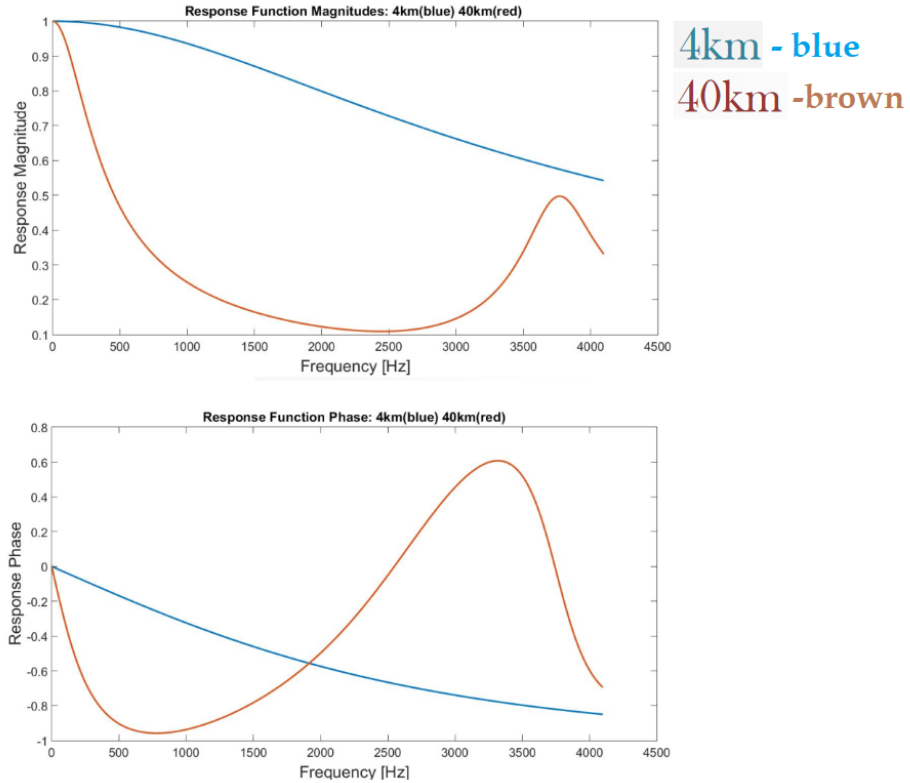
Figure 2.3: The magnitude and phase of the detector response function from (2.11) is shown up to frequencies of a few thousand kHz.

Fig. 2.3 for the case of effective arm lengths of 4km and 40km. Given the response function (2.11), one can see that around 1kHz, around 70% of the signal is lost within the magnitude plot.

As further illustration, simulated supernovae waveforms from different sources are injected [46, 105, 20, 114, 39], which are expected to produce GWs within frequency ranges of a few thousand Hz. Plots of the real part of the frequency are shown in Fig. 2.4. The original waveforms are injected with detector noise from O1 data during GWTC-1 [15] and are plotted against the same waveform projected onto the response function. One can see the amount of waveform that is lost or recovered in this process.

The effect of spacetime symmetry breaking on gravitational waves is considered
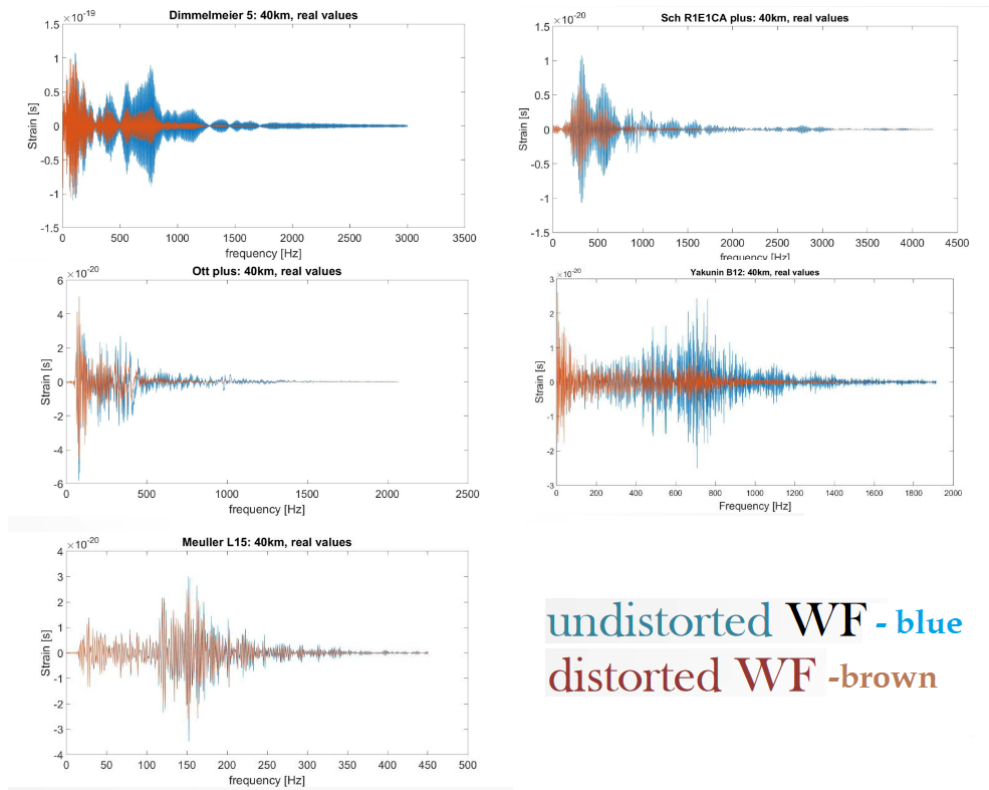
Figure 2.4: The real parts from five different supernovae waveforms injected with O1 detector noise are plotted in blue. The the red shows the distorted waveforms when projecting onto the response function (2.11).

next.

2.3 Spacetime-Symmetry breaking effects on propagating Gravitational Waves

Spacetime-symmetry breaking effects on propagating GWs within the SME framework are considered next. The theoretical framework is first explored before elaborating on the data analysis method and implementation in the following sections.

2.3.1 Illustrative Scalar Field Case

A scalar field example illustrates how to derive the dynamics from the Lagrange within the SME framework [104]. The action for a massless scalar field Φ in flat spacetime, can be described as,

$$I_{sc} = -\tfrac{1}{2} \int d^4x \, \eta^{\mu\nu} (\partial_\mu \Phi)(\partial_\nu \Phi). \tag{2.13}$$

When considering a small variation in the scalar field, i.e., $\Phi \to \Phi + \delta\Phi$, and keeping up to the first order in $\delta\Phi$, the varied action becomes,

$$\delta I_{sc} = - \int d^4x \, \eta^{\mu\nu} (\partial_\mu \delta\Phi)(\partial_\nu \Phi).$$

The Leibniz rule or integration by parts is implemented to arrive at,

$$\delta I_{sc} = - \int d^4x \, [\partial_\mu \left(\delta\Phi(\partial^\mu \Phi) \right) - \delta\Phi \partial_\mu \partial^\mu \Phi]. \tag{2.14}$$

The first term is a total derivative and thus a total 4-divergence. This means it can be considered a surface term that bounds a 3 dimensional hypersurface volume, which can be taken to vanish. The variational principle assumes that the small variation

in the field $\delta\Phi$ vanishes at the boundary surface, and in ensuring the overall action remains unchanged, i.e., $\delta I = 0$, the remaining $\partial_\mu \partial^\mu \Phi$ term also must vanish leaving the dynamical field equations,

$$\Box \Phi = 0, \tag{2.15}$$

where $\Box = \partial_\alpha \partial^\alpha$.

It is expected that within this effective field theory framework, additional terms that allow for Lorentz symmetry breaking can be formed by coupling known matter fields with unknown fixed, background fields: the massless scalar field Φ or the GW field $h_{\mu\nu}$ are coupled to an unknown background coefficient that has an arbitrary number of indices $k^{\mu\nu\lambda\cdots}$ [44, 43]. Two types of Lorentz transformations can be considered. If a particle transformation is performed, the matter fields transform as tensors while the unknown background fields remain fixed [44]. Yet for an observer transformation, both fields transform like tensors, thus showing the physics remains independent of the choice of the coordinate frame [27, 28].

To demonstrate incorporating Lorentz-violating terms, consider a background vector field k_ν that couples to a first derivative of the massless scalar field from above,

$$\Delta I_{sc} = \int d^4 x \, k_\nu (\Phi \partial^\nu \Phi). \tag{2.16}$$

For the first attempt, explicit symmetry breaking is assumed and when applying the Leibniz rule, along with assuming the resulting surface term vanishes, the varied action becomes,

$$\begin{aligned} \Delta I_{sc} &= \tfrac{1}{2} \int d^4 x \, k_\nu \partial^\nu (\Phi^2) \\ &= \tfrac{1}{2} \int d^3 \Sigma_\nu \, k^\nu \, \Phi^2. \end{aligned} \tag{2.17}$$

The $d^3\Sigma_\nu$ is the hypersurface that encloses an "area" element. Yet as before, when implementing a variation in the field $\delta\Phi$ that vanishes on the hypersurface, a resulting expression is found that vanishes overall and thus does not contribute to the equations of motion. Instead of using (2.17), one can apply the variation to (2.16),

$$
\begin{aligned}
\delta\Delta I_{sc} &= \int d^4x \, k_\nu \left[\delta\Phi \, \partial^\nu \Phi + \Phi \, \delta(\partial^\nu \Phi)\right] \\
&= \int d^4x \, k_\nu (\partial^\nu \Phi - \partial^\nu \Phi) \, \delta\Phi,
\end{aligned}
\tag{2.18}
$$

which provides an explicit expression of how the resulting integrand identically is zero.

In order to create an integrand that contributes to the equations of motion, the action is composed as,

$$
I_{sc} = -\tfrac{1}{2} \int d^4x \, \left(\eta^{\mu\nu}(\partial_\mu \Phi)(\partial_\nu \Phi) + (\partial_\mu \Phi)k^{\mu\nu}\partial_\nu \Phi)\right),
\tag{2.19}
$$

where instead of the vector field k_μ, a 2-tensor field $k_{\mu\nu}$ is coupled to the derivatives acting on Φ. Then $k_{\mu\nu}$ are assumed to be small, constant coefficients, i.e., $\partial_\alpha k^{\mu\nu} = 0$, containing ten independent components that dictate the size of the Lorentz violations. When applying the variation principle as before, one arrives at the modified field equations,

$$
\Box\Phi + k^{\mu\nu}\partial_\mu\partial_\nu\Phi = 0.
\tag{2.20}
$$

To relate the previous examples to the case for GWs, the plane wave solutions to (2.20) are considered, and the scalar field is written as,

$$
\Phi = A e^{ip_\mu x^\mu},
\tag{2.21}
$$

where the wave amplitude is A and the phase contains the four-momentum vector $p_\mu = (\omega, \vec{p})$ contracted with the spacetime position vector x^μ. Upon performing a Fourier transformation into momentum space, the equation of motion becomes,

$$p_\mu p^\mu + k_{\mu\nu} p^\mu p^\nu = 0. \tag{2.22}$$

Expanding the four-vectors into their time and spatial components,

$$\omega^2(1 - k_{00}) - 2k_{0j} p^j \omega - k_{ij} p^i p^j - \vec{p}^2 = 0, \tag{2.23}$$

and solving for $\omega(\vec{p})$, a dispersion relation up to the leading order in $k_{\mu\nu}$ is found,

$$\omega \approx |\vec{p}| \left(1 + \tfrac{1}{2}(k_{00} + 2k_{0j}\hat{p}^j + k_{ij}\hat{p}^i\hat{p}^j)\right). \tag{2.24}$$

To see how this will modify the GW propagation speed, the equation is rewritten using $v = \frac{\omega}{\vec{p}}$,

$$v \approx 1 + \tfrac{1}{2}(k_{00} + 2k_{0j}\hat{p}^j + k_{ij}\hat{p}^i\hat{p}^j). \tag{2.25}$$

It is important to note the directional dependence due to the terms containing k_{ij} and k_{0j}, which break the Lorentz symmetry. One could choose a particular isotropic frame where k_{00} is the only nonvanishing component, yet this is a special case.

One could also include higher order terms involving a greater number of indices for the Lorentz-violating background coefficients [76],

$$I_{sc} = -\tfrac{1}{2} \int d^4 x \left(\eta^{\mu\nu}(\partial_\mu \Phi)(\partial_\nu \Phi) + (\partial_\mu \Phi) \sum_d (k^{(d)})^{\mu\nu\lambda\cdots}(\partial_\nu \partial_\lambda \ldots \Phi) \right), \tag{2.26}$$

where the d represents the mass dimension. Terms with higher mass dimension include more spacetime derivatives. In general, the $(k^{(d)})^{\mu\nu\lambda\cdots}$ coefficients will have a mass

dimension of M^{4-d}.

2.3.2 Theoretical Derivation for Modified Gravitational Wave Propagation

A detailed explanation of the derivations outline in Ref. [80] is provided here, as was also done in Ref. [104]

In order to derive a modified form for gravitational waves, one first starts with the simplest action from the gravity sector of the SME. Choosing terms up to second order in $h_{\mu\nu}$ will lead to a set of linearized field equations. For reference, the action for linearized GR is,

$$I_{GR} = -\tfrac{1}{4\kappa} \int d^4x \, h_{\mu\nu} G^{\mu\nu}. \qquad (2.27)$$

The modified action will contain all Lorentz invariant and Lorentz-violating terms, including that for GR,

$$I = \tfrac{1}{8\kappa} \int d^4x \, h_{\mu\nu} \hat{K}^{(d)\mu\nu\rho\sigma} h_{\rho\sigma}, \qquad (2.28)$$

where $\hat{K}^{(d)\mu\nu\rho\sigma}$ are operators consisting if derivatives that act on the metric perturbation field $h_{\mu\nu}$,

$$\hat{K}^{(d)\mu\nu\rho\sigma} = K^{(d)\mu\nu\rho\sigma\epsilon_1...\epsilon_{d-2}} \partial_{\epsilon_1}...\partial_{\epsilon_{d-2}}. \qquad (2.29)$$

These derivatives are contracted with very small, unknown background fields that one can refer to as either coefficients (more common within the SME framework context) or parameters (more common within the LVK data analysis context). Each coefficient has a mass dimension d of M^{d-4}, and one can expect that for higher order fields, their symmetry-breaking effects are smaller. The coefficients are constrained experimentally as shown later in this work.

As done with the previous scalar field example, the action is varied with respect

to the metric fluctuations $\delta h_{\mu\nu}$,

$$\delta I \;=\; \tfrac{1}{8\kappa} \int d^4 x \, [\delta h_{\mu\nu} \, K^{(d)\mu\nu\rho\sigma\epsilon_1...\epsilon_{d-2}} \partial_{\epsilon_1} ... \partial_{\epsilon_{d-2}} \, h_{\rho\sigma}$$
$$+ \, h_{\mu\nu} \, K^{(d)\mu\nu\rho\sigma\epsilon_1...\epsilon_{d-2}} \partial_{\epsilon_1} ... \partial_{\epsilon_{d-2}} \, \delta h_{\rho\sigma}]. \tag{2.30}$$

Then in order to factor out the fluctuations, one needs to perform integration by parts for each derivative acting on $h_{\mu\nu}$. As before, any surface terms are assumed to vanish and the tensor density is unity. If the integration by parts is performed an even number of times (when d is even), the remaining term will have an overall positive sign, and when performed an odd number of times (when d is odd), the remaining term is overall negative. This is represented via $(-1)^d$. The varied action becomes,

$$\delta I = \tfrac{1}{8\kappa} \int d^4 x \delta h_{\alpha\beta} \left[K^{(d)(\alpha\beta)(\mu\nu)\epsilon_1...\epsilon_{d-2}} + (-1)^d K^{(d)(\mu\nu)(\alpha\beta)\epsilon_1...\epsilon_{d-2}} \right] \partial_{\epsilon_1} ... \partial_{\epsilon_{d-2}} h_{\mu\nu},$$
$$\tag{2.31}$$

where one can take advantage of the symmetry in $h_{\mu\nu}$ and indicate other symmetries imposed with parenthesis as in $\hat{K}^{(d)(\mu\nu)(\alpha\beta)}$.

Two considerations are imposed when deriving the field equations. The first is to ensure that all terms included will contribute to the field equations, i.e.,

$$K^{(d)(\alpha\beta)(\mu\nu)\epsilon_1...\epsilon_{d-2}} + (-1)^d \, K^{(d)(\mu\nu)(\alpha\beta)\epsilon_1...\epsilon_{d-2}} \neq 0. \tag{2.32}$$

Secondly, it is ensured that the GR gauge symmetry is upheld under the linear transformation $h_{\mu\nu} \to h_{\mu\nu} - \partial_\mu \xi_\nu - \partial_\nu \xi_\mu$, where ξ^μ is an arbitrary vector.[2] Implementing

---

[2]For general gauge-breaking terms, refer to Ref. [78].

this linear gauge transformation with (2.31), the Lagrange density becomes,

$$
\begin{aligned}
\delta_\xi I &= \tfrac{1}{8\kappa} \int d^4x \, \partial_\alpha \xi_\beta \left[(-1)^d \hat{K}^{(d)(\mu\nu)(\alpha\beta)} + \hat{K}^{(d)(\alpha\beta)(\mu\nu)} \right] h_{\mu\nu}, \\
&= -\tfrac{1}{8\kappa} \int d^4x \, \xi_\nu \left[(-1)^d \hat{K}^{(d)(\rho\sigma)(\mu\nu)} + \hat{K}^{(d)(\mu\nu)(\rho\sigma)} \right] \partial_\mu h_{\rho\sigma}.
\end{aligned}
\tag{2.33}
$$

Since the derivatives of $h\mu\nu$ are not necessarily zero and the gauge field ξ_μ is arbitrary, a resulting relation is,

$$
\left[(-1)^d \hat{K}^{(d)(\rho\sigma)(\mu\nu)} + \hat{K}^{(d)(\rho\sigma)(\mu\nu)} \right] \partial_\mu = 0.
\tag{2.34}
$$

From the two conditions (2.32) and (2.34), it is found that the coefficients can be organized into three categories depending on their properties. One aspect of the coefficients refers to their discrete spacetime symmetry property, determined via their behavior under CPT transformations as either even or odd. Another property refers to the values of mass dimension the coefficient are allowed (refer to the table in Ref. [80] for details). The three categories for the operator coefficients are rewritten as $\hat{s}$, $\hat{q}$, and $\hat{k}$,

$$
\begin{aligned}
\hat{s}^{\mu\rho\nu\sigma} &= s^{(d)\mu\rho\epsilon_1\nu\sigma\epsilon_2\ldots\epsilon_{d-2}} \partial_{\epsilon_1} \ldots \partial_{\epsilon_{d-2}}, \\
\hat{q}^{\mu\rho\nu\sigma} &= q^{(d)\mu\rho\epsilon_1\nu\epsilon_2\sigma\epsilon_3\ldots\epsilon_{d-2}} \partial_{\epsilon_1} \ldots \partial_{\epsilon_{d-2}} \\
\hat{k}^{\mu\nu\rho\sigma} &= k^{(d)\mu\epsilon_1\nu\epsilon_2\rho\epsilon_3\sigma\epsilon_4\ldots\epsilon_{d-2}} \partial_{\epsilon_1} \ldots \partial_{\epsilon_{d-2}},
\end{aligned}
\tag{2.35}
$$

where the $\hat{s}$ operators are CPT even and can take on mass dimensions $d \geq 4$, the $\hat{q}$ operators are CPT odd with possible mass dimensions of $d \geq 5$, and the $\hat{k}$ are CPT even with possible mass dimensions of $d \geq 6$. The term for GR is contained within the mass dimension 4 terms.

The Lagrange density then can be written in terms of the coefficients (2.35),

$$
\begin{aligned}
\mathcal{L} &= \tfrac{1}{8\kappa}\epsilon^{\mu\rho\alpha\kappa}\epsilon^{\nu\sigma\beta\lambda}\eta_{\kappa\lambda}h_{\mu\nu}\partial_\alpha\partial_\beta h_{\rho\sigma} \\
&\quad + \tfrac{1}{8\kappa}h_{\mu\nu}(\hat{s}^{\mu\rho\nu\sigma} + \hat{q}^{\mu\rho\nu\sigma} + \hat{k}^{\mu\rho\nu\sigma})h_{\rho\sigma},
\end{aligned}
\tag{2.36}
$$

where GR is the first term and the second term contains the additional Lorentz invariant and Lorentz-breaking terms where $\epsilon^{\mu\rho\alpha\kappa}$ is the totally antisymmetric Levi-Civita tensor. The Lagrange density (2.36) is the most general form one can produce that is second order in the metric fluctuations that ensures the linearized gauge symmetry and allows for Lorentz invariant and violating terms. The terms can arise as spontaneous symmetry breaking in alternative gravity models, as with Nambu-Goldstone modes and massive modes where additional fluctuations around the vacuum values are "integrated out" or "de-coupled" [24, 17, 117, 115]. The terms can also arise as explicit symmetry breaking as seen in other models. Both means of symmetry breaking will leave us with an "effective" Lagrange density where the metric fluctuations around a vacuum, flat spacetime, will not appear.

The final expression for the field equations are,

$$
0 = G^{\mu\nu} - \left[\tfrac{1}{4}(\hat{s}^{\mu\rho\nu\sigma} + \hat{s}^{\mu\sigma\nu\rho}) + \tfrac{1}{2}\hat{k}^{\mu\nu\rho\sigma} + \tfrac{1}{8}(\hat{q}^{\mu\rho\nu\sigma} + \hat{q}^{\nu\rho\mu\sigma} + \hat{q}^{\mu\sigma\nu\rho} + \hat{q}^{\nu\sigma\mu\rho})\right]h_{\rho\sigma}.
\tag{2.37}
$$

This will reduce to $G^{\mu\nu} = 0$ when there is no Lorentz violation, and further reduce, using the Lorentz gauge, to $\Box\bar{h}^{\mu\nu} = 0$, where $\bar{h}^{\mu\nu} = h^{\mu\nu} - (1/2)\eta^{\mu\nu}h^\alpha{}_\alpha$ and $\partial_\mu\bar{h}^{\mu\nu} = 0$.

Implementing plane wave solutions for propagating GWs into (2.37), i.e., $\bar{h}_{\mu\nu} = A_{\mu\nu}e^{-ip_\alpha x^\alpha}$, yields $p^2 = p^\alpha p_\alpha = 0$. Transforming this into energy-momentum space gives the dispersion relation for GR:

$$
\omega = |\vec{p}|.
\tag{2.38}
$$

Within the TT-gauge, and using the gauge freedom for this limit, the number of independent degrees of freedom can be reduced to 2, where $h_{\mu\nu}$ has the form of (2.9).

Finding the dispersion relation in the case where there is Lorentz violation, the plane wave solution for GWs is implemented into (2.37). To fully solve this, one can choose a gauge condition, given the usual gauge freedom exists, then decompose the terms into their time and spatial components. As an example, consider the temporal gauge as a choice, i.e., $h_{0\mu} = 0$, and project the spatial results onto the helicity basis. Within the first order in the coefficients that allow for Lorentz violation, one still find 2 independent degrees of freedom [89]. As another example, one may use differential forms as a gauge-independent method to derive the dispersion relation [76].

For the Lorentz violating case above, the two independent degrees of freedom differ than in the case for GR in that the two modes can travel at different speeds and their frequencies are highly dispersive. The difference between the two modes is referred to as birefringence within a vacuum. This is different than the scalar field example in (2.24), where there are no birefringence effects yet there can still be dispersion effects where, for example, both modes will experience the same change in speed when compared to another type of physics like light. There is also two additional propagating modes that are $+2$ and -2 helicity projections for the spatial components of h_{ij} when choosing a particular helicity basis. The modified dispersion relation form is then,

$$\omega = |\vec{p}| \left(1 - \zeta^0 \pm |\vec{\zeta}| \right),$$
(2.39)

where

$$|\vec{\zeta}| = \sqrt{(\zeta^1)^2 + (\zeta^2)^2 + (\zeta^3)^2}$$
(2.40)

and

$$
\begin{aligned}
\zeta^0 &= \tfrac{1}{4|\vec{p}|^2} \left(-\hat{s}^{\mu\nu}{}_{\mu\nu} + \tfrac{1}{2}\hat{k}^{\mu\nu}{}_{\mu\nu} \right), \\
(\zeta^1)^2 + (\zeta^2)^2 &= \tfrac{1}{8|\vec{p}|^4} \left(\hat{k}^{\mu\nu\rho\sigma}\hat{k}_{\mu\nu\rho\sigma} - \hat{k}^{\mu\rho}{}_{\nu\rho}\hat{k}_{\mu\sigma}{}^{\nu\sigma} + \tfrac{1}{8}\hat{k}^{\mu\nu}{}_{\mu\nu}\hat{k}^{\rho\sigma}{}_{\rho\sigma} \right), \\
(\zeta^3)^2 &= \tfrac{1}{16|\vec{p}|^4} \left(-\tfrac{1}{2}\hat{q}^{\mu\rho\nu\sigma}\hat{q}_{\mu\rho\nu\sigma} - \hat{q}^{\mu\nu\rho\sigma}\hat{q}_{\mu\nu\rho\sigma} + (\hat{q}^{\mu\rho\nu}{}_{\rho} + \hat{q}^{\nu\rho\mu}{}_{\rho})\hat{q}_{\mu\sigma\nu}{}^{\sigma} \right)
\end{aligned} \tag{2.41}
$$

The derivative operators are also replaced in (2.35) by $\partial_\mu \to ip_\mu$. The plus and minus sign in (2.39) indicate the birefringence effects, where there is a slow and fast mode for the GWs. Also important to note is the affected speed and degree of frequency dispersion depends upon the incoming sky location for the GW, thus allowing for anisotropic effects that one can map out across the celestial sky.

LIGO-Virgo event data uses localization angles for the incoming GW related to the right ascension and declination for the sky position. Thus it is particularly useful when analysing LIGO-Virgo event data to project the coefficients onto a basis containing spin-weighted spherical harmonics,

$$
\zeta^0 = \sum_{djm} \omega^{d-4} Y_{jm}(\hat{\mathbf{n}}) \, k^{(d)}_{(I)jm}, \tag{2.42}
$$

$$
\zeta^1 \mp i\,\zeta^2 = \sum_{djm} \omega^{d-4} {}_{\pm 4}Y_{jm}(\hat{\mathbf{n}}) \left(k^{(d)}_{(E)jm} \pm i k^{(d)}_{(B)jm} \right), \tag{2.43}
$$

$$
\zeta^3 = \sum_{djm} \omega^{d-4} Y_{jm}(\hat{\mathbf{n}}) \, k^{(d)}_{(V)jm}. \tag{2.44}
$$

The spin-weighted spherical harmonics are the usual ${}_{\pm 4}Y_{jm}(\hat{\mathbf{n}})$ (where a spin weight of 0 gives the usual spherical harmonics) and $\hat{n} = -\hat{p}$ is related to what is shown in Fig. 2.2. The $k^{(d)}_{(I)jm}$, $k^{(d)}_{(E)jm}$, $k^{(d)}_{(B)jm}$, and $k^{(d)}_{(V)jm}$ are the symmetry-breaking coefficients in spherical harmonic form that are related to the $\hat{s}$, $\hat{q}$ and $\hat{k}$ coefficients from (2.41), where $j = 0, 1, ..., d-2$ and $-j \leq m \leq j$. The subscripts I, E, B and V refer to

whether the coefficients are CPT odd or even and what mass dimensions they can take as noted in Refs. 2.36.

One can rewrite (2.39) explicitly showing the speed of the GWs,

$$v = 1 - \zeta^0 \pm |\vec{\zeta}|, \tag{2.45}$$

where in the GR case, the two polarizations will together, travel the speed of light, i.e., $v = \omega/|\vec{p}| = 1$ and the ζ terms in (2.45) vanish. Yet in the Lorentz-violating case, the GW polarizations can travel at different speeds with respect to each other. This is due to the dynamical interaction between the GWs and some Lorentz-violating background field, where the degree of effect depends upon relative orientations. Given the large distance between the GW source and the ground-based detectors (between around 40 Mpc to over 8 Gpc), a difference in arrival times can be detectable even with a small Lorentz violation, which is a feature that has been tested with photons [69, 71, 70, 68, 75, 65, 49]. The larger the travel distance for the GW, the more Lorentz-violating effects can build, and the greater the potential in their detection at the interferometers.

In terms of the LVC event data, one can equivalently search for small deviations in the phase of the GW polarizations. Even if no confident deviation from GR detections are made, one can still place tighter constraints on the Lorentz-violating coefficients. In light of this, the dispersion relation in (2.39) can be further developed, first returning to a plane wave solution,

$$h \sim e^{-i(\omega t - kl)}, \tag{2.46}$$

where l is the distance travelled and k is the wave number, $k \sim |\vec{p}| = \omega/v$. The Lorentz-violating effects will create an additional phase shift, $\delta\psi_{\pm}$. Also included are

the effects on the propagation distance from the expanding universe in terms of the cosmological redshift. The expression for this additional phase shift is then,

$$\delta\psi_\pm = \omega_{obs} \int_0^z dz' \frac{(-\zeta^0 \pm |\vec{\zeta}|)}{H(z')}, \tag{2.47}$$

where z is the redshift, $H(z)$ is the Hubble parameter, and the observed frequency is is related to that emitted via $\omega_{obs}(1+z) = \omega_{emit}$. The phase shift can be rewritten as two terms,

$$\delta\psi_\pm = -\delta \pm \beta, \tag{2.48}$$

where

$$\delta = \omega^{d-3}\tau\zeta^{(d)0},$$

$$\beta = \omega^{d-3}\tau|\vec{\zeta}^{(d)}|,$$

$$\tau = \int_0^z dz \frac{(1+z)^{d-4}}{H(z)} \tag{2.49}$$

and $\zeta^0 = \omega^{d-4}\zeta^{(d)0}$, $|\vec{\zeta}| = \omega^{d-4}|\vec{\zeta}^{(d)}|$, and τ is the effective propagation time due to the redshift.

The coefficients can also be rewritten in terms of effective angles, ϑ and φ defined as,

$$\sin\vartheta = \frac{|\zeta^1 \mp i\zeta^2|}{|\vec{\zeta}|}, \quad \cos\vartheta = \frac{\zeta^3}{|\vec{\zeta}|}, \quad e^{\mp i\varphi} = \frac{\zeta^1 \mp i\zeta^2}{\sqrt{(\zeta^1)^2 + (\zeta^2)^2}}. \tag{2.50}$$

Such definitions are for efficiency, yet note that these angles are not the sky localization angles θ and ϕ (there are cases where these different angles can appear to be the same as will be seen later on). The plus and cross expressions can then be rewritten,

incorporating the new phase shift as modified forms, coupled to the GR expressions,

$$
\begin{aligned}
h_{(+)} &= e^{i\delta}(\cos\beta - i\sin\vartheta\cos\varphi\sin\beta)\, h_{(+)}^{LI} \\
&\quad -e^{i\delta}\sin\beta(\cos\vartheta + i\sin\vartheta\sin\varphi)\, h_{(\times)}^{LI} \\
h_{(\times)} &= e^{i\delta}(\cos\beta + i\sin\vartheta\cos\varphi\sin\beta)\, h_{(\times)}^{LI} \\
&\quad +e^{i\delta}\sin\beta(\cos\vartheta - i\sin\vartheta\sin\varphi)\, h_{(+)}^{LI}.
\end{aligned}
\tag{2.51}
$$

where $h_{(+,\times)}^{LI}$ are the Lorentz-invariant gravitational wave for standard GR. Setting $\beta \to 0$ and $\delta \to 0$, one retrieves GR as a limiting case.

An important note refers to the choices in the frame of reference. The Sun-centered Celestial-Equatorial coordinate system (SCF frame) is a standard within literature for component values of the Lorentz-violating coefficients as with the $k_{(I)jm}^{(d)}$, $k_{(E)jm}^{(d)}$, $k_{(B)jm}^{(d)}$, and $k_{(V)jm}^{(d)}$ [81]. Note that one can perform a coordinate transformation on the coefficients as they transform as tensors and it can be treated as global Lorentz transformations in many cases. For the analysis of GWs, the constraints on the coefficients in the SCF frame are reported.

2.3.3   A Note on Units and Dimensions

This section will elaborate on the conversion from natural units to SI units when implementing the previous theory into the analysis code. So far, natural units where $\hbar = c = 1$ are used [3]. In this choice, physical quantities can be described in terms of energy, usually in terms of electron volts (eV). As an example, one refers to a coefficient as having a mass dimension M^{4-d}. When wishing to convert to SI units, one must note the choice of unit for the starting action, which one assumes to be

---

[3]Note there are other unit choices for natural units, e.g., $G_N = c = 1$.

joules meters Jm ^{4} Then for the Einstein Hilbert action written in SI units,

$$I_{EH} = \tfrac{c^4}{16\pi G} \int d^4x \sqrt{-g} R, \tag{2.52}$$

while for the action (2.27), a factor of c^4 is included. Specifically, the $\frac{c^4}{G}$ has units of $\frac{kgm}{s^2}$, the d^4x has units m^4, and the two derivatives within the Einstein tensor provide units of m^{-2}. The metric tensor $g_{\mu\nu}$ is dimensionless. For the Lorentz-violating action in (2.28), each additional derivative operator provides another unit, in SI units, of m^{-2}, with a coefficient's total unit being m^{d-4}.

When converting equations like (2.37) from configuration space to energy-momentum space, each partial derivative will transform as $\partial_\alpha \to \frac{i}{\hbar} p_\alpha$, providing an inverse Planck factor along with a pure imaginary quantity. Thus the form in configuration space,

$$\partial\partial h + s^{(4)} \partial\partial h + q^{(5)} \partial\partial\partial h + ... = 0, \tag{2.53}$$

would transform into energy-momentum space as,

$$(\tfrac{i}{\hbar})^2 pp h + (\tfrac{i}{\hbar})^2 s^{(4)} pp h + (\tfrac{i}{\hbar})^3 q^{(5)} ppp h + ... = 0, \tag{2.54}$$

where $(\frac{i}{\hbar})^{(d-2)} p_{\alpha_1}...p_{\alpha_{d-2}}$ are now in place of the partials in (2.53).

For the four-momenta, the time component will have factors in SI units, i.e., $p_\alpha = (-\frac{\hbar}{c}\omega, \vec{p})$. Then the speed equation (2.45) will appear as

$$v_\pm = \hbar\omega/|\vec{p}| = c\left(1 + c^2(-\zeta^0 \pm |\vec{\zeta}|)\right), \tag{2.55}$$

where there is an additional factor or $(\frac{\hbar}{c})^2$ for each ζ. Then for equations (2.44), given

---

[4] One can also make the choice of the starting action to have units of joules seconds Js as is done in classical mechanics.

each Lorentz-violating coefficient has SI units of m^{d-4}, an additional factor of c^{2-d} is added as in

$$\zeta^0 = c^{(2-d)} \sum_{djm} \omega^{d-4} \, Y_{jm}(\hat{\mathbf{n}}) \, k_{(I)jm}^{(d)}. \tag{2.56}$$

2.3.4 Data Analysis Method and Implementation

Previous works have placed constraints on $\hat{s}$ operators via comparing propagation speeds between the GW signal and electromagnetic signal from the GW170817/GRB170817A observations [80, 118, 126, 1], along with comparative travel speeds across the Earth [86]. Such analysis can constrain the terms within the minimum SME with mass dimension 4, by comparing two different types of physics signals as for cases of multi-messenger astronomy. When using only GW signals to search for symmetry-breaking effects, a minimum mass dimension of 5 is required for birefringence effects between the two polarizations, as expressed within (2.39) with the term containing a plus and minus value. Thus this work focuses on constraining terms with mass dimension 5 that allow for CPT and Lorentz violations. Both isotropic and anisotropic cases are explored for dispersion and birefringence effects, providing a joint estimation of all parameters including source parameters and those for symmetry-breaking. There have been other works within the LVK that have performed such joint estimation for a variety of alternative physics models with respective additional parameters [9]. This work focuses on symmetry-breaking effects on GW propagation, directly analysing the GW strain from the LIGO-Virgo detectors that does not rely on posteriors produced under a GR model. The analysis software is modified to fully consider the source parameters along with additional SME parameters that include possible dispersion and birefringence effects. The LIGO Scientific Collaboration Algorithm Library Suite (`LALSuite`) is used, an algorithm package that contains many available features including waveform generation, injections of dispersed waveforms, inference processes

and so on [121]. Two of the subpackages, `LALSimulation` and `LALInference`, are modified as detailed below. Further details on the implementation can be found within 5.

Implementation into software simulation package

The modified waveforms derived from the SME framework in (2.51) are implemented directly into the `LALSuite` subpackage `LALSimulation`. The simplest additional term that allows for CPT and Lorentz symmetry breaking are those of mass dimension 5. These are the $k_{jm}^{(d)*} = (-1)^m k_{j(-m)}^{(d)}$ coefficients, for $j = 0, 1, 2, 3$, $-j \le m \le j$, and are contained within the β term in (2.51). This coefficient contains sixteen independent coefficients deduced a priori, all additional parameters to be constrained from GW event data. Thus the first few terms within the expression for β of mass dimension 5 in SI units will appear as

$$\beta^{(5)} = \frac{\omega^2 \tau^{(5)}}{2\sqrt{\pi}c} \left| k_{(V)00}^{(5)} - \sqrt{\frac{3}{2}} \sin\theta \left(e^{i\phi}\, k_{(V)11}^{(5)} + e^{-i\phi}\, k_{(V)11}^{(5)*} \right) + \sqrt{3}\cos\theta\, k_{(V)10}^{(5)} + ... \right|. \quad (2.57)$$

where the θ and ϕ angles are sky localization angles that are expressed in the SCF frame. Note this expression allows for anisotropic symmetry-breaking effects, as can also be noted by the dependence on the direction $\hat{n}$ for the spherical harmonics in (2.44).

The observable output signal as expressed in (2.10) will have these modified waveforms implemented along with the included standard detector response functions that depend on the angles relating the different frames, namely the merger frame at the source and the detector frames defined within `LALSuite`.

The effective propagation time τ in (2.57) accounts for the redshift, yet due to additional symmetry-breaking terms, it also depends on the mass dimension as noted

in (2.49). This quantity is evaluated via numerical integration for every SME parameter value being tested. Thus for a feasible computation time, the effective coefficient is probed instead $(k^{(5)}_{(V)jm})_{eff} = \tau \, k^{(5)}_{(V)jm}$. Once convergence of the inference process produces the posterior of this parameter, the recovery of the $k^{(5)}_{(V)jm}$ coefficient is done as discussed later.

Lastly, transformations of the SME coefficients under observer boosts are possible to compute, as possibly important if one wishes to include the Earth's motion, the interferometers, or the motion of the center of mass for the source system relative to the SCF. For this work, the strain measurements are not sensitive enough to consider this effect with boosts for values of $v/c = 10^{-4}$.

Sensitivity Studies for `LALSimulation`

Sensitivity studies are performed to test the implementation within the `LALSimulation`. As an illustrative example, consider a special case where the only nonzero parameter is the time component $k^{(5)}_{(V)00}$ that corresponds to an isotropic, polarization-dependent dispersion. Comparisons of the waveform generated from GR with those for different values of $k^{(5)}_{(V)00}$ are shown in Fig. 2.5 This system is assumed to be a non-spinning binary system at a luminosity distance of 4 Gpc, with equal masses of $m_1 = m_2 = 50 M_\odot$. There are visible differences within the amplitude and frequency of the waveform signal for values as small as 10^{-13}m in the SME coefficient. Values are chosen which can be used to compare to template models presented within [89]. The alterations within the waveform tend to occur at the peak amplitude times for the later work, yet modifications to the waveform appear earlier for the simulation.
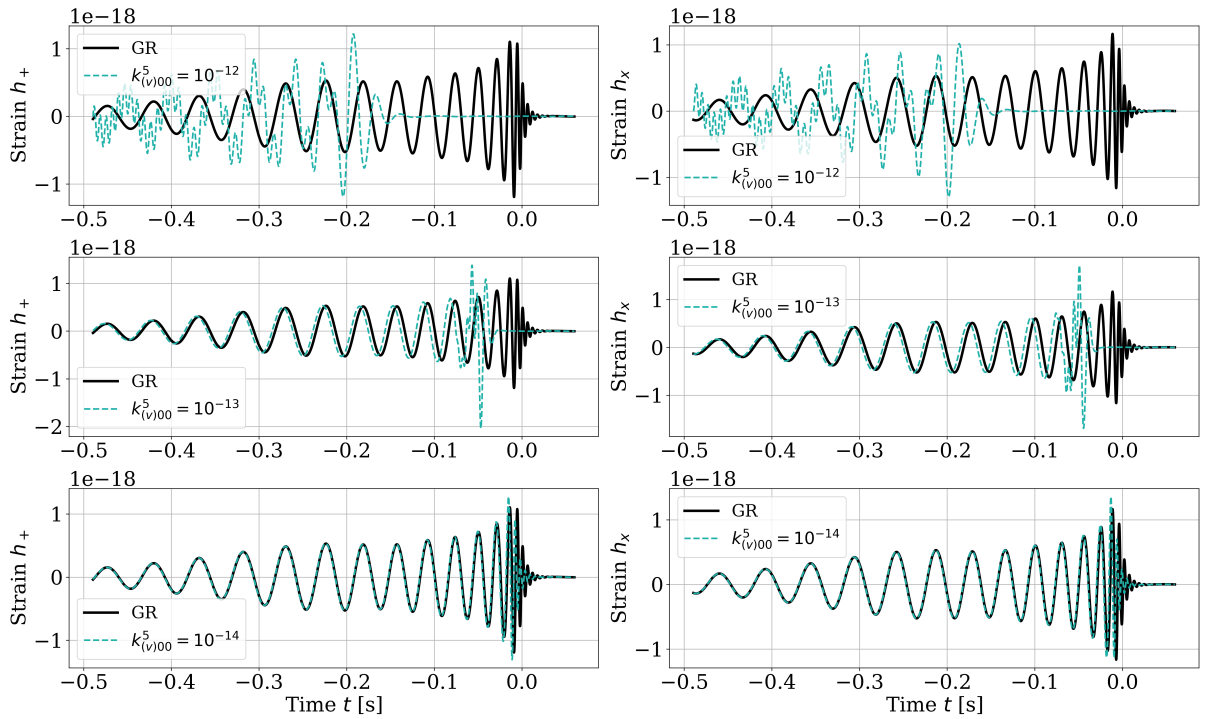
Figure 2.5: Shown are simulated waveform examples above with varying $k^{(5)}_{(V)00}$ values, for the coalescence of a non-spinning binary system of black holes with $m_1 = m_2 = 50 M_\odot$ located at a luminosity distance of 4 Gpc. The solid black lines denotes GR in the case where $k^{(5)}_{(V)00} = 0$ and the dotted lines denoted the waveforms for Lorentz violation where $k^{(5)}_{(V)00}$ has the value specified above the plot.

Bayesian Inference Analysis

The second subpackage of `LALSuite` modified is the parameter estimation package `LALInference`. A Bayesian inference is performed on the posterior probabilities that include the GW source parameters along with the systematic uncertainties from the detector resolutions. The initial vector set of GR prior parameters within the vector array $\vec{\theta}_{GR}$ include the intrinsic parameters associated with the source system, e.g., the masses of the black holes and their spins, along with the extrinsic parameters, e.g., the sky location, the distance from source to detector, and the incoming GW frame's inclination. Additional SME coefficients mentioned in the previous section for the case of mass dimension 5 within the vector array $\vec{\theta}_{SME}$ are added.

A Bayesian inference framework is used in order to compare GW strain from events to a template bank of modified gravitational waveforms that include effects from the SME. A simultaneous inference is done across all parameters, allowing the inclusion correlation between GR parameters and those for the SME, producing a joint posterior probability,

$$P(\vec{\theta}_{GR}, \vec{\theta}_{SME}|d, I) = \frac{P(d|\vec{\theta}_{GR}, \vec{\theta}_{SME}, I)\, P(\vec{\theta}_{GR}, \vec{\theta}_{SME}|I)}{P(d|I)}, \tag{2.58}$$

where $P(\vec{\theta}_{GR}, \vec{\theta}_{SME}|d, I)$ is the posterior probability, $P(d|\vec{\theta}_{GR}, \vec{\theta}_{SME}, I)$ the likelihood, $P(\vec{\theta}_{GR}, \vec{\theta}_{SME}|I)$ the prior probability and $P(d|I)$ the evidence where I contains any pertinent background information to be included. The likelihood function within the frequency domain is,

$$P(d|\vec{\theta}_{GR}, \vec{\theta}_{SME}, I) = \exp\left(\sum_i -\frac{2|\tilde{h}_i(\vec{\theta}_{GR}, \vec{\theta}_{SME}) - \tilde{d}_i|^2}{TS_n(f_i)} - \frac{1}{2}\log\left(\frac{\pi TS_n(f_i)}{2}\right)\right) \tag{2.59}$$

where the template signal is $\tilde{h}_i$, $\tilde{d}_i$ is the interferometer datastream, T is the duration

of the signal and S_n is the PSD of the detector noise. In initial work involving sensitivity studies, a flat prior probability is chosen for the effective SME parameter $(k_{(V)jm}^{(5)})_{eff}$, which is bounded by $|(k_{(V)jm}^{(5)})_{eff}| \in [0; 10^{-10}]$. Resulting max values on the order of 10^{-15} were larger than the constraints found within the work of [118].

The inference process is calculated using a Markov Chain (MC) method in order to effectively handle a large number of parameters that describe the emitted GW from coalescing binary systems. A chain involves semi-random walks inside the n-dimensional parameter space (n being the number of parameters involved), where the steps being recorded are proportional to the posterior probability. There are variations of the MC method, as in the Markov-chain Monte-Carlo (MCMC), that uses paralleled tempering and nesting sampling, which is implemented within the LALSuite algorithm library. The calculated output are joint posterior probabilities of the designated parameters. At this stage, marginalised posterior probabilities can be extracted from a subset of parameters via integrating over the distribution of other variables. One then sums over the volume of the posterior probabilities associated with the intended fraction of confidence to produce credible intervals for the parameters. The structure and methods of the Bayesian inference and the MC algorithms, including any PSD and calibration envelopes that are already developed by the LVK collaboration for parameter estimation are used. One can find these within the `PESummary` package [60], including a list of waveforms models with associated options such as `IMRPhenomPv2` [57].

Sensitivity Studies for `LALInference`

As with the `LALSimulation` package, sensitivities studies are done for the modified `LALInference`. A simulated GW signal with detector noise is created that contains the CPT and Lorentz violations, then a Bayesian inference is performed in order
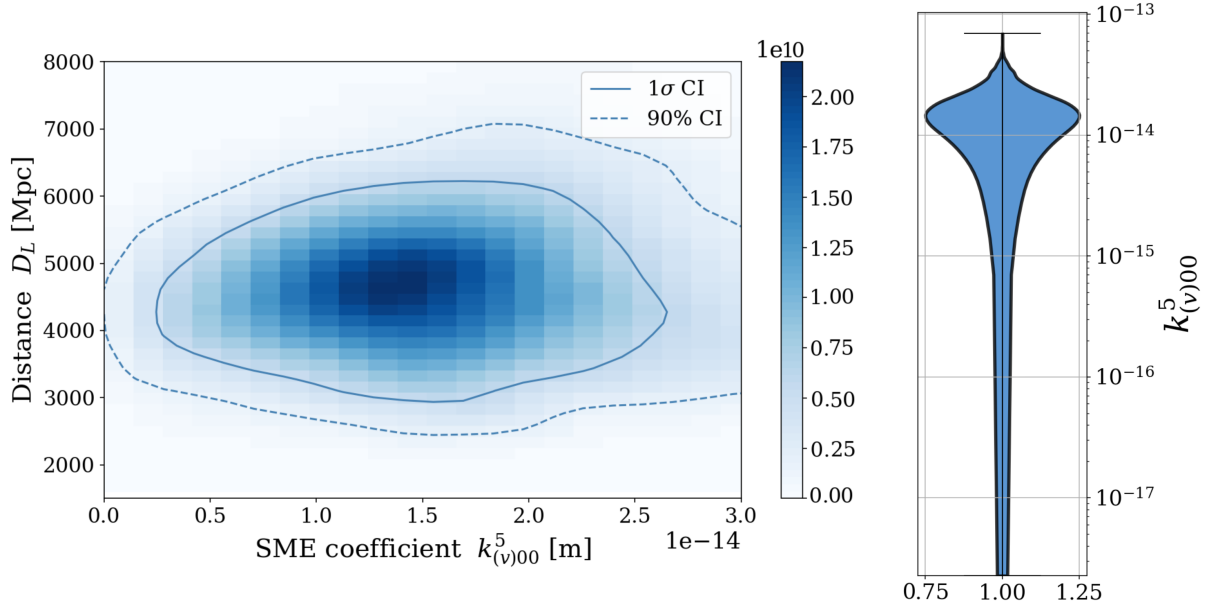
Figure 2.6: Both figures show the posterior probability density on the $k^{(5)}_{(V)00}$ coefficient for a simulated coalescence of a non-spinning binary system of black holes with $m_1 = m_2 = 50 M_\odot$ located at a luminosity distance of 5 Gpc. The left figure shows the 1σ and 90% credible intervals in the $D_L - k^{(d)}_{(V)00}$ plane, while the violin plot on the right shows the posterior probability of $k^{(5)}_{(V)00}$ marginalising the source and systematical uncertainty parameters.

to understand the potential to measure the SME coefficients given an LVK event detection. An example of this was done for a system of non-spinning, coalescing binary black holes with masses of $50 M_\odot$ located at 5 Gpc, and where the symmetry-breaking dispersion effect is incorporated with one SME coefficient set to a value of $k^{(d)}_{(V)00} = 10^{-14}$. The Figure 2.6 shows the resulting posterior probability relation between the luminosity distance and the SME coefficient. The expected values are recovered and an expected degeneracy is observed between the SME coefficient and the luminosity distance: the luminosity distance is degenerate with the SME coefficient considering the farther the distance from the source to the detector, the more the symmetry-breaking effects can compound and the more energy is lost. The constraint for $k^{(d)}_{(V)00}$

shows a 1σ credible interval around the expected value of zero, indicating that the SME coefficient can be measured with a single event given its value is relatively large. The violin plot in the right of the figure shows the $k^{(d)}_{(V)00}$ marginalized posterior probability from the source and systemic uncertainties. The symmetric distribution stems from the absolute form of the SME coefficients as can be seen in (**??**).

The results can be compared to values found for the mass of the graviton, which include a modified dispersion relation in the GW signal. The constraints provide an improved of an order of magnitude. The event GW159014 initially provided a mass constraint of $m_g \leq 1.2{\cdot}10^{-22}$ eV/c^2, where now $m_g \leq 1.76{\cdot}10^{-23}$ eV/c^2 using 33 events from the second GW catalog [4, 9]. The choice of waveform modelling approximate has also been investigated in determining the robustness of the measurement constraints [5], where systematic uncertainties may not lead to a large bias or a re-estimation of the constraints given the current detector sensitivity.

Using the GWTC-3 Catalogue Events to Measure Spacetime Symmetry-Breaking Parameters

For this analysis, 45 events are used from over 90 from the first three observing runs contained within the cumulative catalogue GWTC-3 [7]. There are 10 events from GWTC-1, 23 events from GWTC-2, and 12 events from GWTC-3, all with a signal-to-noise ratio (SNR) between $[9.2; 26.8]$ and luminosity distances between $[0.32; 4.42]$ Gpc. All events are coalescing binary black holes and/or neutron stars that have over a 50% probability of an astrophysical origin.

It was noted that when assuming GR waveforms that best fit the data and accounting for any expected noise, any possible deviations from GR would have to allude to the higher order terms within the model that allow for small modifications in the signal morphology [8]. Hence to avoid possible false deviations from GR that

may be due to transient noise or a model that requires higher order terms, any low-sensitivity events are not included within the analysis [85, 93]. In particular, to ensure only high-confidence signals are used, only events that have a false alarm rate (FAR) lower than 10^{-3} year^{-1} and that have been designated by the LVK to be tested for dispersion effects are chosen.

As noted earlier, an effective coefficient $|k^{(5)}_{(V)00}|$ is sampled over to allow for feasible computation time, assuming a flat prior. This constitutes as an isotropic limit for (2.57). The 45 posterior probability densities from the chosen events are then combined to obtain a measurement for the 16 independent, anisotropic coefficients for $|k^{(5)}_{(V)\mu\nu}|$, which includes the dependence on the sky localization angles. This is done by first writing the sampled effective parameter as a linear combination,

$$\vec{K} = \boldsymbol{Y} \cdot \vec{k^{(5)}_{(V)ij}}, \tag{2.60}$$

where $\vec{K}$ represents the vector of the 45 posteriors, $\boldsymbol{Y}$ is the matrix comprised of spherical harmonics, and $\vec{k^{(5)}_{(V)ij}}$ contains the 16 independent coefficients. The Singular Value Decomposition (SVD) method is implemented in order to invert (2.60),

$$\vec{k} = \boldsymbol{V}\boldsymbol{\Sigma}^{\dagger}\boldsymbol{U^T}\vec{K},, \tag{2.61}$$

which allows one to retrieve values for our anisotropic coefficients. The $\boldsymbol{V}$, $\boldsymbol{\Sigma}^{\dagger}$ and $\boldsymbol{U^T}$ matrices are the SVD factorisation of $\boldsymbol{Y}$.

For the isotropic coefficient, the posterior probability densities are shown in Fig. 2.7 for all 45 events. Most of the events are compatible with GR and show peak values near zero except for 10 events that are shown in colors other than grey. For the 68% credible intervals (CI) the upper bound range is between the orders of magnitude $\mathcal{O}(10^{-14})$ and $\mathcal{O}(10^{-13})$. The 10 events in color show a 68% CI that is not compatible
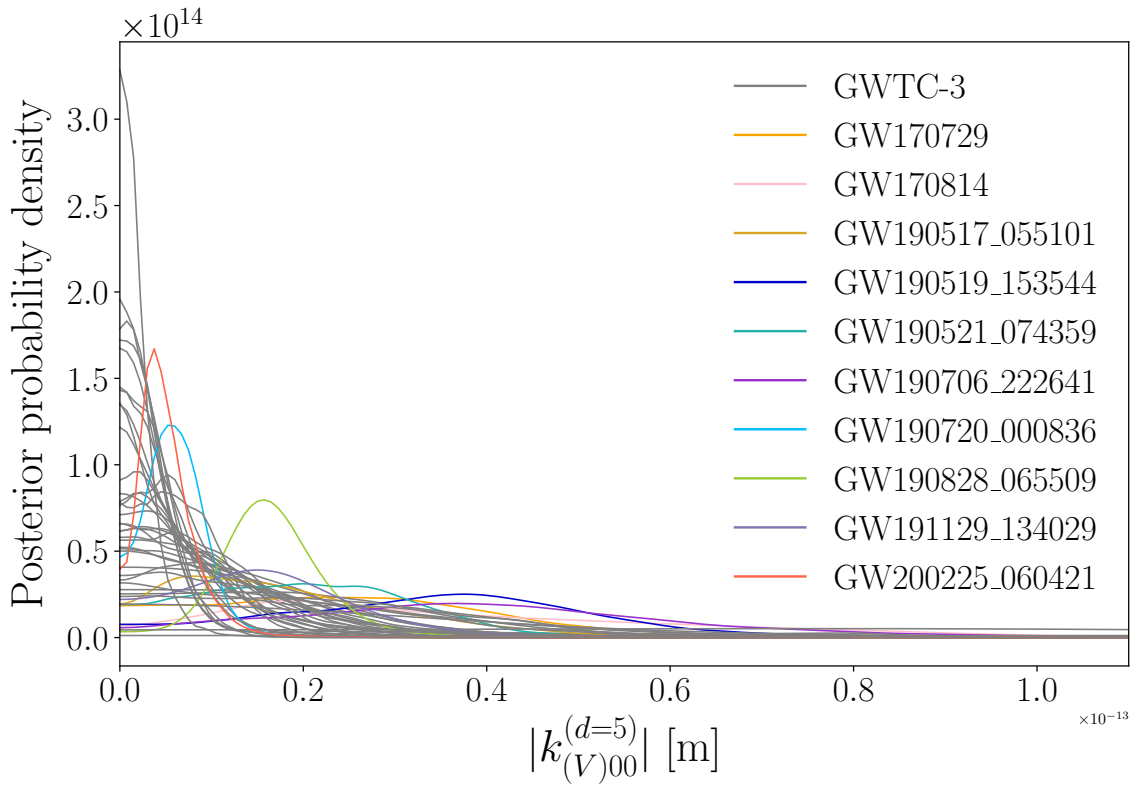
Figure 2.7: The posterior probability on the isotropic coefficient $|k_{(V)00}^{(5)}|$ for GW dispersion is shown for 45 individual events. The events in color presents a 68.3% CI not compatible with the GR case of $|k_{(V)00}^{(5)}| = 0$, while the events in grey are compatible.

with GR and one event, `GW190828_065509`, that is not compatible within the 90% CI range. The combined constraint from all events for $|k^{(5)}_{(V)00}|$ is $3.19 \cdot 10^{-15}$ m at 90% CI while the bound is $5.62 \cdot 10^{-16} < |k^{(5)}_{(V)00}| < 2.81 \cdot 10^{-15}$ m for the 68% CI. The combined deviation from GR is gone when removing three events from the combination, namely `GW190720_000836`, `GW190828_065509` and `GW200225_060421`.

Having more events than the number of independent anisotropic coefficients to constrain, one can extract bounds from the marginalized posterior $|k^{(5)}_{(V)00}|$ for each of these events, reported in imaginary and real values as summarized in Table 2.1. The credible intervals derived from the SVD method and correlations between the 16 parameters are shown in Fig. 2.8. Note that all anisotropic coefficients are

90% lower	68.3% lower	$k^{(5)}_{(V)ij}$ coefficient	68.3% upper	90% upper
0.51	1.21	k_{00}	4.38	7.37
-4.54	-2.13	k_{10}	1.19	3.91
-2.30	-1.00	$Re(k_{11})$	1.73	3.39
-3.64	-1.21	$Im(k_{11})$	2.35	4.45
-7.40	-3.75	k_{20}	1.10	3.78
-1.75	-0.61	$Re(k_{21})$	1.43	3.02
-2.77	-1.16	$Im(k_{21})$	1.71	3.67
-3.58	-1.72	$Re(k_{22})$	1.02	2.55
-2.49	-0.96	$Im(k_{22})$	2.80	5.58
-6.40	-3.31	k_{30}	1.17	3.57
-3.34	-1.65	$Re(k_{31})$	0.98	2.48
-3.90	-1.92	$Im(k_{31})$	1.75	3.87
-2.76	-1.23	$Re(k_{32})$	1.34	2.87
-2.26	-0.90	$Im(k_{32})$	1.82	3.60
-3.95	-1.95	$Re(k_{33})$	1.28	3.18
-3.22	-1.35	$Im(k_{33})$	2.25	4.78

Table 2.1: The table shows the CI on the $k^{(5)}_{(V)ij}$ coefficients (in 10^{-13} m), determined from the marginalised posterior probability distributions estimated with the joint estimation of the 16 $k^{(5)}_{(V)ij}$ coefficients shown in diagonal in Fig. 2.8.

compatible with GR while the isotropic symmetry-breaking coefficient shows devi-
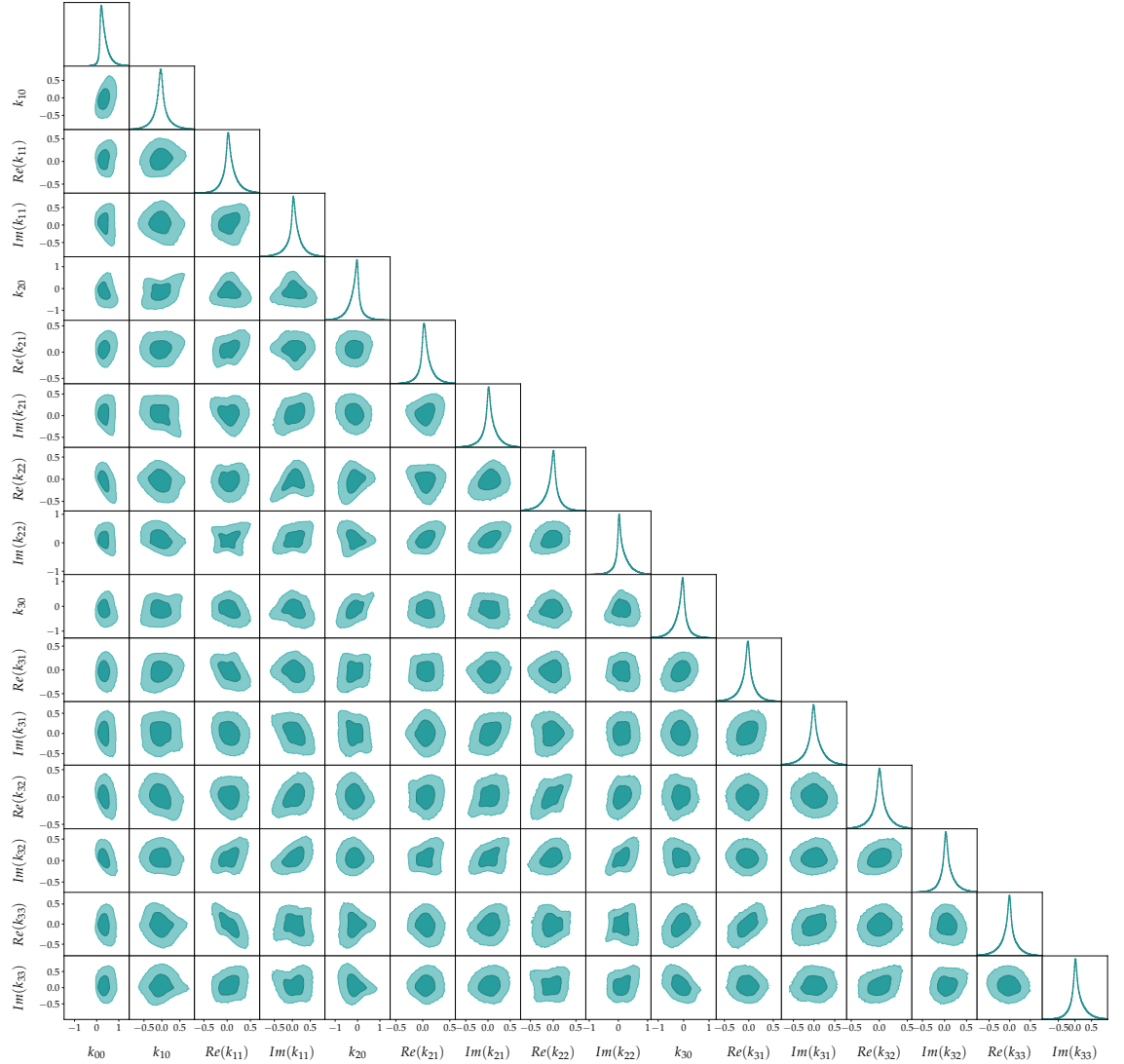
Figure 2.8: Shown are the posterior probabilities of the 16 $k_{(V)ij}^{(5)}$ coefficients (in 10^{-12} m). For the 2-dimensional distribution, dark blue areas are the 68.3% credible intervals and light blue are the 90% credible intervals.

ation from the GR case where $|k_{(V)00}^{(5)}| = 0$ m. Note also that the joint estimation shows weaker constraints than that for individual constraints, being three orders of magnitude larger.

The cases that show possible deviations from GR are investigated to search for other pathological behavior that might account for this. Results within LVK articles refer to such events that show deviation from GR [5, 9, 8] including two events from O2 (GW170729, GW170814), and two from O3 (GW190828_065509, GW200225_060421) for the dispersion relation parameters. There are three events from O3 (GW190519_153544, GW190521_074359, and GW190828_065509) that present deviations when using the post-Newtonian tests and an additional event (GW200225_0604321) that results in poor residual tests. It is possible that these deviations may result from a lack of new physics in the GR model where there should be added features from a new theory. It is also possible that the model used assumes too much of an approximation such as assuming circular orbits or oversimplified approximation of the precession, thus missing needed dynamical phenomena [93].

To test the robustness of the results, different waveform models are included in the inference process across several of our included events. Two events inferred with different waveform models are shown in Fig. 2.9. Initial analysis is done with the waveform IMRPhenomPv2 (inspiral, merger, ringdown phenomenological model up to Post Newtonian term 2) which is a single-precessing-spin waveform model. The results from this waveform are compared to those inferred by SEOBRNv4 which is an effective-one-body waveform model that describes the physics of the spinning binaries [35]. Results inferred by IMRPhenomXPHM, an updated version of IMRPhenomPv2, are also copmared, which include higher harmonics within the expansion terms and an updated calibration for precession [109]. When comparing IMRPhenomXPHM with IMRPhenomPv2 across 23 events, four show a significant modification in the CI while only one presents a devi-
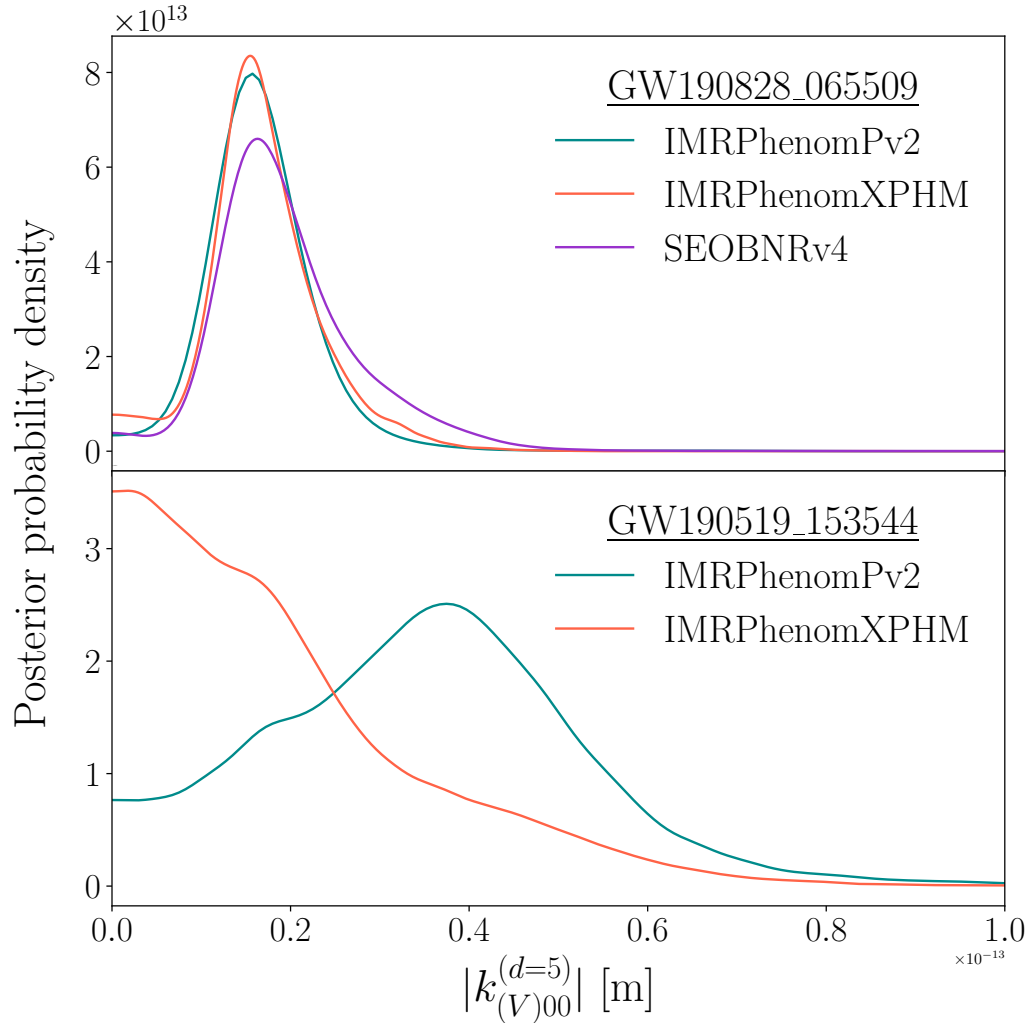
Figure 2.9: The posterior probability for the isotropic dispersion coefficient $|k^{(5)}_{(V)00}|$ is obtained with different waveform models, where comparisons with two events are shown. The top figure presents consistent estimation while the bottom figure presents a case where the probability shape differs between two of the waveform model used for inference.

ation from zero for the mode (`GW190519_153544`, `GW190706_222641`, `GW200219_094415`, `GW200225_060421`). The latter four events are then compared with the `SEOBRNv4` and `IMRPhenomPv2` waveform models, where two then present modifications to the CI (`GW190630_185205`, `GW190720_000836`). 10 events are investigated that have a CI not

containing zero, where only three are compatible with GR when using other waveform models (`GW190519_153544`, `GW190706_222641`, `GW190720_000836`). Thus one can conclude that while apparent deviations are not necessarily due to mismodelling, the high sensitivity requirement of the analysis in finding deviations from GR has become evident. However, a more detailed study is in order when noting that these waveforms share common assumptions and have uncertainty due to the modeling process that is not carried through the analysis (i.e., mismatching with numerical relativity simulations) before one can be more certain to conclude the results are indicative of new physics beyond GR.

The correlation between the source and symmetry-breaking parameters were taken into account during the inference process by the joint estimation. This is investigated by measuring the Pearson coefficients between the coefficient $|k^{(5)}_{(V)00}|$ and the source parameters produced from different waveforms as shown in Fig. 2.10, where the events that produced apparent deviations from GR for the 68% CI are shown. Most of the events show either no or moderate correlation, yet two events, `GW170814` and `GW190519_153544`, show a large anti-correlation with the mass and spin parameters. Events with higher SNR or more accuracy in source parameter measurements would lead to more stringent bounded constraints on the symmetry-breaking coefficients.
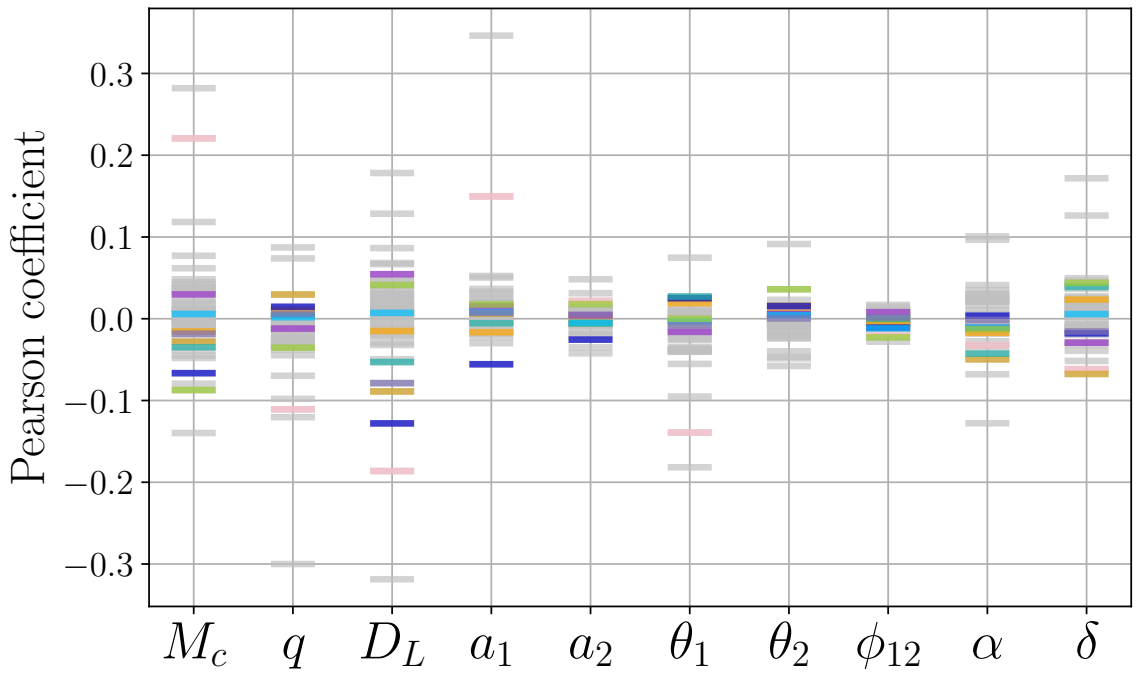
Figure 2.10: The correlations between $|k^{(5)}_{(V)00}|$ and the source parameters are shown for events with apparent deviation within the 68% CI. The x-axis shows the chirp mass M_c, the mass ratio q, the luminosity distance D_L, the spin magnitudes a_1 and a_2, the spin tilt angles $\theta_{1,2}$, the projected angle difference between spins is ϕ_{12}, the right ascension α, and the declination δ. The colored markers are the events corresponding to those presenting a deviation on Fig. 2.7, with GW170814 in pink and GW190519_153544 in blue; the grey markers are the other events.

Chapter 3

3+1 Formulation for the Gravity Sector of the Standard-Model Extension

Solutions to Einstein's Field equations of General Relativity are difficult to solve for most physical systems where only a few solutions have been found for idealized cases. In physical systems where slow velocity, weak field regimes exist, it is sufficient to use Post-Newtonian or general relativistic perturbation theories to describe the dynamics. This is not sufficient for cases were strong-field gravity exist, such as coalescing bodies including black holes and neutron stars and cosmology. The 3+1 formulation, or Numerical Relativity (NR), provides a means to describe nonlinear dynamics that is more easily modeled and provides an alternative means to investigate gravitational dynamics within constrained systems.

When facing complicated dynamical equations for a system containing constraints, the Dirac-Hamiltonian formulation provides an alternative means to better understand and manipulate the dynamics. The analysis in particular provides a systematic

treatment of these systems in order to find an easier, possible transition into quantum mechanics for gravitational physics.

The following work applied the 3+1 formulation with a Dirac-Hamiltonian analysis to the gravity sector of the SME, allowing for a spacetime symmetry breaking analysis to be conducted beyond the weak-field limit [100, 103].

3.1 Starting with the SME Framework

Within the gravity sector of the SME, we focus on the lowest order terms of mass dimension 4 (the minimal SME), and begin with the Lagrange density form,

$$\mathcal{L}_{SME} = \frac{\sqrt{-g}}{2\kappa}(R - 2\Lambda + (k_R)_{\alpha\beta\gamma\delta}R^{\alpha\beta\gamma\delta}) + \mathcal{L}', \tag{3.1}$$

where R, the Ricci scalar, and λ, the cosmological constant, are the usual GR terms while the additional term contracts the Riemann curvature tensor, $R^{\alpha\beta\gamma\delta}$ with $(k_R)_{\alpha\beta\gamma\delta}$, the SME coefficient fields [72]. The G_N is the gravitational constant and $\kappa = 8\pi G_N$. The $\mathcal{L}\prime$ is present to allow for coefficients that would arise from spontaneous symmetry breaking. In general, it is also important to note that the SME action is invariant under general coordinate transformations.

We can write the $(k_R)_{\alpha\beta\gamma\delta}$ coefficients in terms of a scalar, u, a 2-tensor $s_{\mu\nu}$, and a 4-tensor $t_{\alpha\beta\gamma\delta}$ contracted with the Ricci scalar, the trace-free Ricci tensor, $\left(R^{(T)}\right)^{\mu\nu}$, and the Weyl curvature tensor $W^{\alpha\beta\gamma\delta}$,

$$(k_R)_{\alpha\beta\gamma\delta}R^{\alpha\beta\gamma\delta} = -uR + s_{\mu\nu}\left(R^{(T)}\right)^{\mu\nu} + t_{\alpha\beta\gamma\delta}W^{\alpha\beta\gamma\delta}. \tag{3.2}$$

It is important to note that one could redefine the fields u and $s_{\mu\nu}$ in order to transfer them to the matter sector, up to the first order [38]. Either way, we still have observ-

able quantities one can measure. For this work, the additional SME terms within the gravity sector are kept.

There are ten symmetries to consider contained within the action: four from the diffeomorphism symmetry group and six for local Lorentz transformations. Under a general coordinate transformation, the *observer* diffeomorphism is invariant and all the fields transform as tensors: the action is invariant. Yet when applying *particle* diffeomorphisms, one would see that only the coefficients $(k_R)_{\alpha\beta\gamma\delta}$ remain fixed and thus the action breaks *particle* diffeomorphism. This is relevant to case studies later on in this work.

The vierbein $e^\mu{}_a$ maps the metric $g_{\mu\nu}$, defined on the spacetime manifold, to the Minkowski η_{ab} metric for each local point in spacetime, i.e., $\eta_{ab} = e^\mu{}_a e^\nu{}_b g_{\mu\nu}$. Thus when considering *observer* local Lorentz transformations, the curvature fields and coefficients will transform locally. Yet when considering a *particle* local Lorentz transformations, only the coefficients remain fixed and the action breaks local Lorentz transformation symmetries [31].

If the action (3.1) is interpreted to have spontaneous symmetry breaking, the fields including the coefficients $(k_R)_{\alpha\beta\gamma\delta}$ are dynamical. The *particle* local Lorentz transformation symmetries and diffeomorphism symmetries are invariant and one could interpret the dynamical mechanism as potential fields that interact and produce a nonzero vacuum expectation value $\langle (k_R)_{abcd} \rangle$ of the fields [83, 82]. Many other works have explored spontaneous symmetry breaking models with vector and tensor couplings to curvature [32, 33]. Additional works provide more detailed investigations into the differences between explicit and symmetry breaking associated with local Lorentz and diffeomorphism transformations, along with investigating the associated conservation laws [29, 34, 30, 31]. For this work, we assume explicit symmetry breaking.

One derives the conservation equations from the Lagrange, and in the case of either Lorentz or diffeomorphism symmetry breaking, we derive the modified field equations by varying the metric $g_{\mu\nu}$ within (3.1),

$$G^{\mu\nu} = (T_{ust})^{\mu\nu} + \kappa(T_M)^{\mu\nu}, \tag{3.3}$$

where $(T_M)^{\mu\nu}$ is the energy-momentum density tensor for the matter sector and the explicit form for $(T_{ust})^{\mu\nu}$ can be found in [72]. The traced Bianchi identities, $\nabla_\mu G^{\mu\nu} = 0$, are the conservation laws that are usually upheld, and in the modified case lead to

$$\nabla_\mu(T_{ust})^{\mu\nu} = -\kappa\nabla_\mu(T_M)^{\mu\nu}, \tag{3.4}$$

where T_{ust} subscripts of ust refer to the SME coefficients.

3.2   3+1 Formalism

The 3+1 formalism follows the work within [**adm**, 45, 92, 36]. One starts with a 4-dimensional manifold $\mathcal{M}$ with a defined metric $g_{\mu\nu}$. This manifold is decomposed into 3-dimensional spatial hypersurfaces Σ_t that are parameterized by time t. There is a time-like normal vector n^μ for each spatial hypersurface that is normalized, i.e.g, $n_\mu n^\mu = -1$ (one could normalize to $+1$, this is purely a conventional choice associated with the metric signature). In Arnowitt-Deser-Misner (ADM) coordinates, the components of the normalized time vector are $n_\mu = (-\alpha, 0, 0, 0)$, where α is referred to as the lapse function (see Fig. 3.1). This figure shows the connections between two spatial hypersurfaces of Σ_t and one later in time Σ_{t+dt}. The x^i are fixed neighboring points that are mapped through the vector $t^\mu dt$ [25]. The β^i is the spatial shift vector that accounts for the difference between n^ν and t^μ. There is a purely spatial metric
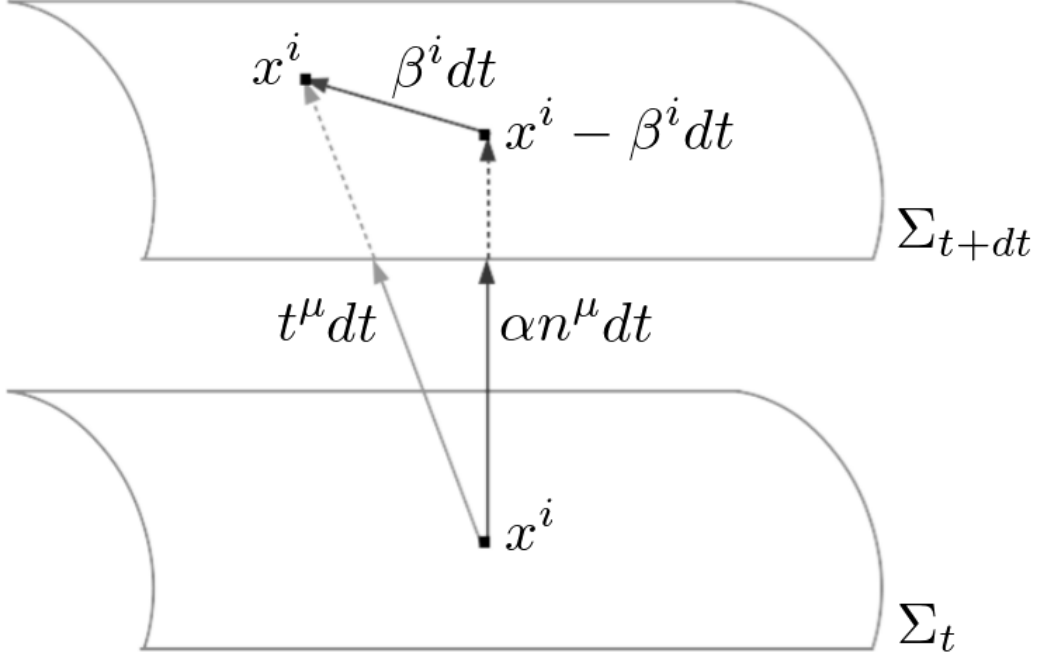
Figure 3.1: The ADM variables connecting spatial hypersurfaces Σ at time t and $t + dt$.

$\gamma_{\mu\nu}$ that that measures proper spatial distances within a hypersurface. It has an inverse and satisfies $\gamma^{il}\gamma_{lk} = \delta^i{}_k$. The spatial metric is written in terms of the metric $g_{\mu\nu}$ and the normal time vectors, $\gamma^{\mu\nu}$,

$$\gamma^{\mu\nu} = g^{\mu\nu} + n^\mu n^\nu. \tag{3.5}$$

As a check, one can note the orthogonality between the spatial metric and time vector, i.e., $\gamma^b_a n_b = 0$. The $\gamma^{\mu\nu}$ and n^μ are used as operators to decompose and project GR tensors into spatial and time-like, and mixed terms. A 3-dimensional covariant derivative is formed from projections with the spatial metric. For a tensor with mixed indices, T^μ_ν, the spatial covariant derivative is

$$\mathcal{D}_\mu T^\alpha{}_\beta = \gamma^\delta{}_\mu \gamma^\alpha{}_\epsilon \gamma^\zeta{}_\beta \nabla_\delta T^\epsilon{}_\zeta, \tag{3.6}$$

where the placement and number of indices indicates the number of spatial metrics required for the projection. This derivative is completely compatible with the spatial metric, i.e., $\mathcal{D}_\mu \gamma^{\mu\nu} = 0$. The components of a spatial covariant derivative acting on an arbitrary covariant vector v_μ satisfying $n^\mu v_\mu = (1/\alpha)(v_0 - \beta^i v_i)$ are

$$
\begin{aligned}
\mathcal{D}_0 v_0 &= \beta^i \beta^j (\partial_i v_j -^3 \Gamma^k_{ij} v_k + n^\mu v_\mu K_{ij}), \\
\mathcal{D}_0 v_i &= \beta^j (\partial_j v_i -^3 \Gamma^k_{ij} v_k + n^\mu v_\mu K_{ij}), \\
\mathcal{D}_i v_0 &= \beta^j (\partial_i v_j -^3 \Gamma^k_{ij} v_k + n^\mu v_\mu K_{ij}), \\
\mathcal{D}_i v_j &= \partial_i v_j -^3 \Gamma^k_{ij} v_k + n^\mu v_\mu K_{ij},
\end{aligned}
\tag{3.7}
$$

where the 3-dimensional Christoffel symbols $^3\Gamma^i_{jk}$ are written in terms of the spatial metric,

$$
^3\Gamma^i_{jk} = \tfrac{1}{2} \gamma^{il} (\partial_j \gamma_{kl} + \partial_k \gamma_{jl} - \partial_l \gamma_{jk}).
\tag{3.8}
$$

A purely spatial 3-dimensional Riemann tensor is defined in terms of the commutator of spatial covariant derivatives acting on a purely spatial vector v_μ,

$$
[\mathcal{D}_\alpha, \mathcal{D}_\beta] \, v_\delta = -\mathcal{R}^\epsilon_{\ \delta\alpha\beta} v_\epsilon,
\tag{3.9}
$$

where $\mathcal{R}^\epsilon_{\ \delta\alpha\beta} n_\epsilon = 0$. The Lie derivative shows how to evolve the spatial metric in time along the normal time vector n^μ. Also defined, the extrinsic curvature $K_{\mu\nu}$ is symmetric, purely spatial tensor. It measures how much a normal vectors (to a spatial hypersurface) change in orientation as it moves along neighboring points. It measures the rate in which a spatial hypersurface curves, and thus is related to the Lie derivative acting on $\gamma_{\mu\nu}$ along n^μ,

$$
K_{\mu\nu} = -\tfrac{1}{2} \mathcal{L}_{\mathbf{n}} \gamma_{\mu\nu}.
\tag{3.10}
$$

It is also useful to define a purely spatial acceleration, $a_\mu = n^\nu \nabla_\nu n_\mu$, where $n^\mu a_\mu = 0$.

There are three types of projections on the Riemann curvature tensor,

$$
\begin{aligned}
\gamma^\alpha{}_\mu \gamma^\beta{}_\nu \gamma^\gamma{}_\kappa \gamma^\delta{}_\lambda R_{\alpha\beta\gamma\delta} &= \mathcal{R}_{\mu\nu\kappa\lambda} + K_{\mu\kappa} K_{\nu\lambda} - K_{\mu\lambda} K_{\nu\kappa}, \\
\gamma^\alpha{}_\mu \gamma^\beta{}_\nu \gamma^\gamma{}_\kappa n^\delta R_{\alpha\beta\gamma\delta} &= \mathcal{D}_\nu K_{\mu\kappa} - \mathcal{D}_\mu K_{\nu\kappa}, \\
\gamma^\beta{}_\mu \gamma^\delta{}_\nu n^\alpha n^\gamma R_{\alpha\beta\gamma\delta} &= \mathcal{L}_{\mathbf{n}} K_{\mu\nu} + \tfrac{1}{\alpha} \mathcal{D}_\mu \mathcal{D}_\nu \alpha + K^\beta{}_\mu K_{\nu\beta}.
\end{aligned}
$$

$$(3.11)$$

From this, the 4-dimensional Ricci tensor can be decomposed,

$$
\begin{aligned}
R^{\mu\nu} &= \mathcal{R}^{\mu\nu} + n^\mu K^{\nu\alpha} a_\alpha + n^\nu K^{\mu\alpha} a_\alpha + K K^{\mu\nu} - \mathcal{L}_{\mathbf{n}} K^{\mu\nu} \\
&\quad + 2 K^{\alpha\mu} K^\nu{}_\alpha - a^\mu a^\nu - \mathcal{D}^\mu a^\nu - n^\mu \mathcal{D}^\nu K - n^\nu \mathcal{D}^\mu K \\
&\quad + n^\mu \mathcal{D}_\alpha K^{\alpha\nu} + n^\nu \mathcal{D}_\alpha K^{\alpha\mu} \\
&\quad + n^\mu n^\nu \left(\mathcal{L}_{\mathbf{n}} K - K^{\alpha\beta} K_{\alpha\beta} + a^2 + \mathcal{D}_\alpha a^\alpha \right).
\end{aligned}
$$

$$(3.12)$$

For this work, it was found to be useful to write the decomposition forms for the Riemann tensor and the Ricci tensor and scalar in terms of the 4-dimensional covariant derivative instead of the purely spatial covariant derivative. After some manipulation

of (3.11), the following expressions are found:

$$
\begin{aligned}
R &= \mathcal{R} + K^{\alpha\beta}K_{\alpha\beta} - K^2 - 2\nabla_\alpha(n^\alpha K + a^\alpha), \\
R^{\alpha\beta} &= \mathcal{R}^{\alpha\beta} - 2K^{\alpha\beta}K + 2K^\alpha{}_\delta K^{\delta\beta} - n^\alpha a^\beta K \\
&\quad + n^\alpha K^\beta{}_\delta a^\delta - n^\alpha n^\beta(K^2 - K^{\alpha\beta}K_{\alpha\beta}) \\
&\quad + \nabla_\delta[n^\alpha n^\beta(n^\delta K + a^\delta) - n^\delta K^{\alpha\beta} - \gamma^{\delta\beta}a^\alpha \\
&\quad - (n^\alpha\gamma^{\beta\delta} + n^\beta\gamma^{\alpha\delta})K + n^\alpha K^{\beta\delta} + n^\beta K^{\alpha\delta}], \\
R^{\alpha\beta\gamma\delta} &= \mathcal{R}^{\alpha\beta\gamma\delta} - 3(K^{\alpha\gamma}K^{\beta\delta} - K^{\beta\gamma}K^{\alpha\delta}) \\
&\quad + (K^{\alpha\epsilon}K^\gamma{}_\epsilon n^\beta n^\delta + sym) - (K^{\alpha\gamma}n^\beta n^\delta K + sym) \\
&\quad - (K^{\alpha\gamma}n^{(\beta}a^{\delta)} + sym) \\
&\quad + \nabla_\epsilon\big[n^\epsilon(K^{\alpha\gamma}n^\beta n^\delta + sym) \\
&\quad\quad + (\gamma^{\epsilon(\alpha}a^{\gamma)}n^\beta n^\delta + sym) \\
&\quad\quad - 2(K^{\alpha\gamma}n^{(\beta}\gamma^{\delta)\epsilon} + sym)\big],
\end{aligned}
\tag{3.13}
$$

where *sym* represents the Riemann symmetric combination of terms with the indices $\alpha, \beta, \gamma, \delta$. As an example, for two symmetric tensors $A^{\alpha\gamma}$ and $B^{\beta\delta}$, $A^{\alpha\gamma}B^{\beta\delta} + sym = A^{\alpha\gamma}B^{\beta\delta} - A^{\beta\gamma}B^{\alpha\delta} - A^{\alpha\delta}B^{\beta\gamma} + A^{\beta\delta}B^{\alpha\gamma}$.

Lastly, the metric line element can be expressed in terms of the spatial and time-like projection operators as,

$$
ds^2 = -(\alpha^2 - \beta^j\beta_j)dt^2 + 2\beta_j dt dx^j + \gamma_{ij}dx^i dx^j,
\tag{3.14}
$$

where it is apparent that there are the usual initial 10 degrees of freedom in GR from α, β^j, and γ_{ij}.

3.2.1 The Decomposition of the GR Action

We start with the decomposition of the GR Lagrange using the 3+1 projection operators,

$$\mathcal{L}_{GR} = \frac{\sqrt{-g}}{2\kappa}[\mathcal{R} + K^{\alpha\beta}K_{\alpha\beta} - K^2 - 2\nabla_\alpha(n^\alpha K + a^\alpha)], \qquad (3.15)$$

where the last term is a surface term that normally does not contribute to the equation of motion and is usually dropped [36]. The last two terms with the extrinsic curvature $K_{\mu\mu}$ include information on how to evolve the spatial metric $\gamma_{\mu\nu}$ in time along the time vector n^μ. The extrinsic curvature is rewritten via evaluating the Lie derivative,

$$K_{ij} = -\frac{1}{2\alpha}(\partial_t\gamma_{ij} - \mathcal{D}_i\beta_j - \mathcal{D}_j\beta_i), \qquad (3.16)$$

showing explicitly the time derivatives. All other components $k_{0\mu}$ do not contain any time derivatives. This is useful when noting the importance of time derivatives in the Hamiltonian formulation: when working with GR, time derivatives only appear on the spatial metric, giving 6 dynamical degrees of freedom. We also have 4 nondynamical degrees of freedom: 1 from α and 3 from β^i, which give 4 primary constraints.

3.2.2 SME decomposition with global background coefficients

With the additional Lorentz-violating coefficients $(k_R)_{\alpha\beta\gamma\delta}$, we decompose the Lagrange in (3.1). During this process, the coefficients for Lorentz violation do not generally vanish when operated on by a covariant derivative. The Lagrange form is

then,

$$
\begin{aligned}
\mathcal{L}_{k_R} = \ & \frac{\sqrt{-g}}{2\kappa}\Big\{(k_R)_{\alpha\beta\gamma\delta}\Big[\mathcal{R}^{\alpha\beta\gamma\delta} - 6K^{\alpha\gamma}K^{\beta\delta} \\
& + 4n^{\alpha}n^{\gamma}(K^{\beta\epsilon}K^{\delta}_{\ \epsilon} - K^{\beta\delta}K^{\epsilon}_{\ \epsilon}) + 4a^{\beta}n^{\gamma}K^{\alpha\delta}\Big] \\
& - 4\Big(n^{\alpha}n^{\gamma}(n^{\epsilon}K^{\beta\delta} + \gamma^{\delta\epsilon}a^{\beta}) - 2n^{\alpha}\gamma^{\gamma\epsilon}K^{\beta\delta}\Big)\nabla_{\epsilon}(k_R)_{\alpha\beta\gamma\delta}\Big\}. \quad (3.17)
\end{aligned}
$$

where all but one term are expressed with the acceleration a^{μ}, the 3-dimensional Riemann curvature tensor, and the extrinsic curvature. The last term shows a covariant derivative on the coefficients that cannot be made to vanish [72]. Also note also that the acceleration a_{μ} has only spatial derivatives, as it can be shown that the components are purely spatial: $a_j = \partial_j \ln \alpha$ and $a_0 = \beta^j a_j$.

The following is a simpler example that investigates the importance of dynamical terms in the 3+1 framework. Consider the covariant derivative of the covariant vector b_{μ} and its projection onto the 3+1 framework while using the Lie derivative properties along n^{μ},

$$
\begin{aligned}
\nabla_{\mu}b_{\nu} = \ & \mathcal{D}_{\mu}b_{\nu} - n_{\nu}\mathcal{D}_{\mu}(n^{\lambda}b_{\lambda}) - 2n_{(\mu}K_{\nu)}{}^{\lambda}b_{\lambda} \\
& - n_{\mu}n_{\nu}(a^{\lambda}b_{\lambda}) + n_{\mu}n_{\nu}\mathcal{L}_{\mathbf{n}}(n^{\lambda}b_{\lambda}) - n_{\mu}\gamma^{\beta}{}_{\nu}\mathcal{L}_{\mathbf{n}}b_{\beta}.
\end{aligned}
$$

$$(3.18)$$

From (3.18), the terms containing spatial covariant derivatives $\mathcal{D}_{\mu}$ do not produce any time derivatives on the metric fields α and β^{μ}. Geometrically, the spatial covariant derivatives live and only describe changes on the 3-dimensional hypersurface Σ_t. Nor are there time derivatives contained within the term with the acceleration, since this only contains spatial partial derivatives on α. This leaves two terms with Lie derivatives that could potentially contain time derivatives on the metric fields. To

investigate, $n^\lambda b_\lambda$ is expanded in terms of its components,

$$n^\lambda b_\lambda = \tfrac{1}{\alpha}(b_0 - \beta^j b_j), \tag{3.19}$$

then applying the Lie derivative,

$$\mathcal{L}_\mathbf{n}(n^\lambda b_\lambda) = -\tfrac{\dot{\alpha}(n^\lambda b_\lambda) + b_i \dot{\beta}^i}{\alpha^2} + \tfrac{1}{\alpha} n^\mu \dot{b}_\mu - \tfrac{1}{\alpha}\beta^j \mathcal{D}_j(n^\lambda b_\lambda). \tag{3.20}$$

The time derivatives within the lapse $\dot{\alpha} = \partial_t \alpha$ and the shift functions $\dot{\beta}^j = \partial_t \beta^j$ are apparent. This alters the number of primary constraints from the GR case. The other term containing a Lie derivative is proportional to $\gamma^i{}_\nu \mathcal{L}_\mathbf{n} b_i$, which will also have time derivatives on α, β^i and γij.

The time dependence on α and β^i is investigated to ensure whether it is simply coordinate artifacts that will disappear under a general coordinate transformation. For instance, the covariant tensor b_μ transforms under a general coordinate transformation in the usual way,

$$b'_\mu = \tfrac{\partial x^\nu}{\partial x'^\mu} b_\nu. \tag{3.21}$$

Yet there are terms containing the projection of b along the normal time-like vector n in (3.20), which produce a scalar that provides no orientation information on the SME background field. An alternative coordinate system is chosen with the contraction $n^{\mu'} b_{\mu'} = b_{0'}$ and the assumption that the unknown background fields are fixed and independent of the gravitational fields. This is a different model to work with, and is an example of an explicit symmetry breaking case of diffeomorphism. This illustrates the importance in specifying the background fields as noted later on.

Similar to the latter example, the form of (3.17) can be rearranged to make the

time derivative acting on fields more explicit,

$$
\begin{aligned}
\mathcal{L}_{k_R} =\ & \frac{\sqrt{-g}}{2\kappa}\Big\{ (k_R)_{\alpha\beta\gamma\delta}\Big[\mathcal{R}^{\alpha\beta\gamma\delta} + 2K^{\alpha\gamma}K^{\beta\delta} \\
& - 12n^\alpha n^\gamma K^{\beta\epsilon}K^\delta{}_\epsilon + 4n^\alpha n^\gamma K^{\beta\delta}K^\epsilon{}_\epsilon + 8K^{\alpha\gamma}n^\beta a^\delta\Big] \\
& + 8K^{\epsilon\zeta}\mathcal{D}_\lambda\big((k_R)_{\alpha\beta\gamma\delta}\gamma^\alpha{}_\epsilon\gamma^{\beta\lambda}\gamma^\gamma{}_\zeta n^\delta\big) \\
& - 4a^\epsilon \mathcal{D}_\zeta\big((k_R)_{\alpha\beta\gamma\delta}\gamma^{\alpha\zeta}\gamma^\gamma{}_\epsilon n^\beta n^\delta\big) \\
& - 4K^{\epsilon\zeta}\mathcal{L}_\mathbf{n}\big((k_R)_{\alpha\beta\gamma\delta}\gamma^\alpha{}_\epsilon\gamma^\gamma{}_\zeta n^\beta n^\delta\big).\Big\},
\end{aligned}
\tag{3.22}
$$

The last term with the Lie derivative is the only one that will contain explicit time derivatives. Expanding the Lie derivative,

$$
\mathcal{L}_{k_R} \supset \frac{4\sqrt{-g}}{\kappa\alpha^2}K^{ij}n^\delta\big((k_R)_{i\beta j\delta}n^\beta\dot\alpha + (k_R)_{ilj\delta}\dot\beta^l\big),
\tag{3.23}
$$

the terms containing $\dot\alpha$ and $\dot\beta^l$ are apparent. As mentioned, this is not the case in GR and in many alternative models for gravity. Yet it is not surprising considering this case has explicit diffeomorphism symmetry breaking, which also breaks the usual GR gauge symmetry.

There are alternative gravity models that incorporate explicit symmetry breaking like that of massive gravity, yet this does not introduce time derivatives on the metric fields. There are also models that contain contractions such as $R_{\alpha\beta}R^{\alpha\beta}$ within the Lagrange density, and even introduce higher order derivatives. Yet still these models do not produce time-dependent metric fields and the gauge symmetry still holds [119]. There are models which allow for higher order time derivatives on the fields, yet they still find a means to hold the GR gauge symmetry [95, 94].

One could assume a spontaneous symmetry breaking scenario, where one relabels $b_\mu \to B_\mu$ to be a dynamical field. Thus additional field equations would appear and

the $\dot{\alpha}$ and $\dot{\beta}^j$ fields would be tied into the dynamics of B_μ; the extra time derivatives on the metric fields appear in combination with the dynamical fields of B_μ. There would be no extra degrees of freedom and $\dot{\alpha}$ and $\dot{\beta}^j$ can be eliminated by performing a particle diffeomorphism. This is analogous to the Nambu-Goldstone modes for spontaneous symmetry [32, 33].

3.2.3 SME Decomposition with Local Background Coefficients

In the explicit symmetry breaking case where the SME coefficients $k_{\alpha\beta\gamma\delta}$ are fixed background fields that are independent of the gravitational fields, different results can be achieved through incorporating the vierbein formalism, relating the global frame to a local frame. For the α, β^j and γ_{ij} fields, the vierbein components $e_\mu{}^a$ are given by,

$$
\begin{aligned}
e_t{}^{\bar{0}} &= \alpha, \\
e_j{}^{\bar{0}} &= 0, \\
e_t{}^{\bar{j}} &= e_i{}^{\bar{j}}\beta^i, \\
\gamma_{ij} &= e_i{}^{\bar{j}}e_{j\bar{j}}, \tag{3.24}
\end{aligned}
$$

where the Latin indices are for spatial components, an explicit t is for time, and the bar over the indices represents the local frame. The full expression for the spatial metric can be calculated once a γ_{ij} form is chosen. This vierbein is not a general solution, and there can be other possible ways to use this formalism. In this case, b_a is the local background field that will break spacetime symmetry [72, 42, 52]. One

can take the scalar contraction within (3.20) and assume,

$$b_\mu n^\mu = b_{\bar{0}}, \tag{3.25}$$

which, when applying the Lie derivative along n^a would give,

$$\mathcal{L}_\mathbf{n}(n^\lambda b_\lambda) = \frac{\partial_t b_{\bar{0}}}{\alpha} - \frac{1}{\alpha}\beta^j \partial_j(b_{\bar{0}}). \tag{3.26}$$

Note there is no explicit time derivatives on α and β^j.

3.3   Dirac-Hamiltonian Analysis

A Dirac-Hamiltonian analysis is done that follows standard procedures performed in [21, 47, 61]. The Lagrange density (3.22) is transformed into a conjugate momentum space where one can more explicitly analyse the system's constraints and degrees of freedom. The decomposition of the coefficient k into u, $s_{\mu\nu}$, and $t_{\kappa\lambda\mu\nu}$ provides three

parts of the Lagrange density,

$$
\begin{aligned}
\mathcal{L}_u &= \tfrac{\sqrt{-g}}{2\kappa}[u\left(\mathcal{R} + K^{\alpha\beta}K_{\alpha\beta} - K^2\right) \\
&\quad + 2(K\mathcal{L}_{\mathbf{n}}u + a^\mu \mathcal{D}_\mu u)] \\
\mathcal{L}_s &= \tfrac{\sqrt{-g}}{2\kappa}[s_{\mu\nu}\mathcal{R}^{\mu\nu} - n^\alpha n^\beta s_{\alpha\beta}(K^{\mu\nu}K_{\mu\nu} - K^2) \\
&\quad + 2s_{\alpha\beta}K^{\alpha\delta}K^\beta{}_\delta + K^{\mu\nu}\mathcal{L}_{\mathbf{n}}s_{\mu\nu} - K\mathcal{L}_{\mathbf{n}}(n^\mu n^\nu s_{\mu\nu}) \\
&\quad + 2K\left(s_{\mu\nu}n^\mu a^\nu + \mathcal{D}_\lambda(s_{\mu\nu}n^\mu \gamma^{\nu\lambda})\right) \\
&\quad - 2K^\lambda{}_\kappa \mathcal{D}_\lambda(s_{\mu\nu}n^\mu \gamma^{\nu\kappa}) \\
&\quad + a_\kappa \mathcal{D}_\lambda(s_{\mu\nu}\gamma^{\mu\lambda}\gamma^{\nu\kappa}) - a^\lambda \mathcal{D}_\lambda(s_{\mu\nu}n^\mu n^\nu)] \\
\mathcal{L}_t &= \tfrac{\sqrt{-g}}{2\kappa}\Big\{ t_{\alpha\beta\gamma\delta}\Big[\mathcal{R}^{\alpha\beta\gamma\delta} + 2K^{\alpha\gamma}K^{\beta\delta} \\
&\quad -12n^\alpha n^\gamma K^{\beta\epsilon}K^\delta{}_\epsilon + 4n^\alpha n^\gamma K^{\beta\delta}K^\epsilon{}_\epsilon + 8K^{\alpha\gamma}n^\beta a^\delta\Big] \\
&\quad + 8K^{\epsilon\zeta}\mathcal{D}_\lambda\big(t_{\alpha\beta\gamma\delta}\gamma^\alpha{}_\epsilon \gamma^{\beta\lambda}\gamma^\gamma{}_\zeta n^\delta\big) \\
&\quad - 4a^\epsilon \mathcal{D}_\zeta\big(t_{\alpha\beta\gamma\delta}\gamma^{\alpha\zeta}\gamma^\gamma{}_\epsilon n^\beta n^\delta\big) \\
&\quad - 4K^{\epsilon\zeta}\mathcal{L}_{\mathbf{n}}\big(t_{\alpha\beta\gamma\delta}\gamma^\alpha{}_\epsilon \gamma^\gamma{}_\zeta n^\beta n^\delta\big)\Big\}.
\end{aligned}
\tag{3.27}
$$

The variation of the actions $L = \int d^3x \mathcal{L}$ is done with respect to all fields that are time dependent using the definition,

$$
\Pi_n = \tfrac{\delta L}{\delta \dot\phi_n},
\tag{3.28}
$$

where $\dot\phi_n$ is substituted for $\dot\alpha$, $\dot\beta^j$ and $\dot\gamma^{ij}$. Assuming the case of global background coefficients, the conjugate momenta are,

$$
\begin{aligned}
\Pi_\alpha &= \tfrac{\sqrt{\gamma}}{\kappa\alpha}n^\mu n^\nu \left(K s_{\mu\nu} + 4K^{ij}t_{i\mu j\nu}\right), \\
\Pi_{\beta,i} &= \tfrac{\sqrt{\gamma}}{\kappa\alpha}n^\mu \left(K s_{\mu i} + 4K^{jk}t_{jik\mu}\right),
\end{aligned}
\tag{3.29}
\tag{3.30}
$$

where $\Pi_\alpha = \delta L/\delta\dot{\alpha}$ and $(\Pi_\beta)_i = \delta L/\delta\dot{\beta}^i$. There is no expression for Π_u since this term vanishes [1]. The conjugate momentum for γ^{ij} is $\Pi_\gamma^{ij} = \delta L/\delta\dot{\gamma}_{ij}$,

$$\Pi_\gamma^{ij} \supset \tfrac{\sqrt{\gamma}}{2\kappa}\left(K\gamma^{ij} - K^{ij} - s_{lm}\gamma^{li}K^{jm} - s_{lm}\gamma^{lj}K^{im} + ...\right),$$

where only the terms relating to $s_{\mu\nu}$ coupled to γ^{ij} are shown to avoid the lengthy expression. Other terms include those with $t_{\kappa\lambda\mu\nu}$ and mixed terms having $s_{\mu\nu}$ and $K_{ij} \sim \dot{\gamma}_{ij} - \mathcal{D}_i\beta_j - \mathcal{D}_j\beta_i$.

The Hamiltonian density is then constructed with the canonical form $\mathcal{H} = \Pi^n\phi_n - \mathcal{L}$. The conjugate momenta expressions must be rewritten as the time dependent fields $\dot{\phi}$ in terms of the conjugate momenta Π_n in order to substitute and find the Hamiltonian density form. This turns out to be an extremely algebraically challenging process, thus the work resorts to first investigating limiting cases in the follow subsections.

3.3.1 First Case Study: Global Frame

The first case study chooses a particular coordinate system where $s_{\mu\nu}$ has only one nonzero, time component, s_{00}. Then the Lagrange density for $\mathcal{L}_s$ from (3.27), with the ADM metric form from (3.14) is,

$$\begin{aligned}
\mathcal{L}_1 &= \tfrac{\alpha\sqrt{\gamma}}{2\kappa}\Big[\mathcal{R} + \tfrac{\alpha^2 - s_{00}}{\alpha^2}\left(K^{ij}K_{ij} - K^2\right) \\
&\quad + K\left(\tfrac{2}{\alpha^4}s_{00}(\dot{\alpha} - \alpha\beta^i a_i) - \tfrac{1}{\alpha^3}(\dot{s}_{00} - \beta^i\partial_i s_{00})\right) \\
&\quad + \tfrac{2}{\alpha^2}s_{00}a^i a_i - \tfrac{1}{\alpha^2}a^i\partial_i s_{00}\Big] + \mathcal{L}_M,
\end{aligned} \qquad (3.31)$$

---

[1] One could assume $u = s_\mu^\mu$ and would obtain a nonzero result for Π_u.

where $\mathcal{L}_M$ contains the matter sector terms. The conjugate momenta densities for the α, β^μ, and $\gamma_{\mu\nu}$ fields are then,

$$
\begin{aligned}
\Pi_\gamma^{ij} &= \frac{\sqrt{\gamma}}{2\kappa}\left[\frac{\alpha^2-s_{00}}{\alpha^2}\left(K\gamma^{ij}-K^{ij}\right)\right.\\
&\qquad\qquad \left. +\frac{1}{2\alpha}\gamma^{ij}(\partial_t-\beta^k\partial_k)\left(\frac{s_{00}}{\alpha^2}\right)\right],
\end{aligned}
\tag{3.32}
$$

$$
\Pi_{\beta,i} = 0,
\tag{3.33}
$$

$$
\Pi_\alpha = \frac{\sqrt{\gamma}s_{00}}{\kappa\alpha^3}K.
\tag{3.34}
$$

For convenience, the definitions are made: $\Pi_\gamma^{ij} \equiv \Pi^{ij}$, $\Pi_i \equiv \Pi_{\beta,i}$, and the trace is abbreviated to $\Pi = \Pi^{ij}\gamma_{ij}$. The vanishing conjugate momenta Π_i provides three primary constraints. The expressions (3.32), (3.34) and that for extrinsic curvature (3.16) can be used together to find expression for $\dot\alpha$ and $\dot\gamma_{ij}$.

A Legendre transformation is applied next on the Lagrange density to obtain the *base* Hamiltonian density,

$$
\mathcal{H}_0 = \pi^{ij}\dot\gamma_{ij} + \pi_\alpha\dot\alpha - \mathcal{L},
\tag{3.35}
$$

which for GR is

$$
\mathcal{H}_{GR} = \frac{2\kappa\alpha}{\sqrt{\gamma}}\left(\Pi_{ij}\Pi^{ij}-\tfrac{1}{2}\Pi^2\right) - \frac{\alpha\sqrt{\gamma}}{2\kappa}\mathcal{R} - 2\beta^i\mathcal{D}_j\Pi^j{}_i.
\tag{3.36}
$$

For this case study, the *base* Hamiltonian density is found to be,

$$
\begin{aligned}
\mathcal{H}_0 &= \frac{2\kappa\alpha^3}{\sqrt{\gamma}(\alpha^2-s_{00})}\left(\Pi_{ij}\Pi^{ij}-\tfrac{1}{3}\Pi^2\right)\\
&\quad +\frac{\kappa\alpha^5(\alpha^2-s_{00})}{3\sqrt{\gamma}s_{00}^2}\Pi_\alpha^2 - \frac{2\kappa\alpha^4}{3\sqrt{\gamma}s_{00}}\Pi_\alpha\Pi + \frac{\alpha\dot{s}_{00}}{2s_{00}}\Pi_\alpha\\
&\quad -\frac{\sqrt{\gamma}}{\kappa\alpha}\left(s_{00}a^i a_i - \tfrac{1}{2}a^i\partial_i s_{00}\right) - \frac{\alpha\sqrt{\gamma}}{2\kappa}\mathcal{R}\\
&\quad +\beta^i\left(\Pi_\alpha[\alpha a_i - \frac{\alpha}{2s_{00}}\partial_i s_{00}] - 2\mathcal{D}_j\Pi^j{}_i\right),
\end{aligned}
\tag{3.37}
$$

where the last line contains the primary constraints. Terms can be removed in (3.37) that include Π_α and s_{00} to retrieve the GR case, yet taking the limit $s_{00} \to 0$ will not provide a smooth connection between the Hamiltonians. This is an artifact of this method where the assumption $s_{00} \neq 0$ is made in order to invert the expression of Π_α in (3.34). This is not a singularity but a parameter singularity. Further investigation is required.

The *augmented* Hamiltonian density is formulated next by adding the primary constraints. The general format includes the *base* Hamiltonian density plus additional terms that contract primary constraints Π_i with the Lagrange multipliers ξ^i. For this case study, the *augmented* Hamiltonian density is found using the three primary constraints (3.34). Then the format becomes $\mathcal{H}_A = \mathcal{H}_0 + \xi^i \Pi_i$. Next, one must proceed to check the consistency condition, observing how the updated Hamiltonian density evolves in time and requiring the derivatives of the constraints to vanish or produce a linear combination of previously found constraints that are *weakly* zero (i.e.,when one imposes the constraints collected and finds the result to vanish) [47]. This requires taking a Poisson bracket between the time-dependent primary constraints and the *augmented* Hamiltonian.

At this point, remarks on the usage of Poisson brackets during the Dirac-Hamiltonian process is made (more information can be found within other literature [36, 116]). Yet during this work, many subtitles arose during the calculations that were not found within other sources, which is discussed in the following. Consider a set of n fields $q_n(t, \vec{r})$ and a set of n momenta $p^n(t, \vec{r})$ as functions of time t and space $\vec{r}$. Functions can be defined from these fields and momenta, $f(q, p)$ and $g(q, p)$. Then the definition of the Poisson bracket is,

$$\{f, g\} = \int d^3z \left(\frac{\delta f}{\delta q_n(t, \vec{z})} \frac{\delta g}{\delta p^n(t, \vec{z})} - \frac{\delta f}{\delta p^n(t, \vec{z})} \frac{\delta g}{\delta q_n(t, \vec{z})} \right), \tag{3.38}$$

where the functions of f and g can be defined at different spatial points within the spatial volume dz^3. The fields are all defined at the same points in time. The number of fields and momenta are chosen to be $n = 1$ for simplicity, i.e., let $q_1 = \phi(t, \vec{r})$ and $p_1 = \Pi = \Pi(t, \vec{r'})$. The Poisson bracket is then,

$$\{\phi(t, \vec{r}), \Pi(t, \vec{r'})\} = \delta^3(\vec{r} - \vec{r'}). \tag{3.39}$$

In classical mechanics, it is common for the functions f and g to be functions of the coordinates and momenta. Yet when one works in field theory, one will often find spatial derivatives of these function involved in the Poisson bracket calculation. Thus for the case when the spatial derivative ∂_i operator is applied to the first function within the Poisson bracket, the following identity is found,

$$\{\partial_i f, g\} = \partial_i \{f, g\}. \tag{3.40}$$

This result can be extended to covariant spatial derivatives as can be illustrated with the momentum constraint term encountered in both GR and the SME: $\mathcal{D}_i \Pi^i{}_k$. Its Poisson bracket with the Hamiltonian H is then,

$$\begin{aligned}
\{\gamma_{kl} \mathcal{D}_i \Pi^{il}, H\} &= \{\gamma_{kl}, H\} \mathcal{D}_i \Pi^{il} + \gamma_{kl} \mathcal{D}_i \{\Pi^{il}, H\} \\
&\quad + \Pi^{ij} \mathcal{D}_i \{\gamma_{jk}, H\} - \tfrac{1}{2} \Pi^{jl} \mathcal{D}_k \{\gamma_{jl}, H\}.
\end{aligned} \tag{3.41}$$

The last two terms in (3.41) emerge after noting a couple subtitles. Firstly, it is important to keep track of the weight of integrand terms: the weight of the three dimensional tensor Π^{ij} is -1. Secondly, one must keep track of the dependence of the covariant derivative on the spatial metric γ_{ij}.

Returning to current case study, one proceeds to check the consistency condition as the new Hamiltonian is evolved in time by taking the Poisson bracket, i.e., $\dot{\Pi}_i = \{\Pi_i, H_A\}$. The result may produce two possibilities: one which produces no new information, or one that provides a new expression relating the fields β^i and their momenta Π. If the result is the latter, this new relation is added as an additional term the the Hamiltonian density and again, the consistency condition must be checked for the new constraints.

The result for this case is a secondary constraint,

$$\dot{\Pi}_i = 2\gamma_{ij}\mathcal{D}_k\Pi^{jk} - \Pi_\alpha \left(\alpha a_i - \tfrac{\alpha}{2s_{00}}\partial_i s_{00} \right) \approx 0. \tag{3.42}$$

Note the above expression *weakly* equals zero when imposing the constraints collected, i.e., $\Pi_i = 0$. Considering this result expresses a new relation between the fields and their momenta, again the consistency condition is checked with the secondary constraint $\Phi_i = \dot{\Pi}_i$. For this, the full expression is required with the explicit time dependence on Φ_i, which will contain terms with time derivatives on s_{00},

$$\begin{aligned} \tfrac{d\Phi_i}{dt} &= \{\Phi_i, H_A\} + \tfrac{\partial \Phi_i}{\partial t} \\ &= \mathcal{D}_j(\beta^j \Phi_i) + \Phi_j \mathcal{D}_i \beta^j + \Psi \partial_i s_{00}, \end{aligned}$$

$$\tag{3.43}$$

where Ψ is a function of coordinates and momenta,

$$
\begin{aligned}
\Psi \;=\;& -\frac{\kappa\alpha^3}{\sqrt{\gamma}(\alpha^2-s_{00})s_{00}}\left(\Pi_{ij}\Pi^{ij}-\tfrac{1}{3}\Pi^2\right) \\
& -\frac{\kappa\alpha^5(\alpha^2-s_{00})}{6\sqrt{\gamma}s_{00}^3}\Pi_\alpha^2 + \frac{\kappa\alpha^4}{3\sqrt{\gamma}s_{00}^2}\Pi_\alpha\Pi + \frac{\alpha\sqrt{\gamma}}{4\kappa s_{00}}\mathcal{R} \\
& +\frac{\sqrt{\gamma}}{4\kappa s_{00}\alpha}\mathcal{D}^2 s_{00} - \frac{\sqrt{\gamma}}{2\kappa\alpha^2}\mathcal{D}^2\alpha \\
& -\frac{\sqrt{\gamma}}{\kappa s_{00}\alpha}a^j\partial_j s_{00} + \frac{3\sqrt{\gamma}}{2\kappa\alpha}a^j a_j.
\end{aligned}
\tag{3.44}
$$

The first two terms in (3.42) are linear in the primary constraint Φ_i, and when imposing the primary constraint $\Pi_i = 0$, the terms are found to be weakly equal to zero. The third term $\Psi\partial_i s_{00}$ can create two possibilities. If we assume that the background coefficients of $s_{\mu\nu}$ are left arbitrary, they can provide new constraints that would update the Hamiltonian and consistency conditions would again be checked. Yet if one chooses a coordinate system where one can impose the spatial partial derivative of the coefficient to vanish, $\partial_i s_{00} = 0$, the secondary constraint would be weakly equal to zero and there would have been no need to find further constraints. The results of (3.42) can be compared to the case for GR, where the third term is an additional term that modifies the usual momentum constraint found in GR, which can be thought of as a "shift" in the conservation law.

We can investigate the implications on the traced Bianchi identities and input the choice of SME coefficient into (3.4),

$$
\nabla_\mu(T_s)^\mu{}_\nu = \tfrac{1}{2}R^{\mu\lambda}\nabla_\nu s_{\mu\lambda} - \nabla_\mu(R^{\mu\lambda}s_{\lambda\nu}).
\tag{3.45}
$$

Then the expression is decomposed by replacing the Ricci tensor with (3.12) and the covariant derivative with the form in (3.18). We explicitly write any tensors in terms of α, β^i and γ_{ij} and the conjugate momenta densities α, β^i and γ_{ij}, using the

expressions from (3.32)-(3.34). Considering the case where $s_{00} \neq 0$ and $\partial_i s_{00} = 0$, the expression becomes,

$$\nabla_\mu (T_s)^\mu{}_j = \frac{\kappa}{\sqrt{\gamma}\alpha} \Psi \partial_j s_{00}, \tag{3.46}$$

which are the same terms found within the third term in (3.43). This provides a comparison check to ensure that the constraint found by evolving the Hamiltonian (3.37) is a constraint expected for the field equations.

Next, a second coordinate assumption for $s_{\mu\nu}$ is made,

$$\partial_i s_{00} = 0, \tag{3.47}$$

where the SME coefficients do not change within the spatial hypersurface parameterized by time.

The Hamilton's equations of motion are then calculated via the standard method using Poisson brackets: $\dot{p}_n = \{p_n, H\}$, where we use the final Hamiltonian for H, containing all constraints found. For this case, this would include the three additional secondary constraints and their associated Lagrange multipliers to (3.37), yet one would find these secondary constraints already to be contained within the primary constraints β^j. This emphasizes the gauge freedom in the case for this framework.

The Hamilton's equations of motion are then,

$$
\dot{\Pi}_\alpha = -\frac{2\kappa\alpha^2(\alpha^2-3s_{00})}{\sqrt{\gamma}(\alpha^2-s_{00})^2}\left(\Pi^{ij}\Pi_{ij} - \tfrac{1}{3}\Pi^2\right) + \frac{8\kappa\alpha^3}{3\sqrt{\gamma}s_{00}}\Pi_\alpha\Pi - \frac{\kappa\alpha^4}{3\sqrt{\gamma}s_{00}^2}\left(7\alpha^2 - 5s_{00}\right)\Pi_\alpha^2
$$
$$
+\mathcal{D}_k\left(\beta^k\Pi_\alpha\right) - \frac{1}{2s_{00}}\Pi_\alpha\dot{s}_{00} + \frac{s_{00}\sqrt{\gamma}}{\kappa\alpha^2}\left(a^i a_i - 2\mathcal{D}_i a^i\right) + \frac{\sqrt{\gamma}}{2\kappa}\mathcal{R}, \qquad (3.48)
$$

$$
\dot{\Pi}_i = 2\gamma_{ij}\mathcal{D}_k\Pi^{jk} - \Pi_\alpha\alpha a_i, \qquad (3.49)
$$

$$
\dot{\Pi}^{ij} = -\frac{4\kappa\alpha^3}{\sqrt{\gamma}(\alpha^2-s_{00})}\left(\Pi^i{}_k\Pi^{jk} - \tfrac{1}{3}\Pi\Pi^{ij}\right) + \frac{\kappa\alpha^3}{\sqrt{\gamma}(\alpha^2-s_{00})}\gamma^{ij}\left(\Pi^{kl}\Pi_{kl} - \tfrac{1}{3}\Pi^2\right)
$$
$$
+\frac{\kappa\alpha^5(\alpha^2-s_{00})}{6\sqrt{\gamma}s_{00}^2}\gamma^{ij}\Pi_\alpha^2
$$
$$
-\frac{\kappa\alpha^4}{3\sqrt{\gamma}s_{00}}\Pi_\alpha(\Pi\gamma^{ij} - 2\Pi^{ij}) - 2\Pi^{k(i}\mathcal{D}_k\beta^{j)} + \mathcal{D}_k\left(\Pi^{ij}\beta^k\right)
$$
$$
-\frac{\sqrt{\gamma}}{2\kappa}\left(\alpha\mathcal{R}^{ij} - \tfrac{1}{2}\gamma^{ij}\alpha\mathcal{R} - \mathcal{D}^i\mathcal{D}^j\alpha + \gamma^{ij}\mathcal{D}^2\alpha\right)
$$
$$
+\frac{\sqrt{\gamma}s_{00}}{\kappa\alpha}\left(\tfrac{1}{2}\gamma^{ij}a^k a_k - a^i a^j\right), \qquad (3.50)
$$

and

$$
\dot{\alpha} = -\frac{2\kappa\alpha^4}{3s_{00}\sqrt{\gamma}}\left[\Pi - \frac{\alpha(\alpha^2-s_{00})}{s_{00}}\Pi_\alpha\right] + \alpha\beta^k a_k
$$
$$
+\frac{\alpha}{2s_{00}}\dot{s}_{00} \qquad (3.51)
$$

$$
\dot{\beta}^i = \xi^i \qquad (3.52)
$$

$$
\dot{\gamma}_{ij} = \frac{4\kappa\alpha^3}{\sqrt{\gamma}(\alpha^2-s_{00})}\left(\Pi_{ij} - \tfrac{1}{3}\Pi\gamma_{ij}\right)
$$
$$
-\frac{2\kappa\alpha^4}{3\sqrt{\gamma}s_{00}}\Pi_\alpha\gamma_{ij} + \mathcal{D}_i\beta_j + \mathcal{D}_j\beta_i. \qquad (3.53)
$$

The next discussion refers to the degrees of freedom in this system, which are represented by the pairs of coordinate and momenta variables that can be freely chosen on the spatial hypersurface.

Initially there are 10 possible degrees of freedom: one from α, three from β^j and 4 from γ_{ij}. Within this case model, there are three primary constraints and three secondary constraints, all having an associated total of six undetermined Lagrange

multipliers. If one adheres to the recipe provided in the equation B11 in the Appendix B in Ref. [61], the degrees of freedom are counted by,

$$
\begin{aligned}
N_{dof} &= N_{dof,initial} - \tfrac{1}{2}(\#constraints) \\
&\quad - \tfrac{1}{2}(\#undetermined\,Lagrange\,multipliers),
\end{aligned}
\tag{3.54}
$$

where *dof* refers to the degrees of freedom. For this case study, this would imply that there are $10 - (1/2)(6) - (1/2)(6) = 4$ degrees of freedom. For the GR case, from the initial 10 possible degrees of freedom, there are four primary constraints, four secondary constraints, and thus eight undetermined Lagrange multipliers, giving a total of $10 - (1/2)8 - (1/2)8 = 2$ degrees of freedom.

One could choose a different choice in the case example for the background coefficients of $s_{\mu\nu}$, providing applicable Hamilton equations for physical systems where one would model strong gravity with numerical simulations, as in CCSNe or Cosmology. This work presents applications in the latter.

3.3.2   Second Case Study: Local Lorentz Frame

In this second illustrative case, a different choice is presented for the background coefficients within the local Lorentz frame. The coefficient s_{ab} is chosen to be diagonal and isotropic,

$$
s_{ab} = \begin{pmatrix}
s_{\bar{0}\bar{0}} & 0 & 0 & 0 \\
0 & \tfrac{1}{3}s & 0 & 0 \\
0 & 0 & \tfrac{1}{3}s & 0 \\
0 & 0 & 0 & \tfrac{1}{3}s
\end{pmatrix},
\tag{3.55}
$$

where $s_{\bar{0}\bar{0}}$ and s are arbitrary functions of spacetime. These local Lorentz coordinates of s_{ab} can be related to that of $s_{\mu\nu} = e_\mu{}^a e_\nu{}^b s_{ab}$ through the vierbein expressions in (3.24). Then the new explicit form for the Lagrange density becomes,

$$
\mathcal{L}_2 = \frac{\alpha\sqrt{\gamma}}{2\kappa}\Big[\mathcal{R}\left(1 + \tfrac{1}{3}s\right) + \left(K^{ij}K_{ij} - K^2\right)\left(1 - s_{\bar{0}\bar{0}}\right)
$$
$$
+ K\mathcal{L}_{\mathbf{n}}\Omega + a^i\partial_i\Omega\Big], \tag{3.56}
$$

where for simplicity, the definition $\Omega = s/3 - s_{\bar{0}\bar{0}}$ is used. This Lagrange density expression appears to be the GR case with scalings of the extrinsic curvature and spatial curvature terms. There is no presence of the α and β^j as time-dependent terms as seen in the first case. Note though, that these coefficients can depend on time and space. Continuing as before, the conjugate momenta densities are calculated,

$$
\Pi^{ij} = \frac{\sqrt{\gamma}}{2\kappa}\Big[\left(K\gamma^{ij} - K^{ij}\right)\left(1 - s_{\bar{0}\bar{0}}\right) - \tfrac{1}{2}\gamma^{ij}\mathcal{L}_{\mathbf{n}}\Omega\Big], \tag{3.57}
$$

$$
\Pi_{\beta,i} = 0, \tag{3.58}
$$

$$
\Pi_\alpha = 0, \tag{3.59}
$$

where now there are four primary constraints for Π_α and $\Pi_{\beta,i}$, as in the GR case. The conjugate momenta for Π^{ij} deviates from that of GR with an additional term containing $s_{\bar{0}\bar{0}}$ and another containing a Lie derivative of the SME coefficients. Note that the results for local Lorentz coefficients in (3.59) is not a limiting case for the general form shown in the global case shown in (3.34). Continuing with the derivation

of the base Hamiltonian,

$$
\begin{aligned}
\mathcal{H}_0 \;=\;& \tfrac{2\kappa\alpha}{\sqrt{\gamma}(1-)}\left(\Pi_{ij}\Pi^{ij} - \tfrac{1}{2}\Pi^2\right) + 2\Pi^{ij}\mathcal{D}_i\beta_j \\
& -\tfrac{\alpha\sqrt{\gamma}}{2\kappa}\left(1 + \tfrac{1}{3}s\right)\mathcal{R} - \frac{1}{2(1 - s_{\bar{0}\bar{0}})}\Pi\Omega' \\
& -\frac{3\sqrt{\gamma}}{16\kappa\alpha(1-s_{\bar{0}\bar{0}})}(\Omega')^2 - \tfrac{\alpha\sqrt{\gamma}}{2\kappa}a^i\partial_i\Omega,
\end{aligned}
\tag{3.60}
$$

where another definition is implemented for simplicity, $\Omega' = (\partial_0 - \beta^i\partial_i)\Omega$. The consistency condition is checked by evolving the primary constraints with respect to the augmented Hamiltonian

$$
H_A = \int d^3x(\mathcal{H}_0 + v\Pi_\alpha + \xi^i\Pi_i),
\tag{3.61}
$$

where the Lagrange multipliers are v and ξ^j. The secondary constraints are found to be,

$$
\begin{aligned}
\{\Pi_\alpha, H_A\} \;=\;& -\frac{2\kappa}{\sqrt{\gamma}(1-s_{\bar{0}\bar{0}})}\left(\Pi^{ij}\Pi_{ij} - \tfrac{1}{2}\Pi^2\right) \\
& +\tfrac{\sqrt{\gamma}}{2\kappa}\left(1 + \tfrac{1}{3}s\right)\mathcal{R} - \frac{3\sqrt{\gamma}}{16\kappa(1-s_{\bar{0}\bar{0}})\alpha^2}(\Omega')^2 \\
& -\tfrac{\sqrt{\gamma}}{2\kappa}\mathcal{D}^2\Omega,
\end{aligned}
\tag{3.62}
$$

$$
\begin{aligned}
\{\Pi_i, H_A\} \;=\;& 2\mathcal{D}_j\Pi^j{}_i - \frac{\Pi}{2(1-s_{\bar{0}\bar{0}})}\partial_i\Omega \\
& -\frac{3\sqrt{\gamma}}{8\kappa(1-s_{\bar{0}\bar{0}})\alpha}\Omega'\partial_i\Omega.
\end{aligned}
\tag{3.63}
$$

There are additional terms beyond GR that contain time and space derivatives Ω containing expressions of the coefficients. Proceeding to check the consistency conditions once more, but noting that the resulting expression will be similar to that for the first case study, one can expect to see a term containing canonical variables that scale with $\partial_i\Omega$. Since this is a lengthy expression, the condition $\partial_i\Omega = 0$ is chosen for

simplicity. This will in effect, reduce the constraints from Π_i in (3.63) to the form for GR, i.e., $\dot{\Pi}_i = 2\mathcal{D}_j\Pi^j{}_i \approx 0$.

Continuing the calculations for the secondary constraint, the following expression is found,

$$
\begin{aligned}
\{\Phi_\alpha, H_A\} + \frac{\partial\Phi_\alpha}{\partial t} &= \mathcal{D}_i(\beta^i\Phi_\alpha) + \frac{2(1+\frac{1}{3}s)}{(1-s_{\bar{0}\bar{0}})}\Phi_i\mathcal{D}^i\alpha + \frac{(1+\frac{1}{3}s)\alpha}{(1-s_{\bar{0}\bar{0}})}\mathcal{D}^i\Phi_i + v\frac{3\sqrt{\gamma}}{8\kappa\alpha^3(1-s_{\bar{0}\bar{0}})}\dot{\Omega}^2 \\
&\quad + \frac{9\sqrt{\gamma}}{64\kappa\alpha^2(1-s_{\bar{0}\bar{0}})^2}\dot{\Omega}^3 + \frac{3}{8\alpha(1-s_{\bar{0}\bar{0}})^2}\dot{\Omega}^2\Pi - \frac{\kappa(\dot{s}+\dot{s}_{\bar{0}\bar{0}})}{2\sqrt{\gamma}(1-s_{\bar{0}\bar{0}})^2}\left(\Pi_{ij}\Pi^{ij} - \tfrac{1}{2}\Pi^2\right) \\
&\quad - \frac{3\sqrt{\gamma}}{8\kappa\alpha^3(1-s_{\bar{0}\bar{0}})}\dot{\Omega}^2\beta^i\mathcal{D}_i\alpha - \frac{\sqrt{\gamma}}{8\kappa(1-s_{\bar{0}\bar{0}})}\left((1+\tfrac{1}{3}s)\dot{\Omega} - \tfrac{4}{3}\dot{s}(1-s_{\bar{0}\bar{0}})\right)\mathcal{R} \\
&\quad - \frac{3\sqrt{\gamma}}{8\kappa\alpha^2(1-s_{\bar{0}\bar{0}})}\dot{\Omega}\ddot{\Omega} - \frac{3\sqrt{\gamma}}{16\kappa\alpha^2(1-s_{\bar{0}\bar{0}})^2}\dot{\Omega}^2\dot{s}_{\bar{0}\bar{0}}, \quad\quad (3.64)
\end{aligned}
$$

$$
\{\Phi_j, H_A\} = \Phi_i\mathcal{D}_j\beta^i + \mathcal{D}_i(\beta^i\Phi_j) + \Phi_\alpha\mathcal{D}_j\alpha, \quad\quad (3.65)
$$

where the following are defined: $\Phi_\alpha = \{\Pi_\alpha, H_A\}$, and $\Phi_i = \{\Pi_i, H_A\}$. Given the secondary constraints of Φ_i and Π_α weakly equal zero, and tertiary constraints in (3.65) are linear in Φ_i and Π_{al} and thus itself weakly equals zero. In contrast to the first case study, there are additional constraints for Π_α, $\Phi_\alpha = \dot{\Pi}_\alpha$ and $\dot{\Phi}_\alpha$ with v being an undetermined Lagrange multiplier.

The undetermined Lagrange multiplier v in (3.61) can be solved for by setting the constraint in (3.64) weakly equal to zero. The first three terms in (3.64) vanish when imposing the secondary constraints, and the expression for v becomes,

$$
\begin{aligned}
v &= -\frac{3\alpha\dot{\Omega}}{8(1-s_{\bar{0}\bar{0}})} - \frac{\kappa\alpha^2\Pi}{(1-s_{\bar{0}\bar{0}})\sqrt{\gamma}} + \beta^i\mathcal{D}_i\alpha \\
&\quad - \frac{4\kappa^2\alpha^3(\dot{s}+\dot{s}_{\bar{0}\bar{0}})}{3\gamma(1-s_{\bar{0}\bar{0}})\dot{\Omega}^2}\left(\Pi_{ij}\Pi^{ij} - \tfrac{1}{2}\Pi^2\right) \\
&\quad + \left((1+\tfrac{1}{3}s)\dot{\Omega} - \tfrac{4}{3}\dot{s}(1-s_{\bar{0}\bar{0}})\right)\frac{\alpha^3\mathcal{R}}{3\dot{\Omega}^2} \\
&\quad + \frac{\alpha\ddot{\Omega}}{\dot{\Omega}} + \frac{\alpha\dot{s}_{\bar{0}\bar{0}}}{2(1-s_{\bar{0}\bar{0}})}. \quad\quad (3.66)
\end{aligned}
$$

As before, there are SME coefficients in some of the term denominators, and so for this solution one would impose the condition that $\dot{\Omega} \neq 0$.

The Hamiltonian can now be updated where the solution for v is labeled as $V = V(\alpha, \gamma_{ij}, \beta^i, \Pi^{ij}, ...)$, a function of canonical variables and the coefficients, giving us the form,

$$
\begin{aligned}
H_F \quad = \quad & \int d^3x (\mathcal{H}_0 + V(\alpha, \gamma_{ij}, \beta^i, \Pi^{ij}, ...)\Pi_\alpha + \xi^i \Pi_i \\
& + \zeta^j \Phi_j).
\end{aligned}
\tag{3.67}
$$

Note the base Hamiltonian $\mathcal{H}_0$ is evaluated when $\partial_i \Omega = 0$ and there are three additional Lagrange multipliers, ζ^j contracted with the secondary constraints. The v is no longer Lagrange multiplier as it has been solved for in (3.66).

To summarize (3.67), four primary constraints are found in (3.58) and (3.59), four secondary constraints (3.62) and (3.63) and six Lagrange multipliers ξ^i and ζ^i. Using the formula (3.54), the degrees of freedom are $10 - (1/2)(8) - (1/2)6 = 3$, one more than for GR.

One can also make a specific choice of setting the coefficients s_{00} and s to be constants, greatly reducing the Hamiltonian to terms that are scalings of GR terms (one can see this by setting $\Omega = 0$ and $\dot{\Omega} = 0$ in (3.60)). In doing so, an explicit symmetry breaking framework is found from the SME that helps find matches to other explicit symmetry models. In this case, two degrees of freedom are found.

3.3.3 The Inclusion of Matter

Next is the addition of the matter sector to the Hamiltonian analysis in order to apply this framework to physical systems including Cosmology or CCSN. The the minimal couplings of the SME symmetry breaking coefficients are retained solely within the

gravity sector. The description of matter can be as simple as a perfect fluid to the inclusion of gauge fields and spinors. In this analysis, the former is chosen.

Turning to the term within the Lagrange density that contains the matter sector, $(T_M)^{\mu\nu}$, and varying this with respect to the metric $g_{\mu\nu}$,

$$(T_M)^{\mu\nu} = \frac{2}{\sqrt{-g}}\frac{\delta S_M}{\delta g_{\mu\nu}}. \tag{3.68}$$

Note the conventional choice in overall sign for this term, which does not effect the resulting physics. The 3+1 decomposition is applied and variations with respect to the fields produce the conjugate momenta forms,

$$
\begin{aligned}
\frac{\delta H_M}{\delta \alpha} &= \alpha^2\sqrt{\gamma}(T_M)^{00}, \\
\frac{\delta H_M}{\delta \beta^i} &= -\alpha\sqrt{\gamma}[(T_M)^{00}\beta_i + (T_M)^{0j}\gamma_{ij}], \\
\frac{\delta H_M}{\delta \gamma_{ij}} &= -\tfrac{1}{2}\alpha\sqrt{\gamma}[(T_M)^{ij} + \beta^i\beta^j(T_M)^{00} + 2(T_M)^{0(i}\beta^{j)}].
\end{aligned}
$$

$$\tag{3.69}$$

One then proceeds to check the consistency condition, or the evolution of the constraints while including the matter terms (3.69). As an example, the secondary constraints that would appear for the second case study for $\Phi_i = \dot{\Pi}_i$ in (3.63) with the inclusion of the extra matter term $-\delta H_M/\delta\beta^i$ gives,

$$
\begin{aligned}
\left\{\frac{\delta H_M}{\delta \beta^i}, H_A\right\} &= \frac{\delta H_M}{\delta \alpha}\mathcal{D}_i\alpha + \mathcal{D}_j\left(\beta^j\frac{\delta H_M}{\delta \beta^j}\right) \\
&\quad + \frac{\delta H_M}{\delta \beta^j}(\mathcal{D}_i\beta^j) - 2\gamma_{ki}\mathcal{D}_j\frac{\delta H_M}{\delta \gamma_{jk}}
\end{aligned}
\tag{3.70}
$$

where the augmented Hamiltonian H_A now also contains the matter section.

3.4 Applications to Cosmology

The following applications focus on solutions within a Friedmann-Lemaitre-Robertson-Walker (FLRW) spacetime [92]. Results from the first case study are used, assuming global background SME coefficients with $s_{m\mu\nu}$ having only one nonzero component, s_{00}, and the coordinate choice of $\partial_i s_{00} = 0$. Then, the general FLRW metric in spherical coordinates is,

$$ds^2 = -dt^2 + a^2(t)\left[\tfrac{dr^2}{1-kr^2} + r^2\big(d\theta^2 + \sin^2\theta d\phi^2\big)\right], \qquad (3.71)$$

where the scale factor for the universe is $a(t)$ and $k = \{+1, 0, -1\}$ depending on whether the universe is closed, flat or open, respectively. When comparing this metric to the 3+1 decomposition fields from (3.14), one can see that $\alpha = 1, \beta^i = 0$ with a vanishing acceleration $a^i = 0$.

As before, the conjugate momenta for the fields that relate to those found in (3.32) and (3.34) are found,

$$\begin{aligned}
\Pi^{ij} &= -\tfrac{\sqrt{\gamma}}{\kappa}(1 - s_{00})\tfrac{\dot{a}}{a}\gamma^{ij} + \tfrac{\sqrt{\gamma}}{4\kappa}\dot{s}_{00}\gamma^{ij}, \\
\Pi_\alpha &= -\tfrac{3s_{00}}{\kappa}\sqrt{\gamma}\tfrac{\dot{a}}{a},
\end{aligned} \qquad (3.72)$$

where one uses the relation $\dot{\gamma}_{ij} = 2\dot{a}\gamma_{ij}/a$ and $\sqrt{\gamma} = a^3 r^2 \sin\theta/\sqrt{1 - kr^2}$. There are three primary constraints for $\Pi_i = 0$ as in the initial first case study. As with

(3.48)-(3.50), one continues with evaluating the Hamilton's equations of motion,

$$
\begin{aligned}
\dot{\Pi}^{ij} &= \frac{\kappa(1-s_{00})}{6\sqrt{\gamma}s_{00}^2}\gamma^{ij}\Pi_\alpha^2 - \frac{\kappa}{3\sqrt{\gamma}s_{00}}\Pi_\alpha(\Pi\gamma^{ij} - 2\Pi^{ij}) \\
&\quad - \frac{\sqrt{\gamma}}{2\kappa}\mathcal{G}^{ij} + \frac{\sqrt{\gamma}}{2}(T_M)^{ij}, \\
\dot{\Pi}_\alpha &= \frac{\sqrt{\gamma}}{2\kappa}\mathcal{R} + \frac{8\kappa}{3\sqrt{\gamma}s_{00}}\Pi_\alpha\Pi - \frac{\kappa}{3\sqrt{\gamma}s_{00}^2}\left(7 - 5s_{00}\right)\Pi_\alpha^2 \\
&\quad - \frac{1}{2s_{00}}\Pi_\alpha\dot{s}_{00} - \sqrt{\gamma}(T_M)^{00},
\end{aligned}
\tag{3.73}
$$

where now there are terms involving the matter couplings (3.69), and $\mathcal{G}_{ij}$ is the three dimensional Einstein tensor. The constraint $\dot{\beta}^i$ from (3.49) still holds in this case.

Matter is described as the usual perfect fluid, i.e., $(T_M)^\mu{}_\nu = diag(-\rho, p, p, p)$, where ρ is the energy density and p is the pressure, related by the equation of state $p = w\rho$, where the barotropic index is w and includes values of $1/3$ for radiation, 0 for dust matter and -1 for vacuum energy. This matter description is also within a homogeneous, isotropic universe for the FLRW case. The three-dimensional Ricci scalar and three-dimensional Einstein tensor are calculated to be $\mathcal{R} = 6k/a^2$, and $\mathcal{G}^{ij} = -k\gamma^{ij}/a^2$.

The Friedman equations are found through combing the equations (3.72) and (3.73),

$$
\left(\frac{\dot{a}}{a}\right)^2 (1 - s_{00}) = \frac{\kappa\rho}{3} - \frac{k}{a^2} - s_{00}\frac{\ddot{a}}{a} + \frac{\dot{a}}{a}\frac{\dot{s}_{00}}{2},
\tag{3.74}
$$

$$
\left[\frac{\ddot{a}}{a} + \frac{1}{2}\left(\frac{\dot{a}}{a}\right)^2\right](1 - s_{00}) = -\frac{\kappa p}{2} - \frac{k}{2a^2} + \frac{\dot{a}}{a}\dot{s}_{00} + \frac{1}{4}\ddot{s}_{00},
\tag{3.75}
$$

where GR is a limiting by setting $s_{00} \to 0$. The modifications to the first equation (3.74) can be seen, which describe the evolution of the scale factor. Modifications in

the second equation (3.73) describe the acceleration of the universe.Both equations contain terms that include first and second time derivatives on the coefficient s_{00}, along with scalings by $(1 - s_{00})$. There is also an additional term with $\ddot{a}$ in the first equation. No further rearranging is done to these equations to better match the standard form of the Friedman equations as the s_{00} still remains an unspecified function.

The implications for the conservation laws, stated generally in (3.4), are studied with respect to the chosen coordinates in (3.45). To ensure consistency with the field equations, one can enforce,

$$\nabla_\mu (T_s)^{\mu\nu} = -\kappa \nabla_\mu (T_M)^{\mu\nu}. \tag{3.76}$$

The spatial component $\nu = i$ for (3.76) is already satisfied by the chosen condition $\partial_i s_{00} = 0$ (3.47), thus the usual conservation of matter still holds: $\nabla_\mu (T_M)^\mu{}_j = 0$. The usual conservation of energy holds within the cosmological solutions as there is no explicit time component $\nu = 0$ within the Hamiltonian calculations.

The left hand side of (3.76) first expanded, containing gravity coupled to the coefficients to find,

$$\nabla_\mu (T_s)^\mu{}_0 = \frac{\ddot{a}}{a} \left(\frac{3}{2} \dot{s}_{00} + 6 s_{00} \frac{\dot{a}}{a} \right) + 3 s_{00} \frac{\dddot{a}}{a}. \tag{3.77}$$

The right hand side containing matter is worked out to give,

$$\nabla_\mu (T_M)^\mu{}_0 = -\dot{\rho} - 3 \frac{\dot{a}}{a} \left(\rho + p \right). \tag{3.78}$$

The next subsections continue to investigate the cosmological solutions through different choices in the functional forms for coefficient s_{00}. The first example will have

the matter stress-energy tensor be conserved by itself, such that (3.78) vanishes. In contrast, the second example will assume the entire conservation expression in (3.76) holds while not satisfying (3.78).

3.4.1 First Cosmological Example: Conserving the Matter Stress-Energy Tensor

In this example, the matter stress-energy tensor alone is assumed to be conserved and thus (3.78) vanishes. A note on terminology: when matter energy equations are conserved, it is referred to as "on-shell". The condition then allows one to solve for s_{00},

$$-\frac{\ddot{a}}{a}\left(\frac{3}{2}\dot{s}_{00} + 6s_{00}\frac{\dot{a}}{a}\right) = 3s_{00}\frac{\dddot{a}}{a}. \tag{3.79}$$

When defining s_{00} as

$$s_{00} = \frac{\zeta}{a^4\ddot{a}^2}, \tag{3.80}$$

an analytical solution can be found, where ζ is an arbitrary constant. Yet this solution was problematic for a couple reasons. If one chooses the acceleration $\ddot{a} = 0$, matching standard cosmological solutions, one would find that the solution diverges. If one chooses the acceleration $\ddot{a}$ to be a constant, the scale factor describing the size of the universe would naturally decrease for an expanding universe. Even more so, when substituting (3.80) into the Friedman expressions (3.72) and (3.73), one discovers up to fourth order time derivatives on the scale factor without making any approximations. When attempting to use a perturbative method, assuming that the dimensionless s_{00} is significantly smaller than unity, an unbounded growth is seen in (3.80). Therefore, the next step pursues a different choice in the coefficient.

3.4.2 Second Cosmological Example: A Modified Conservation Law

The second cosmological example assumes the entire conservation expression in (3.76) holds. The coefficient s_{00} is chosen to remain arbitrary, yet it is enforced that $\dot{s}_{00} = 0$. The result is a modified matter conservation law, where the solutions show a modified evolution of matter. As before, the modified Friedman equations are derived,

$$
\begin{aligned}
\left(\frac{\dot{a}}{a}\right)^2 &= \frac{\kappa\rho}{3(1-\frac{3}{2}s_{00})} - \frac{k}{a^2(1-s_{00})} \\
&\quad + \frac{\kappa p s_{00}}{(2-3s_{00})(1-s_{00})}, \\
\frac{\ddot{a}}{a} &= -\frac{\kappa(\rho+3p)}{6(1-\frac{3}{2}s_{00})}.
\end{aligned}
\tag{3.81}
$$

Scalings can be seen of the usual terms involving the evolution of the scale factor and the acceleration, along with the additional $\ddot{a}/a$ terms that were also found in the first example and a modified pressure term.

Combining equations (3.81) and (3.78) to derive the modified conservation law, or continuity equation,

$$
\dot{\rho} + 3\frac{\dot{a}}{a}f(w, s_{00})\rho = 0,
\tag{3.82}
$$

where $f(w, s_{00})$ is the auxiliary equation defined as

$$
f(w, s_{00}) = \frac{2(1+w-s_{00})}{2+s_{00}(3w-2)}.
\tag{3.83}
$$

One can retrieve the GR limit for when $f \to 1+w$ as $s_{00} \to 0$. Solving for the energy density through integration of the modified continuity equation gives,

$$
\rho = \rho_0 \left(\frac{a}{a_0}\right)^{-3f(w, s_{00})},
\tag{3.84}
$$

where the present day scale factor and energy density is a_0 and ρ_0 respectively. When assuming a universe dominated by matter, i.e., $w = 0$, and setting the auxiliary equation to unity, $f = 1$, no modification to the cosmological evolution ρ^{-3} is found. Yet assuming radiation-dominated universe, $w = 1/3$, a modified evolution equation similar to other modifications to GR is found [53, 113, 106].

The evolution of this matter is investigated and the Friedman equations are derived, using the dimensionless density parameters of Ω_m for matter, Ω_r for radiation, Ω_Λ for the cosmological constant Λ and Ω_k for the curvature of the universe. This describes the ratio of observed energy-matter density to that of the critical $\rho_c = 3H^2/8\pi G_N$. An expression using the Hubble parameter $H = \dot{a}/a$ in terms of the cosmological constants is found. When dividing the Friedman equations (3.81) by the current Hubble constant squared, $H_0^2 = \dot{a}_0^2/a_0^2$, and combining with the evolution equation (3.84), the following expression is found:

$$\frac{H^2}{H_0^2} = \Omega_{m0}a^{-3} + \Omega_{r0}a^{-4\eta_r} + \Omega_{\Lambda0}a^{\eta_\Lambda} + \Omega_{k0}a^{-2}, \tag{3.85}$$

where the definitions $\eta_r = (1 - \frac{3}{4}s_{00})/(1 - \frac{1}{2}s_{00})$ and $\eta_\Lambda = 3s_{00}/(1 - \frac{5}{2}s_{00})$ are used, and the subscripts including 0 refer to the present epoch t_0. There are modifications in the evolution of the radiation and cosmological constant terms, while the terms involving matter and curvature do not differ from GR. The exponent for radiation shows an altered evolution rate while more interesting, the cosmological constant term now is time dependent. One can then find the modified expressions for each of the density parameters,

$$\Omega_X = \frac{\kappa\rho}{3H^2(1 - \frac{3}{2}s_{00})}^{\frac{2+(3w-2)s_{00}}{2(1-s_{00})}}, \tag{3.86}$$

where $X = m, r, \Lambda, k$ for matter, radiation, the cosmological constant, or curvature, respectively. For the curvature, this expression would be $\Omega_k = -k/[H^2(1 - s_{00})]$. Also

note that any scalings with s_{00} are absorbed into the density parameters.

Looking at the expression for the acceleration of the scale factor in terms of the density parameters,

$$
\begin{aligned}
\frac{\ddot{a}}{aH_0^2} =\ & -\tfrac{1}{2}\Omega_{m0}a^{-3} - \Omega_{r0}\tfrac{2(1-s_{00})}{2-s_{00}}a^{-4\eta_r} \\
& +\Omega_{\Lambda 0}\tfrac{2(1-s_{00})}{2-5s_{00}}a^{\eta_\Lambda},
\end{aligned}
\tag{3.87}
$$

where one cannot remove the modified scalings by simply re-defining constants.

From the results in (3.87), rough constraints are found for the coefficient s_{00} by calculating the deceleration parameter $q \equiv -(\ddot{a}/a)H^{-2}$. For present day $t = t_0$, the value of q is negative to match the observed increasing acceleration of the universe, giving the inequality,

$$
-\tfrac{1}{2}\Omega_{m0} - \Omega_{r0}\tfrac{2(1-s_{00})}{2-s_{00}} + \Omega_{\Lambda 0}\tfrac{2(1-s_{00})}{2-5s_{00}} > 0.
\tag{3.88}
$$

The coefficient from the density parameters could not be decoupled, and a more complete analysis is required for using cosmological data [98]. In the least, the effects on the cosmological scale factor are shown by solving the Friendman equations (3.85) as displayed in the plot in Fig. 3.2.

3.5 Mapping to models and frameworks

In theory, any model derived from an action that describes coordinate-independent Lorentz violations can be expected to be contained within the SME framework. As already mentioned, there have been many works that have successfully matched, either completely or in partial, modified physics models to terms within the SME framework. Within the gravity sector, such models include those with dynamical
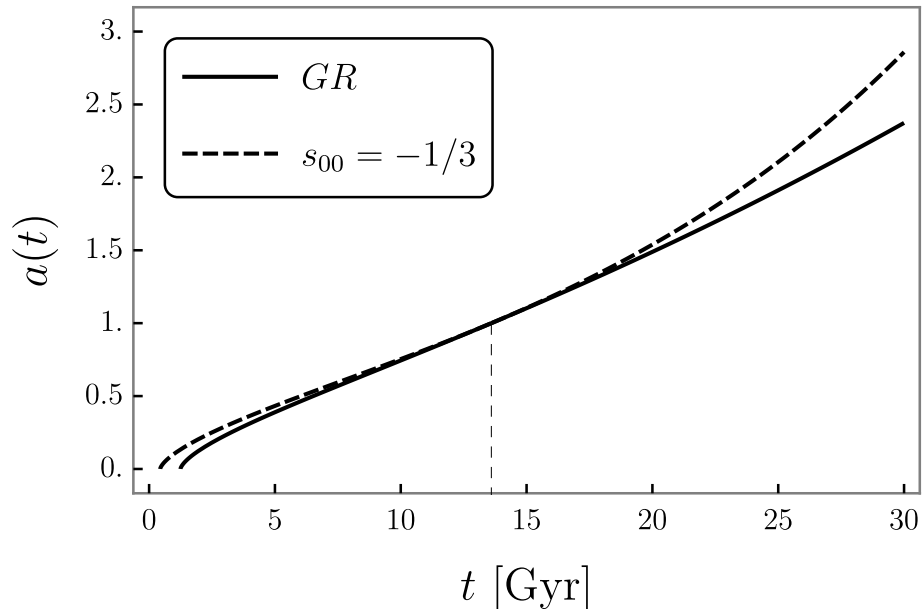
Figure 3.2: In the case of the flat FLRW universe, solutions for the scale factor are compared between the case of GR and the case for constant s_{00}. It is assumed that $\Omega_{r0} = 0$, $\Omega_{m0} = 0.31$, and $\Omega_{\Lambda 0} = 0.69$. The dashed vertical line represents the present day.

vectors and tensors, noncommutative geometry and massive gravity models [31].

In particular, Hořava-Lifshitz (HL) gravity is a proposed model that breaks Lorentz symmetry in the ultraviolet limit yet allows for a renormalizable quantum gravity [59, 122]. In this model, time and space do not evolve in the same manner, where there are only higher order spatial derivatives, thus avoiding Ostrogradsky instabilities and ghosts that can come with higher order time derivatives. Using the 3+1 format for $\mathcal{L}_S$ in (3.27), on can attempt to find a match to the HL model, also in the 3+1 framework. A simple version of the Lagrange density for HL gravity is,

$$\mathcal{L}_H = \alpha\sqrt{\gamma}(K_{ij}K^{ij} - \lambda K^2 + \xi\mathcal{R} + \eta a^i a_i + \ldots) \tag{3.89}$$

where higher the possible higher order spatial derivative terms and the matter sec-

tor terms are within the ellipses [13, 50]. For simplicity, the coupling constant has
been set to $2\kappa = 1$. To better understand how to find a match between (3.89) and
terms within the SME framework, aspects from both expressions are cpompared. The
SME framework adds observer covariant terms to terms of known physics that have
unknown coefficients with indices. The LH model places scalar parameters in front
of GR terms, which can be seen with early kinematic approaches to testing special
relativity [128]. In order to find mappings to these HL terms, components of SME
coefficients are chosen in a particular coordinate system, which has been done with
other models [79, 77].

The equation (3.89) has a form that is in a rotationally isotropic frame. Then the
second case study is used for a local Lorentz frame, assuming the isotropic limit and
coefficients $s_{\mu\nu}$ that are constant in time and space. Focusing on the term with the
contraction $s_{\mu\nu}R^{\mu\nu}$ the form is found,

$$\mathcal{L}_2 = \alpha\sqrt{\gamma}\Big[\mathcal{R}\left(1 + \tfrac{1}{3}s\right) + \left(K^{ij}K_{ij} - K^2\right)\left(1 - s_{\bar{0}\bar{0}}\right)\Big]. \tag{3.90}$$

Initially, the terms $K^{ij}K_{ij} - K^2$ would need to be broken apart to match to the terms
$K_{ij}K^{ij} - \lambda K^2$ in the HL model. Yet, this could not be done with the $s_{\mu\nu}$-type terms
alone, but the SME is a limit to spontaneous symmetry breaking and one can add
dynamical terms to the action as needed [22]. Looking at an action containing higher

order terms,

$$
\begin{aligned}
\mathcal{L}_s \;=\;\; & \frac{\sqrt{-g}}{2\kappa}\Big[a_1 s^\lambda{}_\lambda R + a_2 s_{\mu\nu} R^{\mu\nu} \\
& + a_3 \tfrac{1}{2}(\nabla_\mu s_{\nu\lambda})(\nabla^\mu s^{\nu\lambda}) + a_4 \tfrac{1}{2}(\nabla_\mu s^{\mu\lambda})(\nabla_\lambda s^\beta{}_\beta) \\
& + a_5 \tfrac{1}{2}(\nabla_\mu s^{\mu\lambda})(\nabla_\nu s^\nu{}_\lambda) + a_6 \tfrac{1}{2}(\nabla_\mu s^\nu{}_\nu)(\nabla^\mu s^\lambda{}_\lambda) \\
& + a_7 s_{\mu\nu} s_{\kappa\lambda} R^{\mu\kappa\nu\lambda} + a_8 s_{\mu\nu} s^\mu{}_\lambda R^{\nu\lambda} \\
& + a_9 s^\lambda{}_\lambda s_{\mu\nu} R^{\mu\nu} + a_{10} s^{\mu\nu} s_{\mu\nu} R + a_{11} s^\lambda{}_\lambda s^\mu{}_\mu R \Big],
\end{aligned}
$$

(3.91)

where a_n are dimensionless coupling parameters. The first two terms are the familiar, linear in $s_{\mu\nu}$, yet the remaining terms are all second order in the coefficient[22]. Using the knowledge that $s_{\mu\nu}$ are considered as small and dimensionless, second order terms are considered a special case and are not contained within the minimal SME portion of the framework (see Table V and Table VII of Ref. [74]). These higher order terms, as symmetric 2-tensors, have been considered in other modified physics models [128]. There are other terms not shown in (3.91) including those are were found to equate to mentioned terms after performing an integration by parts on the action as in

$$
\begin{aligned}
0 \;=\;\; & \int d^4 x \sqrt{-g}\big(\nabla_\gamma s_{\alpha\beta} \nabla^\beta s^{\alpha\gamma} - \nabla_\beta s_\alpha{}^\beta \nabla_\gamma s^{\alpha\gamma} \\
& - s_{\alpha\beta} s_{\gamma\delta} R^{\alpha\delta\beta\gamma} + s_{\alpha\delta} s^\alpha{}_\beta R^{\delta\beta}\big).
\end{aligned}
$$

(3.92)

For spontaneous symmetry breaking, one could omit potential terms $V = V(s_\mu{}^\mu, s_{\mu\nu} s^{\mu\nu}, \ldots)$ [108]. After integration by parts, the particular terms in (3.91) that can be used to map to HL terms. In particular,

$$
\Delta\mathcal{L}_s = a_{12} \frac{\sqrt{-g}}{2\kappa} (s^{\mu\nu} \nabla_\mu s_{\nu\lambda})(s^{\kappa\rho} \nabla_\kappa s_\rho{}^\lambda).
$$

(3.93)

Writing out the Lagrange density found in terms of the SME coefficients that are matched to the HL form (3.89),

$$
\begin{aligned}
\mathcal{L}_{SME,Match} \;=\;& \alpha\sqrt{\gamma}\big[\mathcal{R}\left(1+\tfrac{1}{3}s\right)+K^{ij}K_{ij}-K^2 \\
&+a_5\tfrac{1}{2}(\nabla_\mu S^{\mu\lambda})(\nabla_\nu S^{\nu}{}_\lambda) \\
&+a_{12}(S^{\mu\nu}\nabla_\mu S_{\nu\lambda})(S^{\kappa\rho}\nabla_\kappa S_\rho{}^{\lambda})\big].
\end{aligned}
\tag{3.94}
$$

where definition $S_{\mu\nu}$ is used as the set of new coefficients and all terms are nondynamical. Further applying a specific coordinate frame where the only nonzero component of $S_{\mu\nu}$ is the pure time component that must be set to unity, i.e., $S_{00} = 1$, the form is found to be

$$
\begin{aligned}
\mathcal{L}_{SME,Match} \;=\;& \alpha\sqrt{\gamma}\big[\mathcal{R}\left(1+\tfrac{1}{3}s\right)+K^{ij}K_{ij} \\
&-K^2(1+\tfrac{1}{2}a_5)+\left(a_{12}+\tfrac{1}{2}a_5\right)a^i a_i\big].
\end{aligned}
\tag{3.95}
$$

This choice in $S_{\mu\nu}$ is equivalent to $S_{\mu\nu} = n_\mu n_\nu$ when applying the vierbein (3.24), and has been used to match HL gravity to vector models in previous works [62, 63]. Other literature present matter couplings that have been matched to the matter sector for the HL gravity model [31]. The following choices can be made for the coefficients: $\lambda = 1 + a_5/2$, $\xi = 1 + s/3$, and $\eta = a_{12} + a_5/2$, then the (3.95) will match the HL form of (3.89).

As final notes for consideration, the results of this work use subsets of the SME framework in the case of explicit symmetry breaking, which produce extra degrees of freedom when compared to the normal gauge of GR. Thus it would be interesting to explore future investigations into approaches to quantum gravity [45] and the

"problem of time" within the SME [19, 87]. This work also provides the first steps in investigating the degrees of freedom and constraints that are imposed by the Bianchi identities, which stems from the underlying geometrical framework [74]. This remains an open problem to understand. For example, when considering an effective classical Hamiltonian within a homogeneous spacetime and vanishing potential curvature, the cosmological solutions from section 3.4 are derived. The Hamiltonian is then

$$H = \frac{\kappa \alpha^5 (\alpha^2 - s_{00}) p_\alpha^2}{3a^3 s_{00}^2} - \frac{\kappa \alpha^4 p_\alpha p_a}{3a^2 s_{00}} + H_M, \tag{3.96}$$

where H_M is the matter Hamiltonian and the variables are $a(t)$, $\alpha(t)$, and their conjugate momenta $p_a = \partial L / \partial \dot{a}$ and $p_\alpha = \partial L / \partial \dot{\alpha}$ This alters the Wheeler-deWitt equation, which instead has α as a nondynamical parameter and includes a p_α^2 [37, 56]. In (3.96), the usual Hamilton constraint is no longer present and the wave function $\Psi = \Psi(a, \alpha, ..., t)$ would become time dependent, evolving as it would in Schrödinger equation $i \partial_t \Psi = H \Psi$.

Chapter 4

Conclusions

The work in this thesis tests fundamental spacetime symmetries for GR and the SM through an effective field theory, the SME. This is an agnostic, model-independent framework where the focus was within the pure gravity sector.

In chapter 2, terms were implemented from the SME to test for Lorentz and CPT violations within dispersion and birefringence effects of gravitational waves. Notably, this work does not rely on posterior results produced by the LVK that assumes standard GR. Instead, modifications and symmetry-breaking parameters were implemented directly at the level before the Bayesian inference, into the templates that initially contain all parameters. In this way, the full information can be incorporated, which includes symmetry-breaking effects that is provided by the signal morphology. A joint inference across all parameters is performed and constraints on the order of $\mathcal{O}(10^{-13})$m are found.

Within chapter 3, in the case of explicit symmetry breaking, the 3+1 formulation of the lowest-order terms for gravity within the SME were published for the first time. The Dirac-Hamiltonian analysis was applied for global and local Lorentz frames, where in the former produced an addition degree of freedom when compared

to that of GR. Applications to cosmological solutions show modifications to Friedmann equations, altering time-dependent scalings for density parameters including the cosmological constant, and new interpretations of Bianchi identities and conservation laws.

4.1 Outlook

Foundations were laid for a rigorous means of merging the SME framework with the LVK data analysis community. There is present implementations into new, improved algorithms within the LVK, and many more higher order terms yet to be investigated. Teh plethora of events will provide the prospect of mapping out the spacetime symmetry-breaking effects across the celestial sky. In addition, GWs from more stochastic sources such as supernovae, include different algorithms like coherent WaveBurst (cWB) [66], that have yet to be combined with the SME.

The 3+1 formulation provides general equations that can be applied to specific strong field gravity physics systems with black holes and neutron stars and possible traversable wormholes. A subset of the 3+1 formulation equations can be used to study initial value formalism, where numerical relativity techniques that include the spacetime symmetry-breaking can be incorporated with sources including CCSN. This would include the inclusion of matter such as neutrino, to create and analysis the simulated supernovae. Investigating the emergence of extra degrees of freedom for explicit symmetry breaking within the case for global background coefficients 3.3.1, might help better understand the interpretation of time when considering quantum gravity.

There are many future works one can follow from the research presented here, some exist as unfinished projects waiting to be revisited.

Chapter 5

Appendix

This appendix provides the details on the implementation of birefringence effects for gravitational waves into `LALSuite`. Files within `LALSuite` are primarily written with C, C^{++} and various `Python` packages.

5.1   LALSimulation

The following files within the `LALSimulation` are modified to include the dispersion and birefringence effects:

- `lib/LALSimInspiral.c`

- `lib/LALSimInspiral.h`

- `lib/LALSimInspiralWaveformParams.c`

- `lib/LALSimInspiralWaveformParams.h`

Within the C-file `lib/LALSimInspiral.c`, which calls in LAL parameters to be used, an additional function is implemented that introduces isotropic birefringence effects in the frequency domain (FD) for the GW waveform:

```
/* Function to introduce isotropic birefringent Lorentz violating
   effects in FD waveform; implementation is via Eq. 24 along
   with the associated equations for finding the phases and
   angles in arxiv 1905.00409*/
int XLALSMEIsotropicBirefringence(
                                    COMPLEX16FrequencySeries **
                                        hptilde, /**< Frequency-
                                        domain waveform h+ */
                                    COMPLEX16FrequencySeries **
                                        hctilde, /**< Frequency-
                                        domain waveform hx */
                                    LALDict *LALparams
                                                    /**< LAL
                                        dictionary containing
                                        accessory parameters */
                                    )
{
    REAL8 f0, f, df;
    COMPLEX16 hplus, hcross; /*tmpExp, lists of variavles removed*/
    REAL8 beta, betanf;  /*dPhiPref, tmpVal, zeta, Mc, eta, M*/
    UINT4 len, i;

    len = (*hptilde)->data->length;
    if ((*hctilde)->data->length != len) {
        XLALPrintError("Lengths of plus and cross polarization series
            do not agree \n");
        XLAL_ERROR(XLAL_EBADLEN);
    }


    f0 = (*hptilde)->f0;
    if ((*hctilde)->f0 != f0) {
```

```
      XLALPrintError("Starting frequencies of plus and cross
          polarization series do not agree \n");
      XLAL_ERROR(XLAL_EINVAL);
  }


  df = (*hptilde)->deltaF;
  if ((*hctilde)->deltaF != df) {
    XLALPrintError("Frequency steps of plus and cross polarization
          series do not agree \n");
    XLAL_ERROR(XLAL_EINVAL);
  }


 REAL8 SME_kv5_00_eff =
     XLALSimInspiralWaveformParamsLookupNonGRSMEKv500Eff(LALparams
     ); /* Effective SME coefficient in  metres ^d-4*/
 REAL8 SME_d = 5 ; /* the mass dimension of the SME operator */
//printf("XLALSMEIsotropicBirefringence SME_kv5_00_eff %4.1f",
    SME_kv5_00_eff);



UINT4 k = 0;
  if (f0 == 0.0)
    k=1;


 // betanf = 2 * pow(LAL_PI, SME_d -3. -0.5) *  SME_kv5_00_eff / (
     pow(LAL_C_SI, SME_d - 3.));
 betanf = 2 * pow(LAL_PI, 1.5) *  SME_kv5_00_eff / LAL_C_SI;

  for (i=k; i<len; i++) {
    f = f0 + i * df;
    beta = betanf * pow(f, SME_d - 3.);
```

```
    hplus = (*hptilde)->data->data[i] * cos(beta) - (*hctilde)->
        data->data[i] * sin(beta);

    hcross = (*hctilde)->data->data[i] * cos(beta) + (*hptilde)->
        data->data[i] * sin(beta);

    (*hptilde)->data->data[i] = hplus;

    (*hctilde)->data->data[i] = hcross;
  }
  return XLAL_SUCCESS;
}
```

The associated `C` library file `LALSimInspiral.h` also has an additional function:

```
/* Function to introduce isotropic birefringent Lorentz violating
   effects in FD waveform */
int XLALSMEIsotropicBirefringence(COMPLEX16FrequencySeries **
    hptilde, COMPLEX16FrequencySeries **hctilde, LALDict *
    LALparams);
```

The `lib/LALSimInspiralWaveformParams.c` file generates definitions for different parameters included in waveforms. There are three locations where additional definitions are inserted for the SME symmetry-breaking parameter. One is within the section `INSERT FUNCTIONS`,

```
    DEFINE_INSERT_FUNC(NonGRSMEKv500Eff, REAL8, "kv5_00_eff", 0)
    DEFINE_INSERT_FUNC(NonGRSMELogKv500Eff, REAL8, "log_kv5_00_eff
        ", 0)
```

another within the section `LOOKUP FUNCTIONS`,

```
    DEFINE_LOOKUP_FUNC(NonGRSMEKv500Eff, REAL8, "kv5_00_eff", 0)
    DEFINE_LOOKUP_FUNC(NonGRSMELogKv500Eff, REAL8, "log_kv5_00_eff
        ", 0)
```

and the last within the section `ISDEFAULT FUNCTIONS`:

```
    DEFINE_ISDEFAULT_FUNC(NonGRSMEKv500Eff, REAL8, "kv5_00_eff",
        0)
    DEFINE_ISDEFAULT_FUNC(NonGRSMELogKv500Eff, REAL8, "
        log_kv5_00_eff", 0)
```

The associated library file `LALSimInspiralWaveformParams.h` also has three additions, analogous to above:

```
int XLALSimInspiralWaveformParamsInsertEnableSME(LALDict *params,
    REAL8 value);
int XLALSimInspiralWaveformParamsInsertNonGRSMEKv500Eff(LALDict *
    params, REAL8 value);
int XLALSimInspiralWaveformParamsInsertNonGRSMELogKv500Eff(LALDict
    *params, REAL8 value);
```

...

```
REAL8 XLALSimInspiralWaveformParamsLookupEnableSME(LALDict *params
    );
REAL8 XLALSimInspiralWaveformParamsLookupNonGRSMEKv500Eff(LALDict
    *params);
REAL8 XLALSimInspiralWaveformParamsLookupNonGRSMELogKv500Eff(
    LALDict *params);
```

...

```
int XLALSimInspiralWaveformParamsEnableSMEIsDefault(LALDict *
    params);
int XLALSimInspiralWaveformParamsNonGRSMEKv500EffIsDefault(LALDict
    *params);
int XLALSimInspiralWaveformParamsNonGRSMELogKv500EffIsDefault(
    LALDict *params);
```

The library has an additional function that is used to enable the SME symmetry-breaking effects.

5.2 LALInference

The following files within the `LALInference` package are modified to include the dispersion and birefringence effects:

- `LALInferenceInitCBC.c`

- `LALInferenceProposal.c`

- `LALInferenceTemplate.c`

- `LALInferenceReadData.c`

The file `LALInferenceInitCBC.c` is edited to include the flag for the symmetry-breaking effects from the SME. It functions to call for initiating inference runs with the symmetry-breaking parameter. Under the function,

```
LALInferenceModel *LALInferenceInitCBCModel(
    LALInferenceRunState *state) {
char help[]="\
```

within the `Template Arguments`, the additional insertion is:

```
        (--sme) this flag activates the SME parameters kv5* in the
            inference run.\n\
```

Within the `LALInferenceProposal.c` file, additional parameters are included in a list of initial parameters used to generate the waveform:

```
static const char *intrinsicNames[] = {...,"LIV_A_sign","
    kv5_00_eff", "log_kv5_00_eff",NULL};
```

Likewise, a parameter list defined within `LALInferenceTemplate.c` is modified to include the additional parameters:

```
const char list_extra_parameters[40][16] = {...,"LIV_A_sign","
    kv5_00_eff","log_kv5_00_eff"};
```

```
        const UINT4 N_extra_params = 40;
```

It is important to update the number of parameters listed (see two locations above where the number 40 appears). The last mentioned file `LALInferenceReadData.c` provides definitions and responses for injection input commands. The first addition is within the `Data Parameters`, where the options for reading and generating data are provided:

```
    (--inj-sme)                 Set to 1. to activate SME
        injection \n\
    (--inj-kv5_00_eff)          value of kv5_00_eff to be injected
        \n\
    (--inj-log_kv5_00_eff)      value of log_kv5_00_eff to be
        injected\n\
```

Additional conditional statements and functions are used to ensure the correction SME parameters are inserted into an inference run:

```
    //      if(LALInferenceGetProcParamVal(commandLine,"--
        inj-kv5_00_eff") && LALInferenceGetProcParamVal(
        commandLine,"--inj-log_kv5_00_eff")) {
    //      fprintf(stderr, "ERROR: You have injected --inj-
        kv5_00_eff and --inj-log_kv5_00_eff. The first is to
        sample kv5_00_eff with a flat prior, the second is to
        sample kv5_00_eff with a log prior. You must chose only
        one!\n");
    //          exit(1);
    //      }
    //      if(LALInferenceGetProcParamVal(commandLine,"--inj-
        log_kv5_00_eff")) {
    //          log_kv5_00_eff = atof(LALInferenceGetProcParamVal(
        commandLine,"--inj-log_kv5_00_eff")->value);
```

```
//          fprintf(stdout,"ReadData:
   LALInferenceInjectInspiralSignal / log_kv5_00_eff set to
    %f\n",kv5_00_eff);
//      }


if(LALInferenceGetProcParamVal(commandLine,"--inj-sme") ||
   LALInferenceGetProcParamVal(commandLine,"--inj-
   kv5_00_eff")) {
  fprintf(stderr, "WARNING: You are injecting SME parameters
       on a time-domain waveform. SME modifications are only
       supported for FD waveforms") ;
}
```

A similar block of code to the above is also added for the `log_kv5_00_eff` coefficient. Further conditional statements and functions ensure a valid injection of the SME parameter:

```
// Inject kv5_00_eff parameters for SME analysis
REAL8 sme = 0.;
REAL8 kv5_00_eff = 0.;



if(LALInferenceGetProcParamVal(commandLine,"--inj-sme")) {
  if( (!LALInferenceGetProcParamVal(commandLine,"--inj-
      kv5_00_eff")) || ( atof(LALInferenceGetProcParamVal(
      commandLine,"--inj-sme")->value) == 1. && atof(
      LALInferenceGetProcParamVal(commandLine,"--inj-kv5_00_eff
      ")->value) == 0.) ){
    fprintf(stderr,"WARNING: You are asking SME modifications
        but the injected parameter kv5_ij is 0.! Is this what
        you want?\n") ;
  }
```

```
    sme = atof(LALInferenceGetProcParamVal(commandLine,"--inj-sme
        ")->value);
    XLALSimInspiralWaveformParamsInsertEnableSME(LALpars, sme);
 }


if(LALInferenceGetProcParamVal(commandLine,"--inj-kv5_00_eff"))
    {
  if( (!LALInferenceGetProcParamVal(commandLine,"--inj-sme")) ||
        ( atof(LALInferenceGetProcParamVal(commandLine,"--inj-sme
      ")->value) == 0. && atof(LALInferenceGetProcParamVal(
      commandLine,"--inj-kv5_00_eff")->value) != 0.)) {
     fprintf(stderr,"WARNING: You are injecting a non-0 value of
         kv5_ij but SME is not enabled, modifications will not be
          injected. Use '--inj-sme 1' to include the SME
         modifications on the injected waveform. \n") ;
   }
   kv5_00_eff = atof(LALInferenceGetProcParamVal(commandLine,"--
       inj-kv5_00_eff")->value);
   XLALSimInspiralWaveformParamsInsertNonGRSMEKv500Eff(LALpars,
      kv5_00_eff);
}


//  fprintf(stdout,"ReadData:InjectFD / LookupEnableSME = %f\n",
     XLALSimInspiralWaveformParamsLookupEnableSME(LALpars));
//  fprintf(stdout,"ReadData:InjectFD / LookupNonGRSMEKv500Eff =
     %f\n", XLALSimInspiralWaveformParamsLookupNonGRSMEKv500Eff(
     LALpars));
```

Bibliography

[1] B. P. Abbott et al. "Gravitational Waves and Gamma-rays from a Binary Neutron Star Merger: GW170817 and GRB 170817A". In: *Astrophys. J. Lett.* 848.2 (2017), p. L13. DOI: `10.3847/2041-s̄8213/aa920c`. arXiv: `1710.05834` `[astro-ph.HE]`.

[2] B. P. Abbott et al. "Gravitational Waves and Gamma-Rays from a Binary Neutron Star Merger: GW170817 and GRB 170817A". In: *The Astrophysical Journal* 848.2 (Oct. 2017), p. L13. DOI: `10.3847/2041-s̄8213/aa920c`. URL: `https://doi.org/10.3847/2041-s̄8213/aa920c`.

[3] B. P. Abbott et al. "Observation of Gravitational Waves from a Binary Black Hole Merger". In: *Phys. Rev. Lett.* 116 (6 Feb. 2016), p. 061102. DOI: `10.1103/PhysRevLett.116.061102`. URL: `https://link.aps.org/doi/10.1103/PhysRevLett.116.061102`.

[4] B. P. Abbott et al. "Tests of general relativity with GW150914". In: *Phys. Rev. Lett.* 116.22 (2016). [Erratum: Phys.Rev.Lett. 121, 129902 (2018)], p. 221101. DOI: `10.1103/PhysRevLett.116.221101`. arXiv: `1602.03841` `[gr-qc]`.

[5] B. P. Abbott et al. "Tests of General Relativity with the Binary Black Hole Signals from the LIGO-Virgo Catalog GWTC-1". In: *Phys. Rev. D* 100.10

(2019), p. 104036. DOI: `10.1103/PhysRevD.100.104036`. arXiv: `1903.04467`
`[gr-qc]`.

[6] B. P. et al Abbott. "GWTC-1: A Gravitational-Wave Transient Catalog of
Compact Binary Mergers Observed by LIGO and Virgo during the First and
Second Observing Runs". In: *Phys. Rev. X* 9 (3 Sept. 2019), p. 031040. DOI:
`10.1103/PhysRevX.9.031040`. URL: `https://link.aps.org/doi/10.1103/`
`PhysRevX.9.031040`.

[7] R. Abbott et al. "GWTC-3: Compact Binary Coalescences Observed by LIGO
and Virgo During the Second Part of the Third Observing Run". In: (Nov.
2021). arXiv: `2111.03606 [gr-qc]`.

[8] R. Abbott et al. *Tests of General Relativity with GWTC-3*. Dec. 2021. arXiv:
`2112.06861 [gr-qc]`.

[9] R. Abbott et al. "Tests of General Relativity with Binary Black Holes from the
second LIGO-Virgo Gravitational-Wave Transient Catalog". In: (Oct. 2020).
arXiv: `2010.14529 [gr-qc]`.

[10] A. Addazi et al. "Quantum gravity phenomenology at the dawn of the multi-
messenger era—A review". In: *Prog. Part. Nucl. Phys.* 125 (2022), p. 103948.
DOI: `10.1016/j.ppnp.2022.103948`. arXiv: `2111.05659 [hep-ph]`.

[11] B P Abbott et al. "LIGO: the Laser Interferometer Gravitational-Wave Ob-
servatory". In: *Reports on Progress in Physics* 72.7 (June 2009), p. 076901.
DOI: `10.1088/0034-s̄4885/72/7/076901`. URL: `https://doi.org/10.1088%`
`2F0034-s̄4885%2F72%2F7%2F076901`.

[12] B. P. Abbott et al. "GW150914: The Advanced LIGO Detectors in the Era
of First Discoveries". In: *Physical Review Letters* 116.13 (Mar. 2016). DOI:

10.1103/physrevlett.116.131103. URL: https://doi.org/10.1103%
2Fphysrevlett.116.131103.

[13]   D. Blas et al. "Consistent Extension of Hořava Gravity". In: *Phys. Rev. Lett.*
181302 (104 May 2010). DOI: 10.1103/PhysRevLett.104.181302.

[14]   Ling Sun et al. "Characterization of systematic error in Advanced LIGO cal-
ibration". In: *Classical and Quantum Gravity* 37.22 (Oct. 2020), p. 225008.
DOI: 10.1088/1361-6382/abb14e.

[15]   The LIGO Scientific Collaboration et al. *GWTC-3: Compact Binary Coales-
cences Observed by LIGO and Virgo During the Second Part of the Third
Observing Run.* 2021. arXiv: 2111.03606 [gr-qc].

[16]   V. Alan Kostelecký and Robertus Potting. "CPT and strings". In: *Nuclear
Physics B* 359.2 (1991), pp. 545–570. ISSN: 0550-3213. DOI: https://doi.org/
10.1016/0550-3213(91)90071-5. URL: https://www.sciencedirect.
com/science/article/pii/0550321391900715.

[17]   Brett Altschul, Quentin G. Bailey, and V. Alan Kostelecký. "Lorentz violation
with an antisymmetric tensor". In: *Phys. Rev. D* 81 (6 Mar. 2010), p. 065028.
DOI: 10.1103/PhysRevD.81.065028. URL: https://link.aps.org/doi/10.
1103/PhysRevD.81.065028.

[18]   Kevin M. Amarilo et al. "Modification in Gravitational Waves Production
Triggered by Spontaneous Lorentz Violation". In: *PoS* BHCB2018 (2019). Ed.
by Rita Cassia Anjos and Carlos Henrique Coimbra Araujo, p. 015. DOI: 10.
22323/1.329.0015.

[19]   Edward Anderson. *The Problem of Time in Quantum Gravity.* 2012. arXiv:
1009.2157 [gr-qc].

[20] H. Andresen et al. "Gravitational Wave Signals from 3D Neutrino Hydrodynamics Simulations of Core-Collapse Supernovae". In: *Mon. Not. Roy. Astron. Soc.* 468.2 (2017), pp. 2032–2051. DOI: 10.1093/mnras/stx618. arXiv: 1607.05199 [astro-ph.HE].

[21] Claudio Teitelboim Andrew Hanson Tulio Regge. *Cinstrained Hamiltonian Systems*. Accademia Nazionale Dei Lince, 1976.

[22] Quentin G. Bailey. *Recent Developments in Spacetime-Symmetry tests in Gravity*. 2019. arXiv: 1906.08657 [gr-qc].

[23] Quentin G. Bailey, Alan Kostelecký, and Rui Xu. "Short-range gravity and Lorentz violation". In: *Phys. Rev. D* 91.2 (2015), p. 022006. DOI: 10.1103/PhysRevD.91.022006. arXiv: 1410.6162 [gr-qc].

[24] Quentin G. Bailey and V. Alan Kostelecký. "Signals for Lorentz violation in post-Newtonian gravity". In: *Phys. Rev. D* 74 (4 Aug. 2006), p. 045001. DOI: 10.1103/PhysRevD.74.045001. URL: https://link.aps.org/doi/10.1103/PhysRevD.74.045001.

[25] Thomas W. Baumgarte and Stuart L. Shapiro. *Numerical Relativity: Solving Einstein's Equations on the Computer*. 2010.

[26] Emanuele Berti, Kent Yagi, and Nicolás Yunes. "Extreme Gravity Tests with Gravitational Waves from Compact Binary Coalescences: (I) Inspiral-Merger". In: *Gen. Rel. Grav.* 50.4 (2018), p. 46. DOI: 10.1007/s10714-s018-s2362-s8. arXiv: 1801.03208 [gr-qc].

[27] T. H. Bertschinger, Natasha A. Flowers, and Jay D. Tasson. "Observer and Particle Transformations and Newton's Laws". In: *6th Meeting on CPT and Lorentz Symmetry*. Aug. 2013. DOI: 10.1142/9789814566438_0072. arXiv: 1308.6572 [hep-ph].

[28] T. H. Bertschinger et al. "Spacetime Symmetries and Classical Mechanics". In: *Symmetry* 11.1 (2019). ISSN: 2073-8994. DOI: 10.3390/sym11010022. URL: https://www.mdpi.com/2073-s̄8994/11/1/22.

[29] Robert Bluhm. "Explicit versus spontaneous diffeomorphism breaking in gravity". In: *Phys. Rev. D* 91 (6 Mar. 2015), p. 065034. DOI: 10.1103/PhysRevD.91.065034. URL: https://link.aps.org/doi/10.1103/PhysRevD.91.065034.

[30] Robert Bluhm. "Gravity Theories with Background Fields and Spacetime Symmetry Breaking". In: *Symmetry* 9.10 (Oct. 2017), p. 230. DOI: 10.3390/sym9100230. URL: https://doi.org/10.3390/sym9100230.

[31] Robert Bluhm, Hannah Bossi, and Yuewei Wen. "Gravity with explicit spacetime symmetry breaking and the standard model extension". In: *Physical Review D* 100.8 (Oct. 2019). DOI: 10.1103/physrevd.100.084022. URL: https://doi.org/10.1103/physrevd.100.084022.

[32] Robert Bluhm, Shu-Hong Fung, and V. Alan Kostelecký. "Spontaneous Lorentz and diffeomorphism violation, massive modes, and gravity". In: *Physical Review D* 77.6 (Mar. 2008). DOI: 10.1103/physrevd.77.065020.

[33] Robert Bluhm and V. Alan Kostelecký. "Spontaneous Lorentz violation, Nambu-Goldstone modes, and gravity". In: *Phys. Rev. D* 71 (6 Mar. 2005), p. 065008. DOI: 10.1103/PhysRevD.71.065008. URL: https://link.aps.org/doi/10.1103/PhysRevD.71.065008.

[34] Robert Bluhm and Amar Š ehić. "Noether identities in gravity theories with nondynamical backgrounds and explicit spacetime symmetry breaking". In: *Physical Review D* 94.10 (Nov. 2016). DOI: 10.1103/physrevd.94.104034. URL: https://doi.org/10.1103/physrevd.94.104034.

[35] Alejandro Bohé et al. "Improved effective-one-body model of spinning, non-precessing binary black holes for the era of gravitational-wave astrophysics with advanced detectors". In: *Phys. Rev. D* 95.4 (2017), p. 044028. DOI: 10.1103/PhysRevD.95.044028. arXiv: 1611.03703 [gr-qc].

[36] Martin Bojowald. *Canonical Gravity and Applications: Cosmology, Black Holes, and Quantum Gravity.* Cambridge University Press, 2010. DOI: 10.1017/CBO9780511921759.

[37] Martin Bojowald. "Quantum cosmology: a review". In: *Reports on Progress in Physics* 78.2 (Jan. 2015), p. 023901. DOI: 10.1088/0034-s4885/78/2/023901.

[38] Yuri Bonder. "Lorentz violation in the gravity sector: Themml:math xmlns:mml="http://ww display="inline"mml:mit/mml:mi/mml:mathpuzzle". In: *Physical Review D* 91.12 (June 2015). DOI: 10.1103/physrevd.91.125002. URL: https://doi.org/10.1103/physrevd.91.125002.

[39] Stephen W. Bruenn et al. "AXISYMMETRIC AB INITIO CORE-COLLAPSE SUPERNOVA SIMULATIONS OF 12-25 iM/isub/sub STARS". In: *The Astrophysical Journal* 767.1 (Mar. 2013), p. L6. DOI: 10.1088/2041-s8205/767/1/l6.

[40] Sean M. Carroll et al. "Noncommutative Field Theory and Lorentz Violation". In: *Phys. Rev. Lett.* 87 (14 Sept. 2001), p. 141601. DOI: 10.1103/PhysRevLett.87.141601. URL: https://link.aps.org/doi/10.1103/PhysRevLett.87.141601.

[41] The LIGO Scientific Collaboration and the Virgo Collaboration et al. *GWTC-2.1: Deep Extended Catalog of Compact Binary Coalescences Observed by LIGO and Virgo During the First Half of the Third Observing Run.* 2022. arXiv: 2108.01045 [gr-qc].

[42] D. Colladay. "CPT-Violating Gravitational Orbital Perturbations". In: *CPT and Lorentz Symmetry VIII*. May 2019. DOI: `10.1142/11655`.

[43] D. Colladay and V. Alan Kostelecký. "Lorentz-violating extension of the standard model". In: *Phys. Rev. D* 58 (11 Oct. 1998), p. 116002. DOI: `10.1103/PhysRevD.58.116002`. URL: `https://link.aps.org/doi/10.1103/PhysRevD.58.116002`.

[44] Don Colladay and V. Alan Kostelecký. "CPT violation and the standard model". In: *Phys. Rev. D* 55 (11 June 1997), pp. 6760–6774. DOI: `10.1103/PhysRevD.55.6760`.

[45] Bryce S. DeWitt. "Quantum Theory of Gravity. I. The Canonical Theory". In: *Phys. Rev.* 160 (5 Aug. 1967), pp. 1113–1148. DOI: `10.1103/PhysRev.160.1113`.

[46] Harald Dimmelmeier et al. "Gravitational wave burst signal from core collapse of rotating stars". In: *Phys. Rev. D* 78 (6 Sept. 2008), p. 064056. DOI: `10.1103/PhysRevD.78.064056`. URL: `https://link.aps.org/doi/10.1103/PhysRevD.78.064056`.

[47] P.A.M. Dirac. *Lectures on Quantum Mechanics*. Belfer Graduate School of Science. Monographs series. Belfer Graduate School of Science, Yeshiva University, 1964. URL: `https://books.google.com/books?id=oQNRAAAAMAAJ`.

[48] A.F. Ferrari et al. "Lorentz violation in the linearized gravity". In: *Phys. Lett. B* 652.4 (2007), pp. 174–180. ISSN: 0370-2693. DOI: `https://doi.org/10.1016/j.physletb.2007.07.013`. URL: `https://www.sciencedirect.com/science/article/pii/S0370269307008295`.

[49] Andrew S. Friedman et al. "Improved constraints on anisotropic birefringent Lorentz invariance and CPT violation from broadband optical polarimetry of high redshift galaxies". In: *Phys. Rev. D* 102.4 (2020), p. 043008. DOI: 10.1103/PhysRevD.102.043008. arXiv: 2003.00647 [astro-ph.HE].

[50] N. Frusciante. "Cosmological constraints on Lorentz Invariance violation in gravity and dark matter". In: *Phys. Dark Univ.* 13 (7 2016).

[51] Rodolfo Gambini and Jorge Pullin. "Nonstandard optics from quantum space-time". In: *Phys. Rev. D* 59 (12 May 1999), p. 124021. DOI: 10.1103/PhysRevD. 59.124021. URL: https://link.aps.org/doi/10.1103/PhysRevD.59. 124021.

[52] David Garfinkle. *Matters of Gravity: The Newsletter of the Division of Gravitational Physics of the American Physical Society. Number 54. December 2019.* 2019. arXiv: 1912.12352 [gr-qc].

[53] M. Gasperini. "Inflation and broken Lorentz symmetry in the very early universe". In: *Physics Letters B* 163.1 (1985), pp. 84–86. ISSN: 0370-2693. DOI: https://doi.org/10.1016/0370-s2693(85)90197-s2. URL: https: //www.sciencedirect.com/science/article/pii/0370269385901972.

[54] Leıla Haegel. "Searching for new physics during gravitational waves propagation". In: *55th Rencontres de Moriond on Gravitation.* June 2021. arXiv: 2106.05097 [gr-qc].

[55] Leıla Haegel et al. "Search for anisotropic, birefringent spacetime-symmetry breaking in gravitational wave propagation from GWTC-3". In: *Phys. Rev. D* 107.6 (2023), p. 064031. DOI: 10.1103/PhysRevD.107.064031. arXiv: 2210.04481 [gr-qc].

[56]   J. J. Halliwell. *Introductory Lectures on Quantum Cosmology (1990)*. 2009. arXiv: 0909.2566 [gr-qc].

[57]   Mark Hannam et al. "Simple Model of Complete Precessing Black-Hole-Binary Gravitational Waveforms". In: *Phys. Rev. Lett.* 113.15 (2014), p. 151101. DOI: 10.1103/PhysRevLett.113.151101. arXiv: 1308.3271 [gr-qc].

[58]   James B. Hartle. *Gravity: An Introduction to Einstein's General Relativity*. illustrate. Benjamin Cummings, Jan. 2003. ISBN: 0805386629.

[59]   Petr Hoř ava. "Quantum gravity at a Lifshitz point". In: *Physical Review D* 79.8 (Apr. 2009). DOI: 10.1103/physrevd.79.084008. URL: https://doi.org/10.1103%2Fphysrevd.79.084008.

[60]   Charlie Hoy and Vivien Raymond. "PESummary: the code agnostic Parameter Estimation Summary page builder". In: *SoftwareX* 15 (2021), p. 100765. DOI: 10.1016/j.softx.2021.100765. arXiv: 2006.06639 [astro-ph.IM].

[61]   James A Isenberg and James M Nester. "The effect of gravitational interaction on classical fields: A hamilton-dirac analysis". In: *Annals of Physics* 107.1 (1977), pp. 56–81. ISSN: 0003-4916. DOI: https://doi.org/10.1016/0003-4916(77)90202-0. URL: https://www.sciencedirect.com/science/article/pii/0003491677902020.

[62]   Ted Jacobson. "Extended Hořava gravity and Einstein-aether theory". In: *Phys. Rev. D* 81 (10 May 2010), p. 101502. DOI: 10.1103/PhysRevD.81.101502.

[63]   Ted Jacobson. "Undoing the twist: The Hořava limit of Einstein-aether theory". In: *Phys. Rev. D* 89 (8 Apr. 2014), p. 081501. DOI: 10.1103/PhysRevD.89.081501.

[64] Ralf Lehnert, ed. *Testing for Lorentz-Invariance Violations Through Birefringence Effects on Gravitational Waves*. Singapur: WSP, 2020. DOI: `10.1142/11655`.

[65] Fabian Kislat and Henric Krawczynski. "Planck-scale constraints on anisotropic Lorentz and CPT invariance violations from optical polarization measurements". In: *Phys. Rev. D* 95.8 (2017), p. 083013. DOI: `10.1103/PhysRevD.95.083013`. arXiv: `1701.00437 [astro-ph.HE]`.

[66] Sergey Klimenko et al. *cWB pipeline library: 6.4.1*. Version cWB-6.4.1. Dec. 2021. DOI: `10.5281/zenodo.5798976`. URL: `https://doi.org/10.5281/zenodo.5798976`.

[67] Alan V. Kostelecky and Jay D. Tasson. "Matter-gravity couplings and Lorentz violation". In: *Phys. Rev. D* 83 (2011), p. 016013. DOI: `10.1103/PhysRevD.83.016013`. arXiv: `1006.4106 [gr-qc]`.

[68] V. Alan Kostelecky and Matthew Mewes. "Astrophysical Tests of Lorentz and CPT Violation with Photons". In: *Astrophys. J. Lett.* 689 (2008), pp. L1–L4. DOI: `10.1086/595815`. arXiv: `0809.2846 [astro-ph]`.

[69] V. Alan Kostelecky and Matthew Mewes. "Cosmological constraints on Lorentz violation in electrodynamics". In: *Phys. Rev. Lett.* 87 (2001), p. 251304. DOI: `10.1103/PhysRevLett.87.251304`. arXiv: `hep-s̄ph/0111026`.

[70] V. Alan Kostelecky and Matthew Mewes. "Lorentz-violating electrodynamics and the cosmic microwave background". In: *Phys. Rev. Lett.* 99 (2007), p. 011601. DOI: `10.1103/PhysRevLett.99.011601`. arXiv: `astro-s̄ph/0702379`.

[71] V. Alan Kostelecky and Matthew Mewes. "Sensitive polarimetric search for relativity violations in gamma-ray bursts". In: *Phys. Rev. Lett.* 97 (2006), p. 140401. DOI: `10.1103/PhysRevLett.97.140401`. arXiv: `hep-s̄ph/0607084`.

[72] V. Alan Kostelecký. "Gravity, Lorentz violation, and the standard model". In: *Physical Review D* 69.10 (May 2004). DOI: `10.1103/physrevd.69.105009`. URL: `https://doi.org/10.1103/physrevd.69.105009`.

[73] V. Alan Kostelecký and Zonghao Li. "Backgrounds in gravitational effective field theory". In: *Phys. Rev. D* 103 (2 Jan. 2021), p. 024059. DOI: `10.1103/PhysRevD.103.024059`. URL: `https://link.aps.org/doi/10.1103/PhysRevD.103.024059`.

[74] V. Alan Kostelecký and Zonghao Li. "Gauge field theories with Lorentz-violating operators of arbitrary dimension". In: *Physical Review D* 99.5 (Mar. 2019). DOI: `10.1103/physrevd.99.056016`.

[75] V. Alan Kostelecký and Matthew Mewes. "Constraints on relativity violations from gamma-ray bursts". In: *Phys. Rev. Lett.* 110.20 (2013), p. 201601. DOI: `10.1103/PhysRevLett.110.201601`. arXiv: `1301.5367 [astro-ph.HE]`.

[76] V. Alan Kostelecký and Matthew Mewes. "Electrodynamics with Lorentz-violating operators of arbitrary dimension". In: *Phys. Rev. D* 80 (1 July 2009), p. 015020. DOI: `10.1103/PhysRevD.80.015020`. URL: `https://link.aps.org/doi/10.1103/PhysRevD.80.015020`.

[77] V. Alan Kostelecký and Matthew Mewes. "Fermions with Lorentz-violating operators of arbitrary dimension". In: *Phys. Rev. D* 88 (9 Nov. 2013), p. 096006. DOI: `10.1103/PhysRevD.88.096006`.

[78] V. Alan Kostelecký and Matthew Mewes. "Lorentz and diffeomorphism violations in linearized gravity". In: *Phys. Lett. B* 779 (2018), pp. 136–142. ISSN: 0370-2693. DOI: `https://doi.org/10.1016/j.physletb.2018.01.082`. URL: `https://www.sciencedirect.com/science/article/pii/S0370269318301060`.

[79] V. Alan Kostelecký and Matthew Mewes. "Signals for Lorentz violation in electrodynamics". In: *Phys. Rev. D* 66 (5 Sept. 2002), p. 056005. DOI: `10.1103/PhysRevD.66.056005`.

[80] V. Alan Kostelecký and Matthew Mewes. "Testing local Lorentz invariance with gravitational waves". In: *Phys. Lett. B* 757 (2016), pp. 510–514. ISSN: 0370-2693. DOI: `https://doi.org/10.1016/j.physletb.2016.04.040`. URL: `https://www.sciencedirect.com/science/article/pii/S0370269316301137`.

[81] V. Alan Kostelecký and Neil Russell. "Data tables for Lorentz and CPT violation". In: *Rev. Mod. Phys.* 83 (1 Mar. 2011), pp. 11–31. DOI: `10.1103/RevModPhys.83.11`. URL: `https://link.aps.org/doi/10.1103/RevModPhys.83.11`.

[82] V. Alan Kostelecký and Stuart Samuel. "Gravitational phenomenology in higher-dimensional theories and strings". In: *Phys. Rev. D* 40 (6 Sept. 1989), pp. 1886–1903. DOI: `10.1103/PhysRevD.40.1886`. URL: `https://link.aps.org/doi/10.1103/PhysRevD.40.1886`.

[83] V. Alan Kostelecký and Stuart Samuel. "Phenomenological gravitational constraints on strings and higher-dimensional theories". In: *Phys. Rev. Lett.* 63 (3 July 1989), pp. 224–227. DOI: `10.1103/PhysRevLett.63.224`. URL: `https://link.aps.org/doi/10.1103/PhysRevLett.63.224`.

[84] V. Alan Kostelecký and Stuart Samuel. "Spontaneous breaking of Lorentz symmetry in string theory". In: *Phys. Rev. D* 39 (2 Jan. 1989), pp. 683–685. DOI: `10.1103/PhysRevD.39.683`.

[85] Jack Y. L. Kwok et al. "Investigation on the Effects of Non-Gaussian Noise Transients and Their Mitigations on Gravitational-Wave Tests of General Relativity". In: (Sept. 2021). arXiv: `2109.07642 [gr-qc]`.

[86] Xiaoshu Liu et al. "Measuring the speed of gravitational waves from the first and second observing run of Advanced LIGO and Advanced Virgo". In: *Phys. Rev. D* 102.2 (2020), p. 024028. DOI: `10.1103/PhysRevD.102.024028`. arXiv: `2005.03121 [gr-qc]`.

[87] Przemysław Małkiewicz and Artur Miroszewski. "Internal clock formulation of quantum mechanics". In: *Phys. Rev. D* 96 (4 Aug. 2017), p. 046003. DOI: `10.1103/PhysRevD.96.046003`.

[88] T. Mariz, J. R. Nascimento, and A. Yu. Petrov. "Lorentz symmetry breaking – classical and quantum aspects". In: (May 2022). arXiv: `2205.02594 [hep-th]`.

[89] Matthew Mewes. "Signals for Lorentz violation in gravitational waves". In: *Phys. Rev. D* 99.10 (2019), p. 104062. DOI: `10.1103/PhysRevD.99.104062`. arXiv: `1905.00409 [gr-qc]`.

[90] A. A. Michelson and E. W. Morley. "On the Relative Motion of the Earth and the Luminiferous Ether". In: *American Journal of Science* s3-34(203) (1887), pp. 333–345. DOI: `10.2475/ajs.s3-s̄34.203.333`.

[91] Saeed Mirshekari, Nicolás Yunes, and Clifford M. Will. "Constraining Lorentz-violating, modified dispersion relations with gravitational waves". In: *Phys. Rev. D* 85 (2 Jan. 2012), p. 024041. DOI: `10.1103/PhysRevD.85.024041`. URL: `https://link.aps.org/doi/10.1103/PhysRevD.85.024041`.

[92] C. W. Misner, K. S. Thorne, and J. A. Wheeler. *Gravitation.* Ed. by Misner, C. W., Thorne, K. S., & Wheeler, J. A. 1973.

[93] Christopher J. Moore et al. "Testing general relativity with gravitational-wave catalogs: The insidious nature of waveform systematics". In: *iScience* 24.6 (2021), p. 102577. ISSN: 2589-0042. DOI: `https://doi.org/10.1016/j.isci.2021.102577`. URL: `https://www.sciencedirect.com/science/article/pii/S2589004221005459`.

[94] Debottam Nandi and S. Shankaranarayanan. "Complete Hamiltonian analysis of cosmological perturbations at all orders". In: *JCAP* 06 (2016), p. 038. DOI: `10.1088/1475-s̄7516/2016/06/038`. arXiv: `1512.02539 [gr-qc]`.

[95] Debottam Nandi and S. Shankaranarayanan. "Complete Hamiltonian analysis of cosmological perturbations at all orders". In: *Journal of Cosmology and Astroparticle Physics* 2016.06 (June 2016), pp. 038–038. DOI: `10.1088/1475-s̄7516/2016/06/038`. URL: `https://doi.org/10.1088%2F1475-s̄7516%2F2016%2F06%2F038`.

[96] J. R. Nascimento, A. Yu. Petrov, and A. R. Vieira. "On Plane Wave Solutions in Lorentz-Violating Extensions of Gravity". In: *Galaxies* 9.2 (2021). ISSN: 2075-4434. DOI: `10.3390/galaxies9020032`. URL: `https://www.mdpi.com/2075-s̄4434/9/2/32`.

[97] Ralf Lehnert, ed. *3+1 Decomposition of the Gravitational Sector of the Minimal Standard-Model Extension.* Singapur: WSP, 2020. DOI: `10.1142/11655`.

[98] Nils A. Nilsson and Ewa Czuchry. "Hořava–Lifshitz cosmology in light of new data". In: *Physics of the Dark Universe* 23 (2019), p. 100253. ISSN: 2212-6864. DOI: `https://doi.org/10.1016/j.dark.2018.100253`. URL: `https://www.sciencedirect.com/science/article/pii/S2212686418300943`.

[99] Nils A. Nilsson, Kellie O'Neal-Ault, and Quentin G. Bailey. "A 3+1 Decomposition of the Gravitational Sector of the Minimal Standard-Model Extension". In: *8th Meeting on CPT and Lorentz Symmetry*. May 2019. DOI: `10.1142/9789811213984_0050`. arXiv: `1905.10414 [gr-qc]`.

[100] Nils A. Nilsson, Kellie O'Neal-Ault, and Quentin G. Bailey. "A 31 Decomposition of the Gravitational Sector of the Minimal Standard-Model Extension". In: *CPT and Lorentz Symmetry*. WORLD SCIENTIFIC, Apr. 2020. DOI: `10.1142/9789811213984_0050`. URL: `https://doi.org/10.1142%2F9789811213984_0050`.

[101] Rui Niu, Tao Zhu, and Wen Zhao. "Constraining Anisotropy Birefringence Dispersion in Gravitational Wave Propagation with GWTC-3". In: (Feb. 2022). arXiv: `2202.05092 [gr-qc]`.

[102] Kellie O'Neal-Ault. *Recent Progress in Gravity Tests of Spacetime Symmetries*. 2023. arXiv: `2305.13337 [gr-qc]`.

[103] Kellie O'Neal-Ault, Quentin G. Bailey, and Nils A. Nilsson. "mml:math xmlns:mml="http://display="inline"mml:mrowmml:mn3/mml:mnmml:mo/mml:momml:mn1/mml:mn/mml:mr formulation of the standard model extension gravity sector". In: *Physical Review D* 103.4 (Feb. 2021). DOI: `10.1103/physrevd.103.044010`. URL: `https://doi.org/10.1103/physrevd.103.044010`.

[104] Kellie O'Neal-Ault et al. "Analysis of Birefringence and Dispersion Effects from Spacetime-Symmetry Breaking in Gravitational Waves". In: *Universe* 7.10 (2021), p. 380. DOI: `10.3390/universe7100380`. arXiv: `2108.06298 [gr-qc]`.

[105] ChristianD. Ott. "The Gravitational Wave Signature of Core-Collapse Supernovae". In: *Class. Quant. Grav.* 26 (2009), p. 063001. DOI: `10.1088/0264-9381/26/6/063001`. arXiv: `0809.0695 [astro-ph]`.

[106] Joan Solà Peracaula, Javier de Cruz Pérez, and Adrià Gómez-Valent. "Dynamical dark energy vs. = const in light of observations". In: *Europhysics Letters* 121.3 (Apr. 2018), p. 39001. DOI: `10.1209/0295-5075/121/39001`. URL: `https://dx.doi.org/10.1209/0295-5075/121/39001`.

[107] Eric Poisson and Clifford M. Will. *Gravity.* Cambridge University Press, 2014.

[108] Robertus Potting. "Lorentz and CPT violation". In: *Journal of Physics: Conference Series* 447.1 (July 2013), p. 012009. DOI: `10.1088/1742-6596/447/1/012009`.

[109] Geraint Pratten et al. "Computationally efficient models for the dominant and subdominant harmonic modes of precessing binary black holes". In: *Phys. Rev. D* 103.10 (2021), p. 104056. DOI: `10.1103/PhysRevD.103.104056`. arXiv: `2004.06503 [gr-qc]`.

[110] Jin Qiao et al. "Waveform of gravitational waves in the ghost-free parity-violating gravities". In: *Physical Review D* 100.12 (Dec. 2019). ISSN: 2470-0029. DOI: `10.1103/physrevd.100.124058`. URL: `http://dx.doi.org/10.1103/PhysRevD.100.124058`.

[111] M Rakhmanov. "On the round-trip time for a photon propagating in the field of a plane gravitational wave". In: *Classical and Quantum Gravity* 26.15 (July 2009), p. 155010. DOI: `10.1088/0264-9381/26/15/155010`. URL: `https://doi.org/10.1088%2F0264-9381%2F26%2F15%2F155010`.

[112] M Rakhmanov, J D Romano, and J T Whelan. "High-frequency corrections to the detector response and their effect on searches for gravitational waves". In: *Classical and Quantum Gravity* 25.18 (Sept. 2008), p. 184017. DOI: `10.1088/0264-9381/25/18/184017`. URL: `https://doi.org/10.1088%2F0264-9381%2F25%2F18%2F184017`.

[113] Valentina Salvatelli et al. "Indications of a Late-Time Interaction in the Dark Sector". In: *Physical Review Letters* 113.18 (Oct. 2014). DOI: `10.1103/physrevlett.113.181301`. URL: `https://doi.org/10.1103%2Fphysrevlett.113.181301`.

[114] S. Scheidegger et al. "The influence of model parameters on the prediction of gravitational wave signals from stellar core collapse". In: *Astronomy and Astrophysics* 514 (May 2010), A51. DOI: `10.1051/0004-6361/200913220`.

[115] Michael Seifert. "Lorentz-Violating Gravity Models and the Linearized Limit". In: *Symmetry* 10.10 (2018). ISSN: 2073-8994. DOI: `10.3390/sym10100490`. URL: `https://www.mdpi.com/2073-8994/10/10/490`.

[116] Michael D. Seifert. "Constraints and degrees of freedom in Lorentz-violating field theories". In: *Physical Review D* 99.4 (Feb. 2019). DOI: `10.1103/physrevd.99.045003`. URL: `https://doi.org/10.1103%2Fphysrevd.99.045003`.

[117] Michael D. Seifert. "Vector models of gravitational Lorentz symmetry breaking". In: *Phys. Rev. D* 79 (12 June 2009), p. 124012. DOI: `10.1103/PhysRevD.79.124012`. URL: `https://link.aps.org/doi/10.1103/PhysRevD.79.124012`.

[118] Lijing Shao. "Combined search for anisotropic birefringence in the gravitational-wave transient catalog GWTC-1". In: *Phys. Rev. D* 101 (10 May 2020), p. 104019. DOI: `10.1103/PhysRevD.101.104019`. URL: `https://link.aps.org/doi/10.1103/PhysRevD.101.104019`.

[119] W. Szczyrba. "Stephenson-kilmister-yang Theory of Gravity and Its Dynamics". In: *Phys. Rev. D* 36 (1987), pp. 351–374. DOI: `10.1103/PhysRevD.36.351`.

[120] Rhondale Tso and Michele Zanolin. "Measuring violations of general relativity from single gravitational wave detection by nonspinning binary systems: Higher-order asymptotic analysis". In: *Phys. Rev. D* 93.12 (2016), p. 124033. DOI: `10.1103/PhysRevD.93.124033`. arXiv: `1509.02248 [gr-qc]`.

[121] J. Veitch et al. "Parameter estimation for compact binaries with ground-based gravitational-wave observations using the LALInference software library". In: *Phys. Rev. D* 91 (4 Feb. 2015), p. 042003. DOI: `10.1103/PhysRevD.91.042003`. URL: `https://link.aps.org/doi/10.1103/PhysRevD.91.042003`.

[122] Anzhong Wang. "Hoř ava gravity at a Lifshitz point: A progress report". In: *International Journal of Modern Physics D* 26.07 (Mar. 2017), p. 1730014. DOI: `10.1142/s0218271817300142`. URL: `https://doi.org/10.1142%2Fs0218271817300142`.

[123] Yi-Fan Wang et al. "Gravitational Wave Implications for the Parity Symmetry of Gravity in the High Energy Region". In: *Astrophys. J.* 908.1 (2021), p. 58. DOI: `10.3847/1538-s̄4357/abd7a6`. arXiv: `2002.05668 [gr-qc]`.

[124] Yi-Fan Wang et al. *Tests of Gravitational-Wave Birefringence with the Open Gravitational-Wave Catalog.* Sept. 2021. arXiv: `2109.09718 [astro-ph.HE]`.

[125] Sai Wang and Zhi-Chao Zhao. "Tests of CPT invariance in gravitational waves with LIGO-Virgo catalog GWTC-1". In: *The Eur. Phys. J. C* 80.11 (Nov. 2020). ISSN: 1434-6052. DOI: `10.1140/epjc/s10052-s̄020-s̄08628-s̄x`. URL: `http://dx.doi.org/10.1140/epjc/s10052-s̄020-s̄08628-s̄x`.

[126] Ziming Wang, Lijing Shao, and Chang Liu. "New Limits on the Lorentz/CPT Symmetry Through 50 Gravitational-wave Events". In: *The Astrophysical Journal* 921.2 (2021), p. 158.

[127] Steven Weinberg. *Gravitation and Cosmology: Principles and Applications of the General Theory of Relativity.* New York: John Wiley and Sons, 1972. ISBN: 978-0-471-92567-5, 978-0-471-92567-5.

[128] C. M. Will. *Theory and Experiment in Gravitational Physics, 2nd Edition.* Cambridge University Press, 2018.

[129] Rui Xu. "Modifications to Plane Gravitational Waves from Minimal Lorentz Violation". In: *Symmetry* 11.10 (2019), p. 1318. DOI: `10.3390/sym11101318`. arXiv: `1910.09762 [gr-qc]`.

[130] Rui Xu, Yong Gao, and Lijing Shao. "Signatures of Lorentz Violation in Continuous Gravitational-Wave Spectra of Ellipsoidal Neutron Stars". In: *Galaxies* 9.1 (2021), p. 12. DOI: `10.3390/galaxies9010012`. arXiv: `2101.09431 [gr-qc]`.

[131] Nicolás Yunes, Kent Yagi, and Frans Pretorius. "Theoretical physics implications of the binary black-hole mergers GW150914 and GW151226". In: *Phys. Rev. D* 94 (8 Oct. 2016), p. 084002. DOI: `10.1103/PhysRevD.94.084002`. URL: `https://link.aps.org/doi/10.1103/PhysRevD.94.084002`.